

THESIS ON MECHANICAL AND INSTRUMENTAL ENGINEERING E53

# **Novel Methods for Hardmetal Production and Recycling**

RENEE JOOST

**TUT**  
**PRESS**

TALLINN UNIVERSITY OF TECHNOLOGY  
Faculty of Mechanical Engineering  
Department of Materials Engineering

**Dissertation was accepted for the defence of the degree of Doctor of Philosophy in Engineering on May 10, 2010.**

**Supervisor:** Senior researcher Jüri Pirso, Dr Eng, Department of Materials Engineering, Tallinn University of Technology

**Opponents:** Professor Michael Gasik, Department of Materials Science and Engineering, Aalto University School of Science and Technology, Finland.  
Senior researcher Valdek Mikli, PhD, Centre of Materials Research, Tallinn University of Technology, Estonia.

Defence of the thesis: June 18, 2010, at 12:00  
Lecture hall: A V-215  
Tallinn University of Technology, Ehitajate tee 5, Tallinn

Declaration:

Hereby I declare that this doctoral thesis, my original investigation and achievement, submitted for the doctoral degree at Tallinn University of Technology has not been submitted for any academic degree.



*/Töö autori nimi ja allkiri/*

Copyright: Renee Joost, 2010  
ISSN 1406-4758  
ISBN 978-9949-23-002-0

MASINA- JA APARAADIEHITUS E53

# **Uudsed meetodid WC-Co kõvasulamite valmistamiseks ja taaskasutamiseks**

RENEE JOOST



## **Acknowledgements**

First I would like to thank my supervisor Dr. Eng. Jüri Pirso for introducing me to the subject, providing excellent working conditions and continuous support throughout the studies.

I would like to thank the co-authors of the papers related to the thesis and all my colleagues in Department of Materials Engineering of TUT for their assistance and support, especially Mart Viljus from Centre of Materials Research for materials characterization.

This work was supported by Estonian Science Foundation (grant no. 6758) and target financing projects T062 ("Design and technology of multiphase tribomaterials"). This work has been partially supported by graduate school „Functional materials and processes“ receiving funding from the European Social Fund under project 1.2.0401.09-0079 in Estonia and graduate school "New Product Technologies and Processes".

Finally, I would like to thank my family for the help and encouragement.

## **The author's contribution**

The author of this thesis took part in the sample preparation routine, was responsible for carrying out of the experiments, collecting, processing and further analysis of experimental data. The author also took in discussion of the content. The intellectual merit which is the result of the framework where the contribution of every author of related papers should not be underestimated.



## Contents

Symbols and abbreviations .....	10
Introduction .....	11
1. Literature review and aims of the study .....	12
1.1 Production of hardmetals .....	12
1.1.1 Processing of ammonium paratungstate (APT) and tungstic acid .....	12
1.1.2 Conventional method for production of WC by reduction and carburization .....	13
1.1.3 Direct carburization of $WO_3$ as an alternative route for making tungsten carbide .....	17
1.1.4 Production of Co powder .....	18
1.2 Reactive sintering .....	19
1.2.1 The production of fine grain hardmetals .....	19
1.2.2 Thermodynamic analysis of tungsten carburization .....	19
1.2.3 Reactive sintering process: powder preparation, changes in phase composition during sintering .....	20
1.3 Methods for hardmetals recycling .....	22
1.3.1 Conventional methods for WC-Co recycling .....	23
1.3.1.1 Coldstream method .....	24
1.3.1.2 Hydrothermal treatment method .....	25
1.3.1.3 High-temperature fracture method .....	25
1.3.1.4 Zinc method .....	26
1.4 Oxidation-reduction methods .....	27
1.4.1 Carbothermal reduction in vacuum .....	27
1.4.1.1 Thermodynamic analysis for in situ synthesis of WC-Co composite powder from metal oxides .....	28
1.4.2 Reduction mechanism of $WO_3$ by hydrogen .....	34
1.4.3 Reduction and carburization with hydrocarbons .....	36
1.4.4 Reduction and carburization in inert gas atmosphere .....	37
1.4.5 The effect of Co content to the carburization .....	38
1.5 Conclusion to the chapter and aims of the study .....	39
2. Experimental procedures. Investigated materials and test methods .....	41
2.1 Technological parameters of studied hardmetal production methods .....	41
2.1.1 Reactive sintering process .....	41
2.1.2. Carbothermal reduction process .....	44

2.1.2.1 The preparation of powder and green parts from mixture of oxides and graphite.....	45
2.1.2.2 Reduction and sintering process .....	46
2.2 Materials tested .....	48
2.3 Property and wear testing methods .....	50
2.3.1 Methods for microstructure and property testing.....	50
2.3.2 Erosive wear testing method .....	51
2.3.3 Abrasive wear test methods .....	52
3. Reactive sintering: development of method for hardmetal production from W, Co and C powders. ....	53
3.1 Changes in phase composition during reactive sintering process.....	53
3.2 Densification and shrinkage behavior.....	58
3.3 Effect of grain growth inhibitors.....	61
3.4 Mechanical properties .....	64
3.5 Conclusions to the chapter .....	66
4. Recycling by oxidation and carbothermal reduction .....	67
4.1 Oxidation process.....	67
4.2 The determination of content of additional carbon black .....	69
4.3 Carbothermal reduction of $WO_3$ , $CoWO_4$ and graphite mixture powders in vacuum.....	70
4.4 Carbothermal reduction of green parts in vacuum. The main parameters of process: carbon addition, temperature and time. ....	74
4.4.1 Phase formation in compacted green parts during carbothermal reduction and reactive sintering .....	74
4.4.2 Densification and shrinkage behavior during carbothermal reduction and following reactive sintering.....	77
4.4.3 The effect of milling technology.....	81
4.4.4 The influence of plasticizer content and compaction pressure to the microstructure and mechanical properties .....	82
4.4.5 Mechanical properties of hardmetal produced by carbothermal reduction in combination with reactive sintering.....	88
4.5 Conclusions to the chapter .....	89
5. Wear resistance of hardmetals produced by reactive sintering method.....	90
5.1 Abrasion .....	90
5.2 Wear mechanism in abrasion .....	95
5.4 Erosion .....	97
5.4 Conclusions to the chapter .....	99



Conclusions.....	100
References.....	101
List of publications.....	110
Abstract.....	111
Kokkuvõte.....	112
ELULOOKIRJELDUS.....	113
CURRICULUM VITAE.....	115

## Symbols and abbreviations

### *Abbreviations*

ASTM	American Society for Testing and Materials
APT	ammonium paratungstate
BET	Brunauer, Emmett and Teller method for specific surface area estimation
BPR	Ball to Powder Ratio
CAK	centrifugal accelerator of Kleis
COV	Coefficient of Variation
FSSS	Fisher Sub Sieve Sizer
HB	Brinell hardness
HIP	Hot Isostatic Pressing
HV	Vickers hardness
IMTA	integrated mechanical and thermal activation
MAS	Mechanically Activated Synthesis
RPM	Rounds per minute, rotation speed, 1/min
SEM	Scanning Electron Microscopy
Sinter/HIP	concurrent vacuum sintering and HIP process
SSA	Specific Surface Area
TGA	Thermal Gravimetric Analysis
TRS	Transverse Rupture Strength
XRD	X-ray diffraction

### *Symbols*

$d$	average grain size
$F_n$	normal load, N
$K$	erosion rate
$k$	wear coefficient
$K_p$	equilibrium constant
$P$	pressure, Bar
$R_z$	surface finish parameter
$\Delta G$	Gibbs free energy
$\eta$ -phase	$W_xCo_yC$
$\gamma$	density, $g/cm^3$
$S$	specific surface area, $m^2/g$
$\Delta A_i$ ( $i = 1-5$ )	the thermodynamic data of reactant

## Introduction

WC-Co hardmetals are most widely used as tool materials in machining and forming application as well as materials for wear component because of their excellent hardness-ductility combination. The shortage of WC-Co hardmetals is the high prices of tungsten and cobalt. To reuse hardmetals scrap and to work out cost-effective manufacturing is very actual.

Many methods have been used to synthesize tungsten carbide. WC is conventionally synthesized through a solid/solid reaction by heating a mixture of tungsten powder and carbon black at temperatures in the range of 1400-1800 °C under a hydrogen atmosphere.

The present thesis "Novel methods for hardmetals production and recycling", is devoted to hardmetals produced by cost-effective reactive sintering process. In this study we focused on the formation of dense WC-Co from the mixture of W, Co and C elemental powders as well as on the development of technology for the reactive sintering of  $WO_3+CoWO_4+C$  mixtures. The author of present study focuses on the experimental manufacturing and recycling processes, as it is important from practical point of view that the established technology could be used in Estonian small and medium-sized enterprises. The estimated quantity of hardmetals scrap in Estonia is ca 3 tons annually. This waste material can be reentered to the manufacturing by economical recycling method. The introduction of new cost-efficient manufacturing processes has a decisive influence on the further development of hardmetals industry. This thesis is divided into five Chapters. Following the introduction, literature overview is given in Chapter 1. In chapter 2, the preparation of materials and the experimental methods are reviewed.

Chapter 3 consists of five sections. The sections are dedicated to development of reactive sintering method for hardmetals production from W, Co and C powders.

Chapter 4 is divided into five sections. The first section is dedicated to the hardmetals oxidation process. The second section describes the determination of additional carbon content in the carbothermal reduction and carburization process. The third section is a study about carbothermal reduction and carburization of  $WO_3$ ,  $CoWO_4$  and C powders in vacuum. The fourth section of fourth chapter is dedicated to the carbothermal reduction and reactive sintering of green parts in vacuum.

The last chapter presents the results of wear tests made with reactive sintered and recycled hardmetals. After the last chapter the general conclusions of study are presented.

The main results of present research have been presented in 4 international conferences.

## 1. Literature review and aims of the study

WC-Co hardmetal alloys have been used for application as various wear resistance machine parts and tools, including rollers, inserts, drills, dies and others. These alloys are composed of a large amount of tungsten carbide and cobalt (or Fe and Ni), and a small amount of titanium carbide and tantalum carbide [1].

The starting materials for the manufacture of hardmetals are hard refractory carbides and metal binder, both in the form of the powder. The most widely used refractory carbide phases are WC, TiC, TaC and their mixed carbides. In addition niobium carbide (NbC), chromium carbide ( $\text{Cr}_3\text{C}_2$ ), vanadium carbide (VC), and their alloys are used. The primary metal binder is cobalt (Co), although some of other iron group elements have also been tried to use [2].

### 1.1 Production of hardmetals

#### 1.1.1 Processing of ammonium paratungstate (APT) and tungstic acid

The starting materials for the manufacture of WC are concentrates of scheelite or wolframite ore from which ammonium paratungstate (APT) or tungstic acid is prepared by hydrometallurgical processing, today often implying solvent extraction and ion exchange. After reduction to tungsten metal and mixing with graphite, tungsten carbide is obtained by exothermic reaction at temperature range 1350–1600 °C. Tungsten carbide powder is subsequently mixed with cobalt, and if appropriate with other carbides and comminuted hardmetals scrap to the desired overall composition. After mixing and milling, the powder mixture is agglomerated, consolidated and sintered. For many products there will be finishing and coating operations but these will only be given a perfunctory treatment in this context. The various processing steps are summarized in Fig. 1.

There are many techniques for making concentrates of the common tungsten minerals, scheelite ( $\text{CaWO}_4$ ) and wolframite ( $(\text{Fe}, \text{Mn})\text{WO}_4$ ): flotation, magnetic or electrostatic separation [4, 5].

In virtually all processing of tungsten bearing minerals to tungsten products, ammonium paratungstate  $(\text{NH}_4)_{10}\text{H}_2\text{W}_{12}\text{O}_{42} \cdot 4\text{H}_2\text{O}$  (also written  $5(\text{NH}_4)_2\text{O}, 12\text{WO}_3, 5\text{H}_2\text{O}$ ) or APT for short, is an intermediate product. With modern techniques this compound can be made to almost any desired purity and granulometry [2].

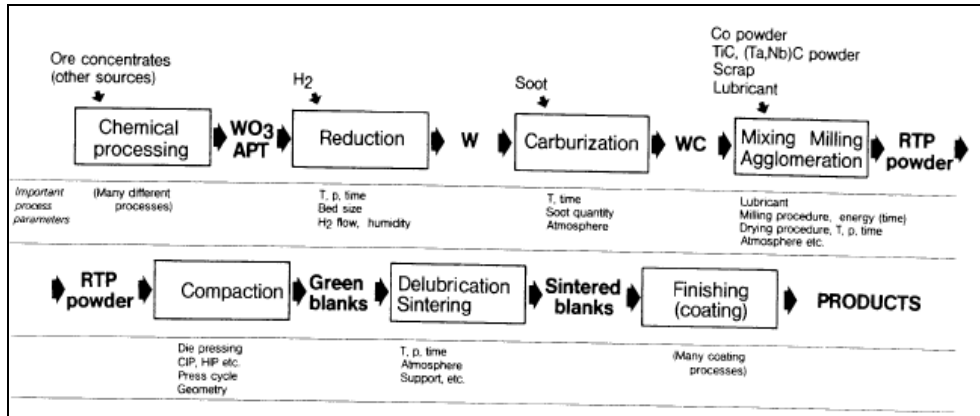


Figure 1. Processing steps in the making of cemented carbide [2, 3]

Nowadays concentrates with 10–40%  $WO_3$  are often fed-directly into the chemical plant where they are, for instance, treated by sodium carbonate in an autoclave [2]. APT obtained by fractional crystallization in the acid route process has purity which is satisfactory for many applications. The sodium tungstate solution obtained by the alkaline route can be purified by a series of chemical treatments or by modern techniques such as solvent extraction and ion-exchange [4, 5].

Tungsten-containing scrap is also treated chemically and converted to sodium tungstate and APT [6]. This is particularly appropriate for contaminated scrap. An interesting new method for treating such starting material is electrolytic dialysis. It can sometimes be advantageous to oxidize scrap and dissolve it in salt baths for subsequent leaching to sodium tungstate solution and a modification of this process route has recently been presented [7].

### 1.1.2 Conventional method for production of WC by reduction and carburization

Tungsten monocarbide (WC), a primary component in WC-Co hardmetals is obtained by the carburization of tungsten prepared by hydrogen reduction of  $WO_3$ . The primary sources of the tungsten are the minerals, Scheelite ( $CaWO_4$ ) and Wolframite ( $(Fe,Mn)WO_4$ ).

The content of  $WO_3$  in Scheelite and Wolframite is between 0,3% and 3,5% [2]. Due to the extremely high melting point of tungsten, its extraction is carried out by hydro-, rather than pyrometallurgical processes. The intermediate product is

ammonium paratungstate (APT) which is converted to either blue oxide ( $WO_{2.9}$ ) or yellow oxide ( $WO_3$ ).

The most common process is hydrogen reduction of APT or  $WO_3$  in which intermediate oxides are being formed. The “blue oxide” sometimes referred to as  $W_4O_{11}$  is a mixture of  $W_{18}O_{49}$  and  $W_{20}O_{58}$ , while the “brown oxide” is  $WO_2$ . The variation of the equilibrium constant  $K_p$  with temperature is shown in Fig. 2.

The reaction is reversible and the direction of the reaction is dependent on temperature and  $P_{H_2O}/P_{H_2}$ . The size of the W powder particles APT, blue oxide,  $WO_3$  and  $H_2WO_4$  will be reduced by hydrogen at temperature between 800 and 1000 °C. Production of tungsten powder of any desired size (FSSS) between 0,5 and 15  $\mu m$  is carried out by varying the reduction parameters. The important reduction parameters are temperature, time, hydrogen flow rate, height of oxide powder mass and apparent density of the oxide [8].

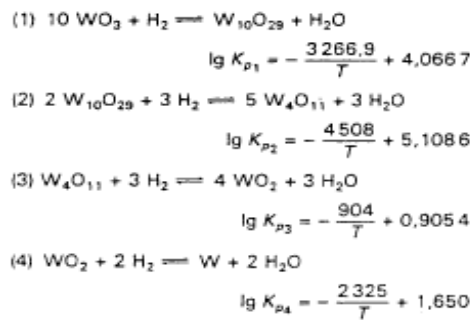
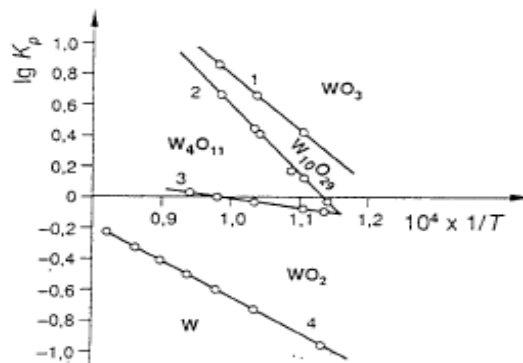


Figure 2. Reduction of tungsten oxides by hydrogen: variation of equilibrium constant  $K_p$  with temperature  $T$  (K) [9]

Of particular importance for the subsequent processing are the purity, the granulometry and the morphology of the tungsten powder obtained during the reduction, and this has been the subject of many publications, particularly concerning the influence of small amounts of impurities [10,11].

On regulating temperature, humidity of the hydrogen gas and the bed size, the average grain size of the tungsten powder can be varied between 0,3 and 10 microns or more. The reduction agents and temperatures are given in Table 1. The mechanisms and kinetics of reduction of  $WO_3$  are well described in [12]. The use of an oxygen probe (yttria-stabilized zirconia) at present permits the study and soon the control of the composition of the furnace atmosphere during reduction [13].

For fine-grained materials it may be advantageous to stop the reaction at the “blue oxide” stage and mill this, before continuing the reaction [14, 15]. Coarse-grained materials require the addition of particular dopants of which the alkaline metals are the most important ones.

Table 1. Reduction processes [16]

Reduction process/ furnace type	Compound	Reducing agent	Temperature [°C]
<i>Batch operations</i>			
1. Carbon reduction	APT	Carbon or Hydrocarbons	1300-1400
2. Hydrogen reduction	Oxide, acid	H <sub>2</sub>	700-900
<i>Continuous operations</i>			
3. Walking beam or belt type	APT Oxide Acid	H <sub>2</sub>	700-1000
4. Multitube pusher type	Oxides	H <sub>2</sub>	700-1000
5. Rotary kiln	APT Oxides	H <sub>2</sub>	700-1200
6. Plasma	Chlorides APT Oxides	H <sub>2</sub>	≥ 5000
7. Fluidsed bed	Oxide	H <sub>2</sub>	≥ 700
<i>Melting operations</i>			
Carbothermic Silicothermic Aluminothermic	ore concentrates	C Fe Si Al	≈ 2500

The next stage in the process, after tungsten powder production, is the manufacture of WC. To do this, the appropriate grade of tungsten metal is mixed with carbon black and heated to a temperature between 1400 °C and 1800 °C. The grain size of WC obtained lies generally in the range of 0,8–7,0 μm to meet the requirements of the sintered hardmetal. Some changes in grain size can be effected by variation of the carburizing temperature. Accurate carbon control is very important in hardmetal production. A slight deficiency of carbon results in the formation of extremely embrittling "eta" phase and an excess of carbon gives fine flakes of free graphite, which weakens the hardmetal and lowers the resistance to abrasive wear.

Prior to carburization, mixing is carried out to get a homogeneous mixture of tungsten metal powder and lamp black. Simple blending does not serve the purpose because of the high density difference of tungsten metal and carbon. The most widely used method for efficient mixing is either ball milling or mixing in a "V" type blender with a higher rpm intensifier. Depending upon the characteristics of the tungsten powder, the method of mixing tungsten and carbon black can have an important effect upon the grain size of the carbides produced.

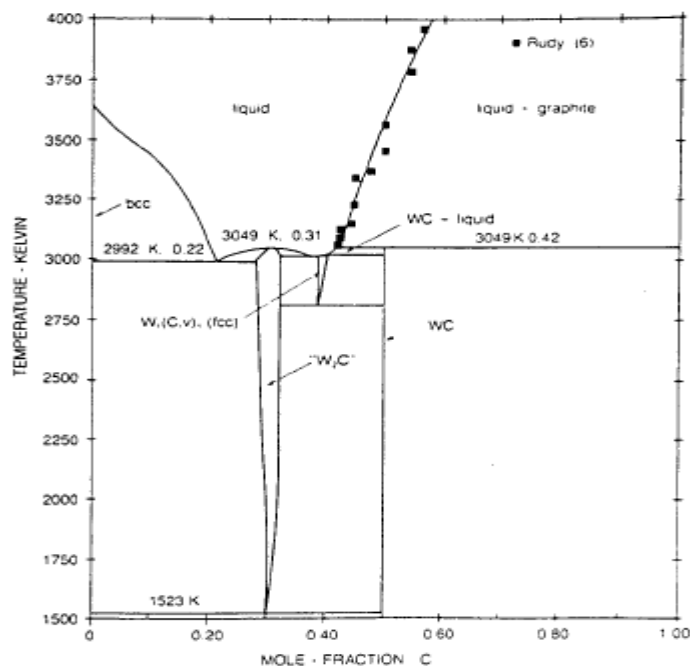


Figure 3. The W-C phase diagram [17]



Tungsten monocarbide used in preparing hardmetal is produced primarily by carburizing tungsten powder with carbon black. In the carburization process, the presence of a gas with a definite partial pressure of carbon is essential for the formation of the carbide.

As seen the W-C phase diagram (Fig. 3) the tungsten monocarbide has a very narrow homogeneity range and decomposes peritectically at 2776°C. It is made by reacting pure tungsten carbide powder with carbon black of low ash content, at 1350–1600°C. Even during this high temperature reaction there is a considerable elimination of impurity elements. The reaction is exothermic ( $G_{273}^{\circ} = -39.63 \text{ kJ}$ ) and this may give rise to temperature gradients and a concomitant scatter in grain-size in batch production. The continuous carburization process gives a more homogenous grain size: the mixture W + C is poured into graphite boats circulating under a counter-current hydrogen flow in a pusher-type Tamman furnace – a graphite tube is used as a heating element. Coarse and polycrystalline WC powders ( $d > 2 \mu\text{m}$ ) are obtained from coarse tungsten powders at a relatively high temperature (1600 °C), while fine and nearly monocrystalline WC powders ( $d < 1 \mu\text{m}$ ) are produced from submicron tungsten powders at 1350–1400 °C. Small amounts of cobalt influence the carburization of coarse tungsten powder [18]. During the carburization process the hemicarbide  $\text{W}_2\text{C}$  is also obtained as an intermediate phase [19]. The carburization temperature is correlated with the WC phase substructure and consequently with the mechanical properties of WC-Co alloys; it influences the subgrain size, microstrain and microhardness of WC [20, 21]. A good summary of the mechanisms and kinetics of tungsten powder carburization is given in [22].

### 1.1.3 Direct carburization of $\text{WO}_3$ as an alternative route for making tungsten carbide

In addition to the conventional carburizing of tungsten there are several other ways of making WC. Direct carburization of *tungstic* oxide  $\text{WO}_3$  is obviously of interest since it would eliminate one processing step. Studies are confirmed this possible route but there is still uncertainty about its advantages over the traditional route. The tungsten trioxide reduction-carburization with CO-CO<sub>2</sub> mixtures leads to the production of submicron WC powders ( $< 0,4 \mu\text{m}$ ) at 900 °C [23].

A new fairly direct method for making WC from ore concentrates has been developed by the US Bureau of Mines [2, 24]. In a system with two immiscible salt melts, the gangue is concentrated in the silicate melt while the tungsten-rich component is in the sodium chloride melt. The latter is subsequently subjected at 1070 °C to a gas sparing operation using natural gas (methane) which will give precipitation of WC which is cleaned by a wet chemical treatment. Submicrometer crystals of WC

are initially produced which then grow into thin plates up to 100  $\mu\text{m}$  on a side or into popcorn-shaped conglomerates.

The still used “menstruum technique” [23, 24], based on old patents, consists of dissolving tungsten in a graphite-covered melt of iron, nickel or cobalt (the so-called “auxiliary bath”) and extracting the carbide crystals from the cooled and crushed material by acid treatment. Very pure (low oxygen content) and well crystallized carbide can be obtained.

Alumino-thermic reduction of *tungstic* compounds combined with carburization is also an established procedure but with limited economic attraction, as is also the case for preparation of WC by molten salt electrolysis.

Tungsten carbide with special structure and properties (coatings for instance) can be prepared via gaseous tungsten compounds:  $\text{WF}_6$ ,  $\text{WCl}_6$ ,  $\text{W}(\text{CO})_6$ . Plasma technology has also been used for making WC, but again, the economy of these processes (involving consideration of energy consumption and protection of environment) has not made them widely applicable.

Direct carburization of  $\text{WO}_3$  is very much desirable from a practical point of view, but the problem arises in controlling both particle size and carbon content. Generally reduction of  $\text{WO}_3$  is done between 800  $^\circ\text{C}$  and 1000  $^\circ\text{C}$  for adequate control of particle size, whereas a minimum temperature of 1200  $^\circ\text{C}$  is required for carburization. This big difference makes it difficult, in practice, to combine both the processes in a single operation.

A mixture of cobalt and tungsten carbide can also be made by gas phase reduction/carburization of cobalt tungstate ( $\text{CoWO}_4$ ) and there is complete information on the thermodynamics of this reaction [25] which, so far, has not been commercially exploited. Several workers [26, 27] have found that carburization of tungsten at around 900  $^\circ\text{C}$  is possible in the presence of cobalt due to the catalytic effect. Ushijima [26] reported that  $\text{WO}_3$  can be carburized in hydrogen at about 900  $^\circ\text{C}$  in the presence of  $\text{Co}_3\text{O}_4$ .

#### **1.1.4 Production of Co powder**

Cobalt is found in the ores of other metals. Economically exploitable minerals for cobalt production are sulphides, arsenides, oxides, and hydroxides. Originally, cobalt powder was made by reducing cobalt oxide in hydrogen. Ultra-fine cobalt powders, regarded as essential for hardmetal industries, are made by pyrolysis of cobalt salt, such as cobalt oxalate, which is made by reacting oxalic acid and cobalt chloride. The powders are around 2  $\mu\text{m}$  but during milling with the carbide, break down even more finely. A new method has been developed to the production of "Polyol Cobalt" (spherical monodisperse and non-agglomerated Co powder). The method is based on

the reduction of cobaltous hydroxide by mixture of ethylene-glycol and diethylene-glycol [2, 8].

## 1.2 Reactive sintering

### 1.2.1 The production of fine grain hardmetals

The increasing use of materials with special properties and the introduction of new cost-efficient manufacturing processes have a decisive influence on the further development of hardmetals. It is well known that the mechanical properties of hardmetals can be improved by the reduction of a carbide grain size up to nanosize scale [28–30]. Nanograin and sub-micron WC-Co composites have superior properties and more homogeneous microstructure than those of the conventional WC-Co composites. They have potential to replace standard materials for tools, dies and wear parts because of their increased hardness and wear resistance. When the grain size in the WC-Co cemented carbides is reduced to a range of submicron or nanometer, the hardness and the strength of cemented carbides increase remarkably, and the toughness improves greatly as well [31, 32].

WC is conventionally synthesized through a solid/solid reaction by heating a mixture of tungsten powder and carbon black at temperatures in the range of 1400–1800 °C under a hydrogen atmosphere [33]. For fabricating sub-micron or nanocrystalline WC-Co composites, nanosize WC powder is used as a starting powder [1]. There are many ways to produce nanocrystalline WC and WC-Co powders, such as spray conversion process [34, 35], electric discharge machining [36], chemical vapor condensation [37, 38], thermal plasma process [39], high energy milling [40], integrated mechanical and thermal activation [41].

### 1.2.2 Thermodynamic analysis of tungsten carburization

Tungsten carbide (WC) and ditungsten carbide ( $W_2C$ ) are two stoichiometric compounds of the products of tungsten carbonization, with the reaction equations expressed as below:

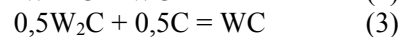


Fig. 4 shows the corresponding  $\Delta G-T$  curves of the Eqs. (1), (2) and (3). The  $\Delta G$  of the reaction (2) has obviously the lowest value, thus in the condition of sufficient concentration of carbon, the reaction product is WC. As the reactants are heated up, the  $\Delta G-T$  curve of producing WC rises and the curve of producing  $W_2C$  goes down.

Therefore, the  $W_2C$  phase is more stable than the WC phase at higher temperatures. From the  $\Delta G-T$  curve corresponding to Eq. (3), the  $\Delta G$  can be larger than zero at above 1500 K, thus the reaction will not occur, that is to say, at high temperatures  $W_2C$  can't transform into WC even with excess carbon [42].

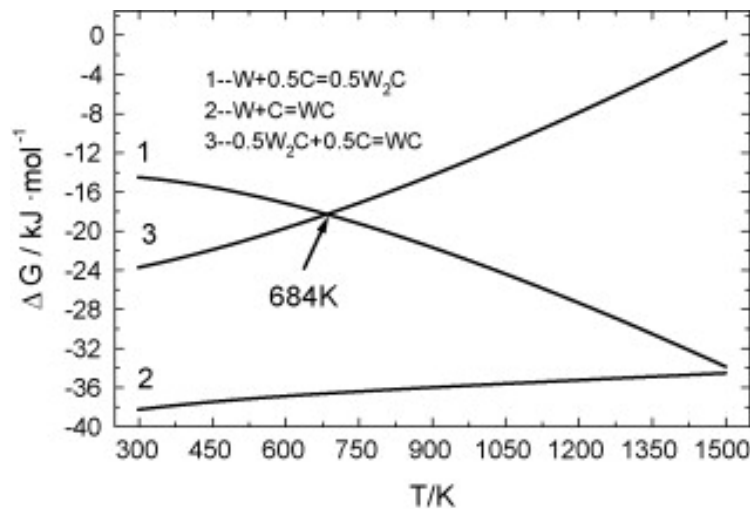


Figure 4. Changes of  $\Delta G$  with the temperature of the tungsten carburization reactions [42]

### 1.2.3 Reactive sintering process: powder preparation, changes in phase composition during sintering

High energy ball milling, a well-known process for preparing amorphous alloys, intermetallides, metal nitrides, metal carbides and nanocrystalline materials, has been considered as a powerful technique for synthesizing numerous nanocrystalline materials due to its simplicity and relatively inexpensive equipment [40]. The ball milled nanocrystalline powders have some unique characteristics compared to the other nanocrystalline powders, prepared by various techniques [41]. These powders are heavily work-hardened with a high density of lattice defects and an excess stored enthalpy [43]. The advantage of the method is that it can be used to synthesize designed compound with nano-size scale at room temperature, a method also known as reactive milling. The direct room temperature synthesis of metal carbides by high-energy milling of metal/carbon powders has been investigated by M. Sherif El-Eskandarany [44].

Reactive milling solely cannot be applied for the synthesis of carbide, if the reaction has small negative free energy of formation. Synthesis of the tungsten carbide at room temperature by high energy milling is also not reasonable, needing too long milling time and a considerable amount of mechanical activation. Tungsten carbide powder, manufactured by high-energy ball milling and following annealing may behave unpredictably during heat-treatment because of different amounts of absorbed energy and structural microdefects, oxidation, and loss of carbon.

The integrated mechanical and thermal activation (IMTA) process has been developed as a viable technique for producing large quantities of nanostructured carbides [41]. This process combines mechanical and thermal activation to enhance the formation of carbides *in situ* (the carbide grains are formed during sintering). The process is also called reactive sintering. The basic form of the IMTA process is to mechanically activate reactants (usually a mixture of the oxide and graphite powders) at room temperature through high energy milling (the mechanical activation step), followed by completing the synthesis reaction at higher temperatures (the thermal activation step). Because of the mechanical activation, the synthesis reaction of the IMTA process can be carried out at much lower temperatures and/or shorter time than those used in the conventional method for making coarse-grained carbides.

The carbon content has a great importance to the properties of the sintered WC-Co compositions. At a stoichiometric content of 6,13% C in the monotungsten carbide (WC) [45], the household is in balance. There is a very narrow range of  $\pm 0.1$ wt.% carbon where the WC-Co microstructure still remains in the two phase region (Fig. 3). At a W:C atomic ratio of less than 1 the carbon precipitates in the form of graphite and at a W:C ratio of significantly over 1  $\text{Co}_x\text{W}_y\text{C}$  ( $\eta$ -phase) is formed in the structure.

During a high energy milling and following drying, oxide layers are formed on the W and Co particles. During sintering the reduction of the oxide layers and some loss of the carbon occur. However, this drawback can be avoided, adding some “extra” carbon to the mixture in order to compensate the decarburization in the furnace during sintering. Free carbon is generally considered detrimental to the mechanical properties of sintered WC-Co since its presence reduces the hardness and wear resistance. Thus, it is necessary to adjust the free carbon concentration in nano-phase WC-Co powder, depending on the application desired. Free carbon is often present in the nanostructured WC-Co powder, obtained by the IMTA process because of the extra carbon added at the beginning of this process [46]. The nanocrystalline powder is expected to suffer greater levels of decarburization than the conventional coarse-grained powder because of the higher surface areas per unit volume of particles. The powder is extremely sensitive to the processing conditions: enhanced WC grain growth starts early in the sintering cycle while abnormal grains can form [47]. The fact that nanosized powder melts at lower temperatures than the equilibrium eutectic temperature has been demonstrated for nanocrystalline WC-Co powders [48].

According to work [49] shrinkage of fine-grained WC-Co composites occurs mainly during solid state phase and is completed in the liquid phase step. The solid-state shrinkage results of Co spreading on the WC particles and rearrangement of the WC particles, dissolved in Co and became faceted.

The grain growth during liquid phase sintering of the WC-Co alloys can be described as an Ostwald ripening process [50]. Within this model, the reduction in surface energy of the solid particles is the major driving force for small grains to dissolve and large grains to grow. Although this solution/re-precipitation requires diffusion through the liquid phase binder, the rate is controlled by interface kinetics due to the faceted morphology of the WC grains, where growth occurs by a 2-dimensional nucleation or defect assisted process [51]. Another mechanism for WC grain growth is the particle coalescence, involving atomic diffusion across a solid/solid grain boundary.

### **1.3 Methods for hardmetals recycling**

The annual worldwide hardmetals production is 45–50 thousand tons. As the hardmetal is expensive, the recycling of hardmetal has subsequent importance. Today there are different recycling rates of WC-Co in different industrial regions:

- EU less than 30% [52]
- US up to 60% [53]
- China, Russia less than 15% [52]
- Japan less than 20% [54].

The world wide scrap market is estimated to be 12 000 - 15 000 tons (except China) and available open market ca 10 000 tons [52].

There are two categories for the recycling of the WC-Co hardmetals. One is based on the carbide decomposition and refining by chemical agents [55]. This method can recycle the WC-Co into the elemental forms, i.e., tungsten, cobalt, titanium and tantalum. However, this method has the possibility of producing environmental pollution since this recycling method is based on chemical refining process, and requires various chemical equipments [56]. The other is based on separating the carbide and cobalt by metallurgical and crushing process [57, 58]. This method can obtain WC powder from the WC-Co hardmetal alloy. The obtained WC powder has a large particle size and impurities.

### 1.3.1 Conventional methods for WC-Co recycling

Various recycling processes of WC-Co hardmetals, such as chemical modification method, thermal modification method, zinc melt method, cold stream method and electrochemical method have been investigated and some of them are actually employed in industry (Fig. 5).

Recycling of hardmetal scrap is today mainly done in two different ways:

- Zink process
- Chemical process (oxidation and subsequent leaching treated like a concentrate).

Most chemical processes are based on the production of APT out of hard scrap like it is done from concentrate. In terms of quality the WC process via a chemical route is like "virgin" WC [52]. It is possible to feed hardmetal scrap to the chemical processing described in previous paragraph 1.1, and this is always done when the scrap is contaminated. However there are also vast amounts of "pure" scrap available, since in many applications only a small portion of a tool or a wear part is actually used. Such scrap can be recycled by less costly processes. Before any processing the scrap has to be cleared and sorted [59].

In this thesis three conventional recycling methods are analyzed: coldstream method, high-temperature fracture method and zinc method. The advantage with all three methods is that the costly chemical processing can be circumvented. The other side of the coin is that there is no purification and rather some risks of contamination. The composition and granulometry of the powder obtained by these methods may also not correspond to what is required in commercial production. Some loss of carbon is usually unavoidable and requires addition of graphite to the reclaimed powder. There is also likely to be accumulation of some impurities such as iron and aluminum. To some extent this can be compensated for by adding virgin carbide and cobalt powders of high purity but, sooner or later, scrap has to be recycled by the chemical route in order to decrease the contents of impurities [2].

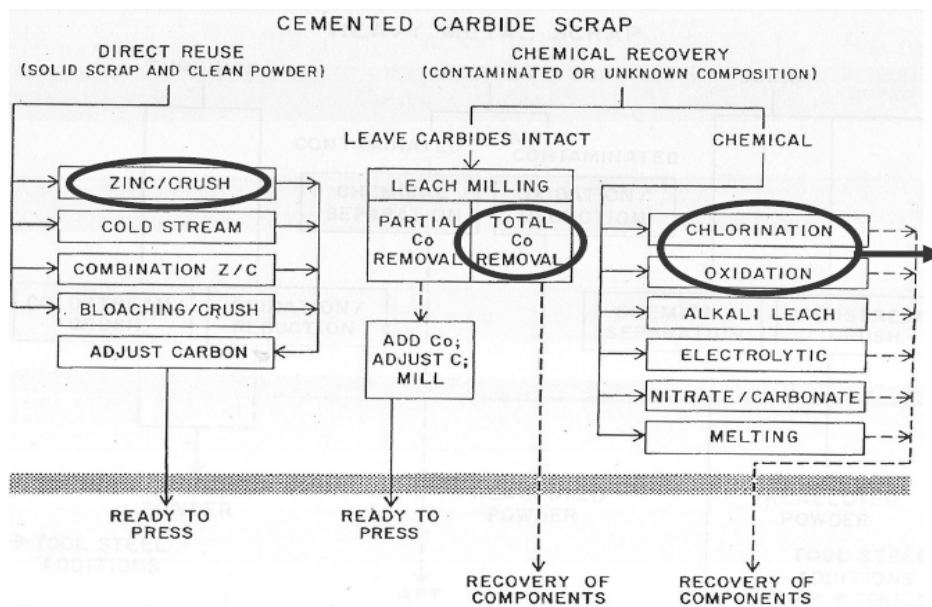


Figure 5. Treatment of hardmetals scrap (the methods deployed in industrial scale are marked) [52, 60]

However, these conventional methods have many problems to be solved and there are not always established technologies. For example, chemical modification method requires comparatively large-scale equipment and it takes relatively long reaction time. The recycling by thermal modification process usually undergoes the decomposition of WC and it leads to the formation of  $\eta$ -phase, which degrades the mechanical properties. Zinc melt and cold stream processes have problems with contamination by undesirable elements [61]. Therefore there is a need to develop more economical and high-quality recycling procedure.

### 1.3.1.1 Coldstream method

In the "COLDSTREAM" process the crushed scrap (passing through mesh 3,4–6 mm) is fed into a blast chamber and drawn by vacuum into a primary classifier. The full charge thus collected is pressurized and metered into a high pressure dried air system and accelerated through a venture toward the blast chamber. The fragments are impinged against a fixed target of hardmetal. The air expands as it leaves the venture, creating an adiabatic cooling which lowers the possible oxidation of the particles. After blasting the powder is transported to a primary classifier, a secondary classifier or a



finer collector, depending on the size. Oversize particles are returned to the blast chamber and the process is repeated [2].

### **1.3.1.2 Hydrothermal treatment method**

Hydrothermal process is known as an effective technique for the synthesis of new inorganic materials, leaching of ore resources, treatments of organic waste etc. One of the merits of this method is relatively low energy consumption because of the high chemical reactivity and excellent solubility of materials in hot water [62–63].

The WC-Co hardmetal specimens are hydrothermally treated with  $\text{HNO}_3$ ,  $\text{HCl}$ ,  $\text{FeCl}_3$  or  $\text{HCl}+\text{FeCl}_3$  aqueous solutions at temperatures 110–200 °C. The Co will be leached out into the acid solution, while the WC will be oxidized to insoluble  $\text{WO}_3 \cdot 0,33\text{H}_2\text{O}$  hydrate which could be separated by filtration. The recovered  $\text{WO}_3 \cdot 0,33\text{H}_2\text{O}$  powder can be easily returned to the industrial process for the synthesis of WC powder [64].

The hydrothermal oxidation method is more energy saving than other convention recycling methods and more versatile to be applied to hardmetal with various WC grain size, Co contents and even hardmetal containing carbide additives [64]. However, this method has the possibility of producing environmental pollution since this recycling method is based on chemical refining process and requires various chemical equipments.

According to patent IN157146 (1986), a molten salt consisting of alkali hydroxide, preferably  $\text{KOH}$  or  $\text{NaOH}$ , and an alkali nitrate as oxidizing agent, preferably  $\text{KNO}_3$  or  $\text{NaNO}_3$ , is employed for the working up of hardmetal scrap. The melting temperature varies between 350 and 460 °C. It was established that at 400 to 420 °C the yields of tungsten are 90 to 94%. At 440 to 460 °C the yield of tungsten can be increased to 99%. In this case the reaction can be controlled only with difficulty. In addition emission of nitrogen oxides occurs. The disadvantage of all reactions in nitrate and/or nitrite media is that the highly exothermic reaction is difficult to control. Consequently the overall reaction is considered to be problematic as regards industrial safety. In addition there is a frequently uncontrollable emission of nitrous gases. Nitrite and nitrate contained in the sodium tungstate solution and in the filtration residues render working up extremely difficult when a solvent extraction has to be subsequently carried out [64].

### **1.3.1.3 High-temperature fracture method**

In high-temperature fracture method WC-Co scrap is heat-treated in an inert atmosphere at 1800–2000 °C. Bloating of the hardmetal binder leads to the easy pulverization of the scrap in the subsequent quenching and milling processes [2, 65]. This method requires a high energy for heating and usually undesirable  $\text{W}_2\text{C}$ , C and

$\eta$ -phases form in the recovered powders. Moreover, the grain growth of carbide is inevitable due to the high treatment temperature.

According to Trapp US Pat. No. 2485175, tungsten carbide is recovered from cemented tungsten carbide by a process wherein a mass of the cemented carbide is heated to a temperature above the melting point of the cobalt bonding metal which causes the mass to swell and become porous, the porous mass is leached with acid to remove the cobalt metallic bond, and the resultant mass is subjected to mechanical reduction to produce powdered tungsten carbide. This process leaves a portion of the cobalt associated with the powdered tungsten carbide and produces grain growth of the metal carbide particles, both of which are undesirable for reuse of the recovered metal carbide powder.

#### 1.3.1.4 Zinc method

The most common method for recycling hardmetals scrap is the “zinc process” [66]. The process route is illustrated in Fig. 6. A method involves treatment of the hardmetal with molten Zn. The scrap is first cleaned with particular attention to remnants of brazing alloys or coating.

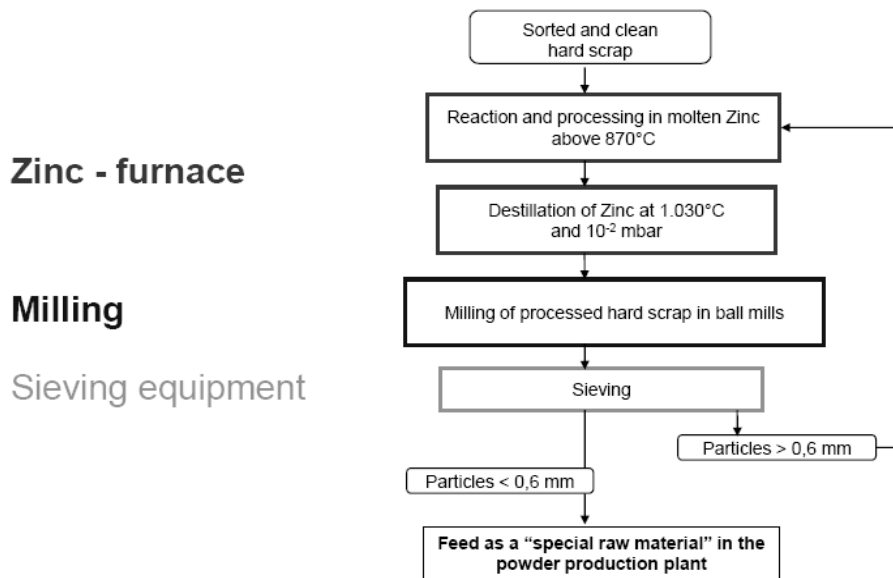


Figure 6. Route of Zinc process [52]

Hardmetals scrap is immersed in a molten Zn bath, and with diffusion of Zn or its vapor towards Co binder a Zn-Co alloy forms via a eutectic reaction at 950 °C, which results in the disintegration of the bulk scrap. The reaction between Zn and Co takes several hours. There is a volumetric change due to forming intermetallic Co-Zn phases, which are higher in volume (Fig.7) [52]. As a result, the scraps are powdered into WC grains, which stick on the bottom of the zinc bath. Then the scrap is treated at a higher temperature on 1000–1050 °C to vaporize Zn in a vacuum distillation processor in the inert gas atmosphere. The resulted porous sponge-like scrap is easily pulverized [67, 68]. The obtained WC powder has a low quality with a large particle size and high impurities. However, main problem still remains as the contamination of Zn in the recovered powders. At present some 30% of all hardmetals is recycled by this route [2].

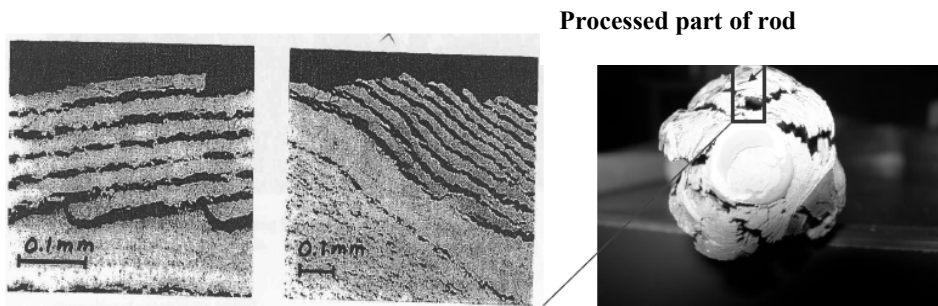


Figure 7. The outer part of the processed WC-Co rod [52]

## 1.4 Oxidation-reduction methods

### 1.4.1 Carbothermal reduction in vacuum

In this chapter, I focus on describing the investigations which have been done to develop a new recycling process of the waste WC-Co hardmetal alloy by a combination of oxidation, mechanical milling and carbothermal reduction processes.

It is known that WC-Co hardmetal can be easily transformed into a sub-micron particle size oxide mixture of  $\text{CoWO}_4$  and  $\text{WO}_3$  by oxidation and mechanical milling processes [65, 68, 69]. Generally reduction of  $\text{WO}_3$  is done between 800 °C and 1000 °C for control of particle size, whereas a minimum temperature of 1200 °C is required for carburization. This big difference in temperature for reduction and carburization makes it difficult, in practice, to combine both the processes in a single operation [33].

WC-Co composite powders with pure phases and homogeneous and ultrafine particles can be synthesized from tungsten oxide, cobalt oxide and carbon black at 1050 °C under vacuum conditions. Compared with conventional reaction methods, while intermediate products, such as CoWO<sub>4</sub>, play an important role in reducing the activation energies of the reactions, this novel method has the distinct advantage of lower reaction temperature and shorter holding time [42, 70]. It was further reported that it is possible to achieve dense hardmetal bulk by *in situ* synthesis in the SPS (Spark Plasma Sintering) system [71].

Investigating the mechanical properties and microstructure of hardmetals produced by carbothermal reduction of oxide powders it was found that the properties of recycled WC-Co materials were mainly influenced by the content of additional graphite. The same phenomenon also occurs with reactive sintering of bulk WC-Co parts from W, Co and carbon black mixtures. Carbon content has a great effect on the properties of sintered WC-Co composites. As it was mentioned earlier, there is a very narrow range of ±0.1 wt.% carbon where the WC-Co microstructure remains in the two-phase region (Fig. 3). At a W:C atomic ratio of less than 1 the carbon precipitates in the form of graphite, and at a W:C ratio of significantly over 1, Co<sub>x</sub>W<sub>y</sub>C (η-phase) is formed in the structure. During carbothermal reduction and sintering, reduction of the oxides and a loss of carbon occur. However, this drawback can be overcome through the addition of some “extra” carbon to the mixture to compensate for the carbothermal reduction and decarburization in the furnace during sintering [72].

Due to the several disadvantages of conventional recycling methods described in previous chapters, in this thesis I propose a new route for the recycling of hardmetals by a combination of oxidation, carbothermal reduction and reactive sintering. This new method has the advantage of simpler processing.

#### 1.4.1.1 Thermodynamic analysis for *in situ* synthesis of WC-Co composite powder from metal oxides

It is known that in the reaction thermodynamics, the first law of thermodynamics is used to explain processes related to energy transformation, and the second law of thermodynamics is used to determine the direction of the chemical reactions. Generally, the change of the Gibbs free energy,  $\Delta G$ , is used to judge the spontaneous direction of a process. In a condition when  $\Delta G = 0$ , the system exists at an equilibrium state, while  $\Delta G < 0$ , the reactions may occur. To characterize the transformation of heat in reaction,  $\Delta G$  can be calculated by the following equation:

$$\begin{aligned} \Delta G = & -\Delta A_1 T \ln T - \frac{1}{2} \times 10^{-3} \Delta A_2 T^2 - \frac{1}{2} \times \Delta A_2 T^2 - \frac{1}{2} \times 10^5 \Delta A_3 T^{-1} \\ & - \frac{1}{6} \times 10^{-6} \Delta A_4 T^3 - \frac{1}{6} \times 10^8 \Delta A_5 T^{-2} + A_6 T + A_7 \end{aligned} \quad (4)$$

where  $\Delta A_i$  ( $i = 1-5$ ) is the thermodynamic data of reactant and products at the standard state,  $A_6$  and  $A_7$  are the integrated constants. The initial reaction temperature can be obtained when  $\Delta G = 0$ . Moreover, the reactions sequence, the relative stability and transformation rule of the phases can be further investigated based on the thermodynamic principle [42].

When the mixed powder of tungsten oxides, cobalt oxides and carbon black is heated to a certain temperature, there are several reactions that may occur, including not only the reduction of tungsten oxides and cobalt oxides by the carbon, leading to the formation of different intermediate lower valence metal oxides, but also the reactions through which the tungsten carbides form.

#### *Thermodynamic analysis of carbon reducing tungsten trioxide $WO_3$*

In the case of reduction and carburizing treatment with solid carbon it is interesting that there is thermodynamic probability of direct transition of  $WO_3$  into WC at 600 °C (873 K) (Fig. 8 C). At this temperature if free graphite remains there is formation of WC. At 700 °C (973 K) it is possible to reach the stoichiometric composition of WC and establish equilibrium in the gas system CO+CO<sub>2</sub>. A further increase in temperature leads to the situation that the partial pressure in the gas mixture leads shifts in the direction of forming CO according to the reaction  $C+CO_2=2CO$ , which in turn leads to partial consumption (burn up) of carbon from the hard alloy mixture and an insufficient amount of it in order to form WC. Intermediate oxide  $WO_2$  develops. As temperature increases there is an increase in the percentage of metal tungsten, and a decrease in the amount of carbon bonded with tungsten into carbide [73].

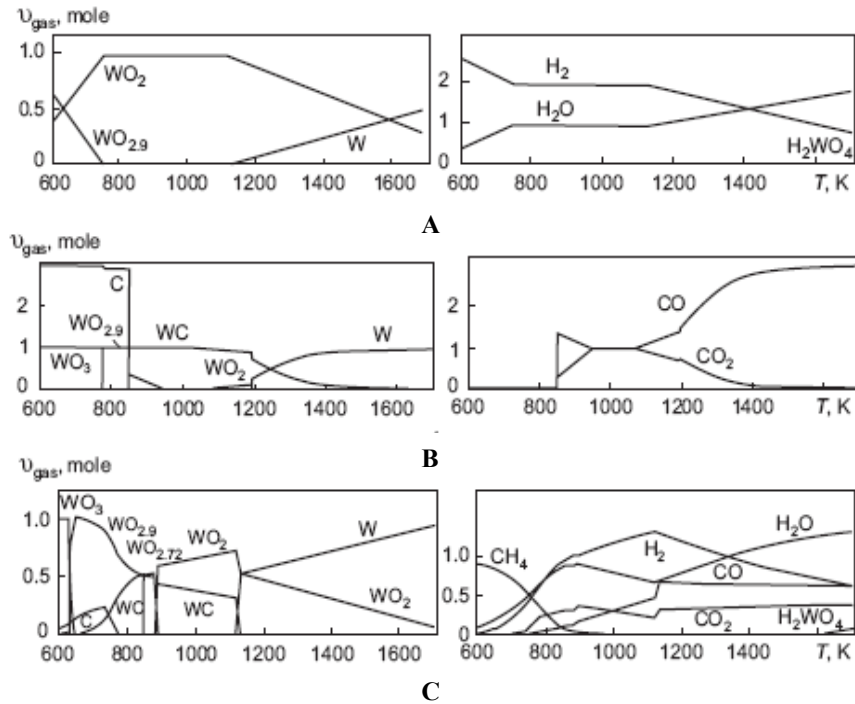
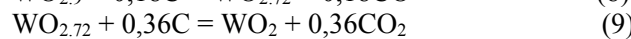
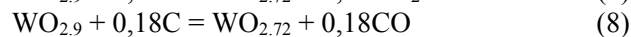
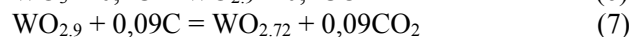
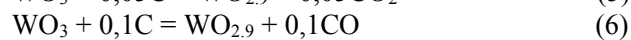
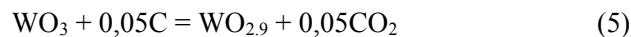
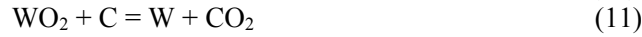
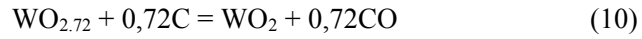


Figure 8. Equilibrium composition diagrams for reduction and carburizing treatment of  $WO_3$  at 1.0333 Pa in atmospheres of  $H_2$  (A), carbon (B), and  $CH_4$  (C) [73]

In the reactions of  $H_2$  reducing  $WO_3$ , it was reported [74] that before pure  $W$  is finally obtained, different tungsten oxides form during the reaction process, e.g., the blue tungsten oxide ( $WO_{2.9}$ ), the purple tungsten oxide ( $WO_{2.72}$ ) and tungsten dioxide ( $WO_2$ ), which were produced in a range from low to high temperatures. From the viewpoint of thermodynamics, a similar phenomenon may occur that several intermediate phases form in the solid–solid-state reactions of carbon reducing  $WO_3$ , with the reaction equations expressed as below:





The  $\Delta G$  values for the above reactions at the standard pressure at different temperatures can be calculated with Eq. (4) by applying the thermodynamic data that were provided in [42]. The changes of  $\Delta G$  with the temperature of the four tungsten oxides, i.e.,  $\text{WO}_3$ ,  $\text{WO}_{2.9}$ ,  $\text{WO}_{2.72}$  and  $\text{WO}_2$ , with the gas products of CO and  $\text{CO}_2$ , respectively, are shown in Fig. 9. As seen in Fig. 9 (a), for the reactions as described in Eqs. (5) and (6), when the temperatures are higher than 390 and 705 K, respectively, the  $\Delta G$  values for Eqs. (5) and (6) are both lower than zero, which means that the two reactions can take place according to the criterion of the reactions. When the temperature is lower than 970 K,  $\Delta G$  of Eq. (5) in which the gas product is  $\text{CO}_2$  is less than that of Eq. (6) in which the gas product is CO at the same temperature. It means that at different reaction temperatures the same reactants can have different reaction products. At temperatures higher than 970 K, the gas reaction product is CO instead of  $\text{CO}_2$  at lower temperatures. In Figure 9 (b), the  $\Delta G$  of the two reactions of carbon reducing  $\text{WO}_{2.9}$  as described in Eqs. (7) and (8) are lower than zero at the room temperature, thus the reactivity of  $\text{WO}_{2.9}$  reduction is very high, and the reactions can take place at low temperatures. The  $\Delta G$  of Eq. (7) is always lower than that of Eq. (8), hence the gas product of carbon reducing  $\text{WO}_{2.9}$  to  $\text{WO}_{2.72}$  is  $\text{CO}_2$  at above room temperature. Similar to Fig. 9 (a), 9 (c) shows that when the temperatures are higher than 905 and 940 K, respectively, the  $\Delta G$  of Eqs. (9) and (10) of carbon reducing  $\text{WO}_3$  are lower than zero, thus these reactions can occur correspondingly. As the temperature is lower than 970 K, at the same temperature, the  $\Delta G$  of Eq. (9) in which the gas product is  $\text{CO}_2$  is lower than that of Eq. (10) in which the gas product is CO. Therefore, at temperatures lower than 970 K the gas product should be  $\text{CO}_2$ , while at higher temperatures than 970 K the gas phase should be CO. Figure 9 (d) shows the initial temperatures for the reaction described in Eqs. (11) and (12), which are 1015 and 1055 K, respectively. It is noted that the two  $\Delta G$  curves intersect at 970 K, which corresponds to  $\Delta G > 0$ , implying that the gas product is only CO as carbon reduces  $\text{WO}_2$  [42].

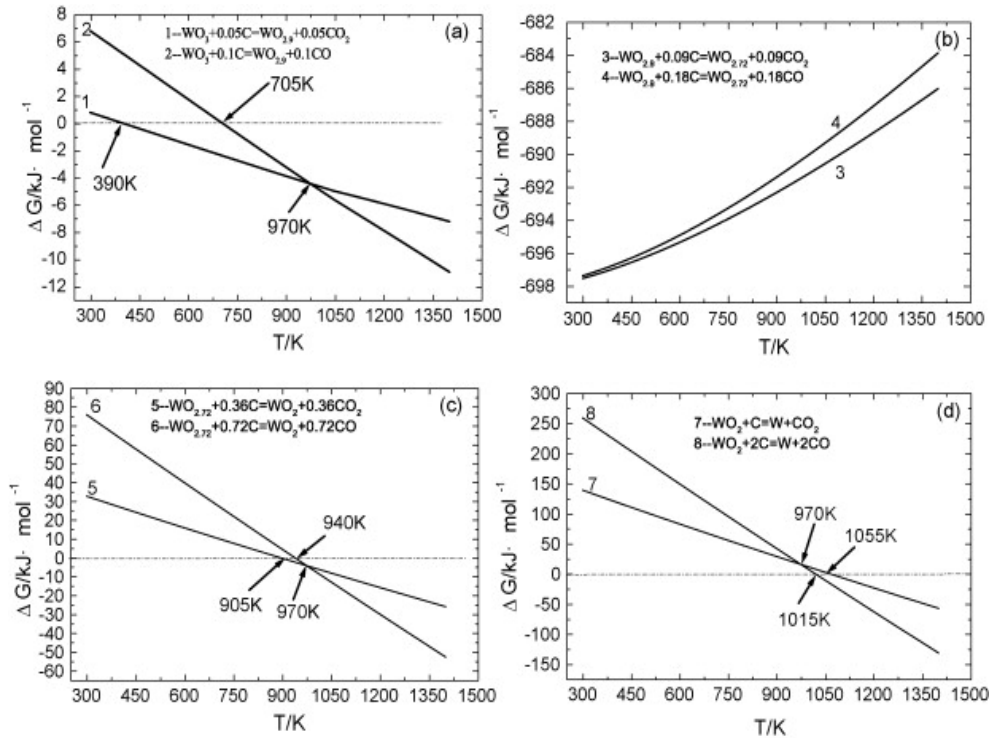


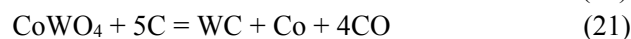
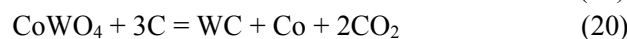
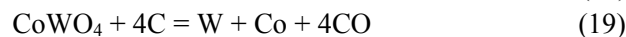
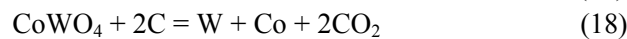
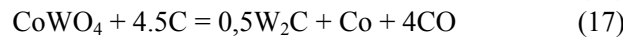
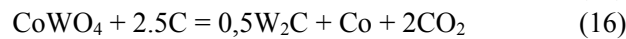
Figure 9. Changes of  $\Delta G$  with the temperature of four tungsten oxides of (a)  $WO_3$ , (b)  $WO_{2.9}$ , (c)  $WO_{2.72}$  and (d)  $WO_2$  when reacting with carbon [42]

In one word, the four kinds of tungsten oxides (i.e.,  $WO_3$ ,  $WO_{2.9}$ ,  $WO_{2.72}$  and  $WO_2$ ) can all be reduced by carbon above a certain temperature. The gas products of carbon reducing  $WO_3$  and  $WO_{2.72}$  can be two phases of CO and  $CO_2$ , which correspond to the lower and higher temperatures, respectively. Whereas, reaction of carbon reducing  $WO_{2.9}$  or  $WO_2$  has only one single gas product, which is  $CO_2$  or CO correspondingly. The sequence of the initial reaction temperature of the tungsten oxides is  $WO_{2.9}$ ,  $WO_3$ ,  $WO_{2.72}$  and  $WO_2$  from the low to the high temperatures.



*Thermodynamic analysis of intermediate product of cobalt tungstate CoWO<sub>4</sub>*

CoWO<sub>4</sub>, synthesized at low temperature, is an unstable compound since it can be decomposed at high temperature. The reactions of the synthesis and decomposition can be expressed as follows:



In Figure 10 are the corresponding  $\Delta G-T$  curves of the above reactions. Where, we can see that all the  $\Delta G$  values are lower than zero, implying that all the reactions can occur spontaneously. The  $\Delta G$  of Eq. (13) is the lowest and the gas product of the reaction is CO<sub>2</sub>. If CoO and WO<sub>3</sub> are reactants, they can be synthesized into CoWO<sub>4</sub> directly. The decomposition reactions occur at high temperature. The initial reaction temperature of Eq. (20) is 945 K, which is the lowest of the reaction temperatures, and the products are WC, Co and CO<sub>2</sub>. The initial reaction temperature of Eq. (18) is the highest, reaching 1050 K, and the products are W, Co and CO<sub>2</sub>. When the temperature exceeds 975 K, the  $\Delta G$  of Eq. (19) is the lowest and the reaction products are WC, Co and CO. Therefore, when CoWO<sub>4</sub> reacts with carbon, the gas product is CO<sub>2</sub> at low temperature and CO at high temperature. Solid products depend on the reaction temperature and the content of carbon. At the same temperature, with the decrease of the carbon content, the reaction product is WC, W<sub>2</sub>C or W.

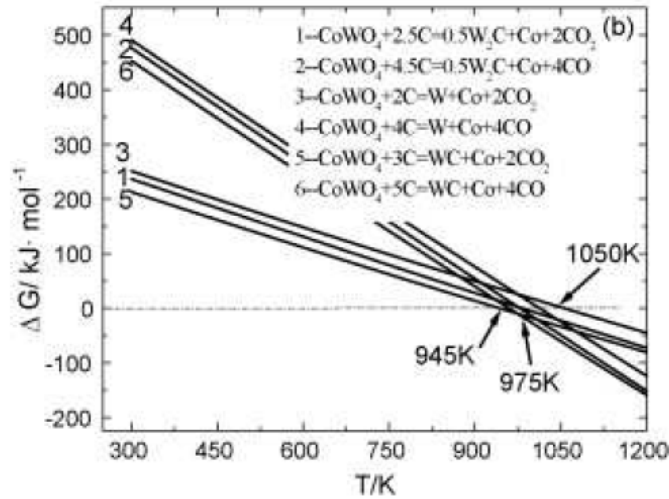


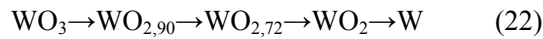
Figure 10. Changes of  $\Delta G$  with the temperature of  $\text{CoWO}_4$  decomposition [42]

#### 1.4.2 Reduction mechanism of $\text{WO}_3$ by hydrogen

Nowadays, the production of nano-sized WC powder became important for tool materials. The solution technique was developed to make nano-sized WC/Co particles from 60 to 300 nm in size [75]. The reduction and carburization process of mixed powders, tungsten oxide, cobalt oxide and graphite, in  $\text{H}_2$  gas became the production method of nano-sized WC-Co composite powder [76]. The process parameters were temperature, time, and gas species and flow rate of  $\text{H}_2$  in producing nano-sized WC-Co powders [77].

Oxidation-reduction process also can direct recycle heavy metal scrap to powder, which can re-enter the production of heavy metal alloys. Direct recycling is combined with minimum of energy consumption, chemical waste and lowest production costs. The hardmetal scrap can be completely oxidized at different temperatures if the temperature is above 850 °C. It is found that the oxide mainly consists of  $\text{WO}_3$  and  $(\text{Co},\text{Ni},\text{Fe})\text{WO}_4$  phases [78]. After reduction by hydrogen, the powder is comprised of single substance of W, Co, Ni and Fe. Fe and Co form a solid solution with metallic Ni [79]. In the reactions of  $\text{H}_2$  reducing  $\text{WO}_3$ , it was reported [74] that before pure W is finally obtained, different tungsten oxides form during the reaction process, e.g., the blue tungsten oxide ( $\text{WO}_{2.9}$ ), the purple tungsten oxide ( $\text{WO}_{2.72}$ ) and tungsten dioxide ( $\text{WO}_2$ ), which were produced in a range from low to high temperatures. The reduction mechanism is very complicated, which is determined by the interaction among

temperature, humidity, and kinetics of phase formation [79], the phase transition from  $\text{WO}_3$  to  $\text{W}$  is illustrated with Eq. (22).



Under equilibrium conditions reduction of tungsten from  $\text{WO}_3$  in hydrogen below  $900^\circ\text{C}$  occurs down to  $\text{WO}_2$  and at  $900^\circ\text{C}$  tungsten and tungstic acid  $\text{H}_2\text{WO}_4$  (Fig. 11) form. With an increase in temperature there is an increase in the thermodynamic probability of forming metal tungsten and  $\text{H}_2\text{WO}_4$ , and also there is a decrease in the partial pressure of hydrogen. Under thermodynamic equilibrium conditions it is not possible to obtain pure tungsten [73].

For complete occurrence of the reduction reaction an increase is suggested for increasing the hydrogen partial pressure in accordance with the calculated amount of reducing agent [80].

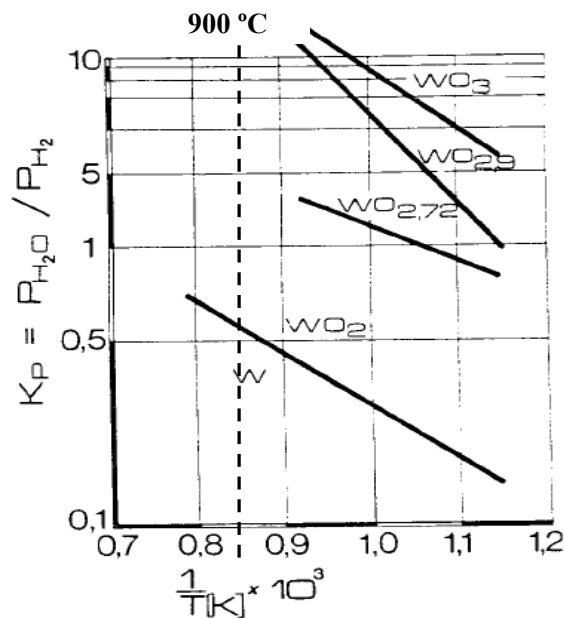


Figure 11. Reduction of tungsten oxides by hydrogen, variation of the equilibrium with temperature [2]

In the reduction process by hydrogen at elevated temperature, it will present water vapor. Thus a volatile oxide hydrate  $[\text{WO}_2(\text{OH})_2]$  was formed by the water vapor and  $\text{WO}_3$ . The flowing hydrogen took away small amounts of oxide hydrate, leading to the

loss of tungsten. On the other hand, it is responsible for chemical water vapor transport of tungsten, which occurs throughout the reduction sequence, and which decisively codetermines the physical, chemical properties and surface of powder particle of the reduced alloy powder [81].

The surface shape of the reduced powder particles is irregular and complicated at high temperature. As the reduction temperature increases, the powder particle becomes larger and the whiskers become more and thicker directionally growth, resulting in more complicated surface shape of the powder particle. Decreasing the temperature of reduction can produce fine and regular alloy powder particle.

### **1.4.3 Reduction and carburization with hydrocarbons**

Reduction and carburizing treatment of tungsten-containing oxides in an atmosphere of thermally destroyed high-molecular hydrocarbons with or without addition of carbon black makes it possible to obtain a four- or five component system W (or Co-W) - C - H - O. Thermodynamically formation of tungsten carbide with reduction and carburizing treatment of  $WO_3$  in a methane atmosphere is possible at 500 °C (Fig. 8 C). In this case  $WO_{2,9}$  and WC form and 7% of free carbon is present. According to data [80] in contrast to reduction and carburizing treatment with solid carbon, in methane formation of pure WC is thermodynamically impossible under equilibrium conditions.

With reduction and carburizing treatment in atmosphere of thermally destroyed high-molecular hydrocarbons taking account of the thermodynamic properties it is possible to avoid on one hand burn-up of carbon from the reducing mixture, which is typical for the process carried out in an atmosphere of hydrogen continuously fed into the reaction zone, and on the other hand deposition of additional carbon, which was observed with reduction and carburizing treatment in a flow of methane-hydrogen mixture with deviation of the composition from equilibrium [80]. Data about the complete occurrence of the carburizing reaction in a mixture of  $CoWO_4+WO_3$  only in the presence of solid carbon agrees with data in [82]. With no carbon black in the mixture the reduction and carburizing treatment in a similar temperature-time regime occurs with formation of intermediate carbide  $Co_3W_3C$  [73].

Takatsu and Bandarenko [27, 83] studied the carburization of WC-Co mixed powder by  $CH_4$  in rotary kiln. According to him, a continuous production of WC-Co mixed powder can be done by serial connection of three rotary kilns. Of these three kilns, the first one was used for reduction, whereas second and third were used for carburization and additional carburization respectively. Under optimum carburization conditions, the carbon content of the obtained powder could be adjusted to the theoretical carbon content of WC within 0,2%. As the reduction and carburization temperatures were low, WC powders in the submicron range could be produced by

direct carburization of WC-Co mixed powder without any grain growth problem as that which occurs in the conventional carburization of fine tungsten powder .

#### **1.4.4 Reduction and carburization in inert gas atmosphere**

Miyake [84] discovered that tungsten carbide can be produced directly from  $WO_3$  by heating the mixture of  $WO_3$  powder and carbon in nitrogen atmosphere. Here the problem imposed by water vapor does not arise as the reduction of  $WO_3$  takes place by carbon, but tungsten carbide having theoretical carbon content is difficult to get, unless hydrogen does participate in the carburization reaction [84]. The authors suggest that this problem can also be solved by two step reaction: heating the mixture at a temperature higher than  $1000\text{ }^\circ\text{C}$  in nitrogen atmosphere, and then heating at a temperature of higher than  $1400\text{ }^\circ\text{C}$  in hydrogen atmosphere, thereby forming tungsten carbide directly from the corresponding oxide.

The tests made by Gil-Geun Lee proved, that WC-8wt.%Co hardmetal was completely transformed into the oxide state within oxidation time of 24 hours by the oxidation at  $800\text{ }^\circ\text{C}$  in air without regard to shape and dimensions [56].

The total amount of the solid carbon was based on the formation of WC-8wt.%Co with stoichiometric composition by the reduction and carburization reactions. The powder mixture showed a remarkable decrease in the weight fraction-temperature diagram for the carbothermal reduction suggests a significant carbothermal reaction occurs at this temperature. The synthesized WC-Co composite powder at  $1100\text{ }^\circ\text{C}$  for 30 minutes from WC-8wt.% Co hardmetal has an average particle size on  $0,5\mu\text{m}$  [56]. Ho-Soon Im [85] found that  $WO_3$  and  $Co_3O_4$  mixed with carbon black, can be reduced and carburized at  $900\text{-}980\text{ }^\circ\text{C}$  for 3 hours flowing Ar gas in tube furnace. The content of free carbon in WC/Co mixed powders decreased as the reaction temperature increased. It was also seen that carbon content of sample was reduced about 2-3 wt.% after dry ball-milling, it seems that carbon consumed to reduce the oxide powders during dry milling.

Dean S. Venables [86] report that at higher temperatures  $CO_2$  will react more rapidly with graphite, resulting in a higher ratio of CO to  $CO_2$ . The flow rates of inert gas affects the concentration of gaseous species in the system, which may in turn influence the reaction rate. D.S. Venables [86] report that the mass loss curve (Fig. 12) show that decreasing the flow rate results in a large increase in the mass lost during the reaction.

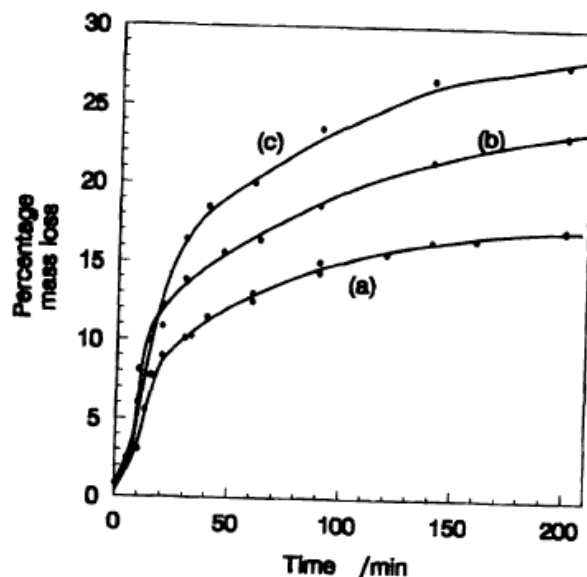


Figure 12. Mass loss curves of mixtures of  $WO_3$  and graphite in a 1:4 mole ratio at  $985^\circ C$  and at flowrates of (a) 100 and (b) 50 and (c) 25 ml/min. [86]

The increased mass loss at lower flow rates proves that the reaction is not predominantly a solid-solid reaction. As has been found for the reduction of other metal oxides with carbon, the reduction almost certainly proceeds via reaction with CO formed in reaction. The final mass loss is also significantly higher at low flowrates, which means that more CO is formed at lower flow rates forming a more reducing atmosphere [86].

#### 1.4.5 The effect of Co content to the carburization

Cobalt has an activating effect in a number of cases on carburizing treatment of the chemical mixture of tungsten oxides and cobalt  $CoWO_4+WO_3$ . This is observed in the case of appearance of cobalt in the system not bound into intermetallic [87, 88]. Cobalt accelerates the methane decomposition reaction as a result of which there is an increase in carbon concentration at the surface of carbide phases. Also, cobalt accelerates carbon diffusion and promotes transportation of it to reaction zone at the tungsten interface with tungsten oxides (tungsten carbide) since the diffusion coefficient for carbon in cobalt is greater by four orders of magnitude than in the WC phase. At the same time it has been shown that with formation of intermetallic  $Co_7W_6$  and  $Co_3W$  the degree of carburizing falls sharply. The rate of carburizing, as was established in [82], increases in the presence of 7% cobalt and decreases with a higher content of it.

Several workers [83, 89] have found that carburization of tungsten around 900 °C is possible in the presence of cobalt due to the catalytic effect. Ushijima [89] reported that  $WO_3$  can be carburized in hydrogen at about 900 °C in the presence of  $Co_3O_4$ . The starting material was a ball milled mixture of  $WO_3$ ,  $Co_3O_4$ , and carbon black. The mixture was heated in carbon boats in hydrogen atmosphere at 800 °C for the reduction of oxides. After reduction was completed, the temperature was raised to 900–950 °C for carburization. The obtained WC-Co mixed powder was ball milled and the conventional method was followed for the production of hardmetals. The carbon black content of WC-Co mixed powder, however, was scattered in a wide range due to the fluctuation in carburizing conditions such as temperature, concentration of carburizing gas, and contact between powder and gas, etc. An additional carburizing treatment was necessary to control content within 0,1–0,2 % and make it suitable as a raw material for hardmetals production.

## **1.5 Conclusion to the chapter and aims of the study**

In the previous sections of first chapter the overview of conventional methods for hardmetal recycling and production were given. The conventional hardmetal recycling methods have many problems to be solved and there are not always established technologies. For example, chemical modification method requires comparatively large-scale equipment and it takes relatively long reaction time. The recycling by thermal modification process usually undergoes the decomposition of WC and it leads to the formation of  $\eta$ -phase, which degrades the mechanical properties. Zinc melt and cold stream processes have problems with contamination by undesirable elements. Therefore there is a need to develop more economical and high-quality recycling procedure. One of the alternative recycling method can be oxidation-reduction method, where the oxide mixture is reduced by the hydrogen or graphite.

Reactive sintering is modern technology for the ultra fine and nanoscale hardmetal manufacturing. Reactive sintering technology is cost effective way for the hardmetal production and can be utilized as the alternative to the conventional WC+Co powder mixtures, which are conventional raw material for hardmetal production. Theoretically the combination of reduction with reactive sintering is possible

As seen in the literature review there has been many trials to produce WC-Co powder from oxide mixture by reduction and carburization in different atmospheres, but from the practical point of view it would be more economical to produce hardmetal parts directly from the oxide mixture. The novelty of proposed technology is combination of carbothermal reduction, carburization and reactive sintering in one sintering route.

The aims of the present work are:

1. to develop a novel method for WC-Co recycling by oxidation-reduction and reactive sintering method;
2. to study the influence of different amounts of carbon addition to the phase formation, microstructure and mechanical properties of WC-Co manufactured by reactive sintering method;
3. to study the influence of technological factors on the microstructure and mechanical properties of recycled and reactive-sintered WC-Co;
4. to study phase formation and microstructure evolution during sintering;
5. to determine the basic technological parameters of the novel recycling technology: milling parameters, compaction pressure and sintering route.



## 2. Experimental procedures. Investigated materials and test methods

### 2.1 Technological parameters of studied hardmetal production methods

#### 2.1.1 Reactive sintering process

For producing the hardmetals via reactive sintering (Fig. 13 ) the elemental powders of tungsten , cobalt and graphite (carbon black) were mild in a high-energy ball-mill (attritor).

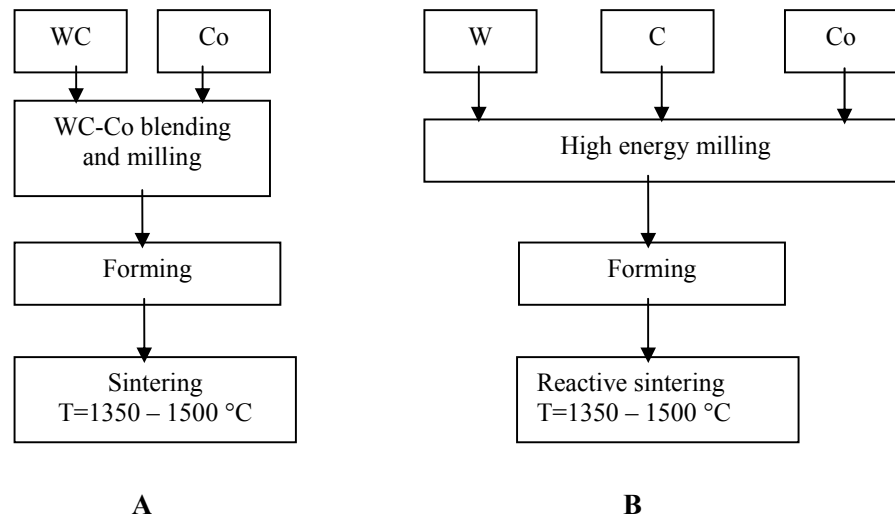


Figure 13. WC-Co manufacturing routes: (A) conventional technology, (B) reactive sintering

Five types of powder mixtures were investigated with the same binder content, but different graphite content. The mixtures of elemental powders of nominal composition of WC-Co were prepared using 99,5% pure tungsten (Sylvania Tungsten ) with the particle size of 1–3  $\mu\text{m}$ , carbon black KS6 (TIMCAL Ltd) and cobalt powder with the particle size below 10  $\mu\text{m}$ . The amount of carbon black was varied from 1 to 1,2 times of stoichiometric content in order to reduce the oxides and avoid the decarbidization of tungsten carbide.

In order to determine the milling time and ball-to-material weight ratio the experimental tests were carried out. The specific surface area of W, Co and carbon

black mixture powder was measured after 2, 4, 8, 12 and 16 milling hours and without milling. The average particle size of the powders was calculated from the specific surface area measured with the BET method (sorbometer Kelvin 1040). The particle size was calculated according to Eq. (23):

$$D = (6/\gamma) / S \quad (23)$$

where,  $\gamma$  - density,  $\text{g/cm}^3$ ;  
 $S$  - specific surface area,  $\text{m}^2/\text{g}$ .

Test results are given in Fig. 14 A and B. It was seen that rapid increase of specific surface takes place during first 2 hours of milling. As seen in Fig. 14 the influence of attritor blades rotation speed is small but the ball-to-material weight ratio (B:M) has significant role in milling procedure.

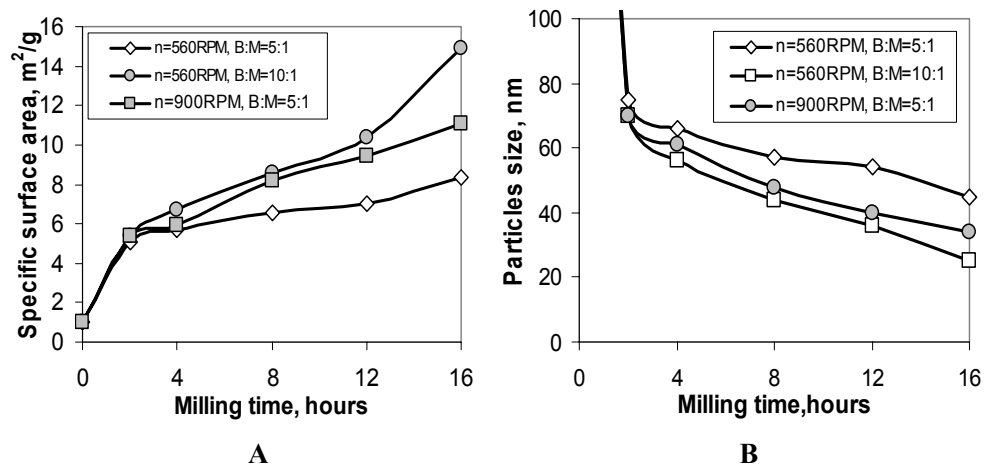


Figure 14. Changes in specific surface (A) and particle size (B) during the milling procedure in attritor

It can be seen that using high energy milling it is possible to manufacture nanoscale powders with particle size ca. 45 nm. During the carburizing and sintering tests it was seen that milling time 8 hours and B:M ratio 5:1 is sufficient to produce WC-Co sintered material by reactive sintering method.

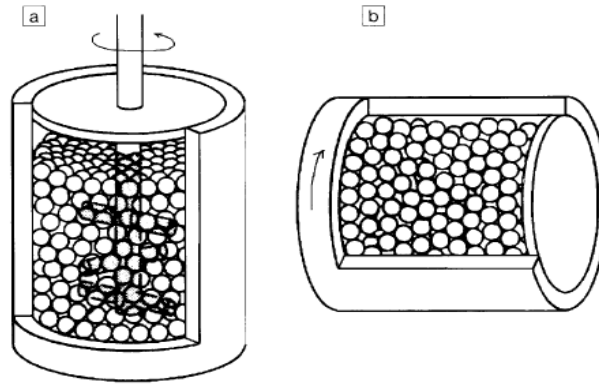


Figure 15. Vertical attritor (a) and ball-mill (b) [90]

In this work the milling of Co, W and graphite powders with different W:C mole ratios were carried out in an attritor mill (Fig. 15 A) for 8 hours. The milling speed was set at 560 1/min. The mixture of the starting powders was placed in the vial (1 l) with the ball-to-powder weight ratio of 5:1. The initial carbon black concentration in the W powder mixture was from 6,12 up to 9,1 wt%. Graphite was added over a stoichiometric to compensate the decarburization during debinding and sintering. In order to minimize any possibility of contamination, the vial, impellers and milling balls were made from WC-Co cemented carbides.

The vial was cooled with water circulation throughout the process. Paraffin wax (3%) solution in kerosene was added into the powder to protect the powder from oxidation. After milling the powders were dried at 40 °C in the air and palletized into small spherical shape with about 200  $\mu\text{m}$  diameter. The mechanically activated W, Co and graphite mixture was compacted to 28 $\times$ 18 $\times$ 6 mm green parts by uniaxial pressing at 80 MPa. The green compacts were directly sintered at different temperatures and times (depending on their binder content) in a graphite-heated furnace in a vacuum better than  $10^{-4}$  Bar.

### 2.1.2. Carbothermal reduction process

WC-Co hardmetal scrap was used as raw material. The scrap parts were manufactured from Boart Longyear G30 hardmetal powder by the conventional hardmetal production method. Hardmetal scrap with 6, 13 and 15 wt.% Co binder phase content was used. The WC-Co scrap was washed ultrasonically with distilled water. The technological scheme of hardmetal production process from scrap is shown in Fig.16.

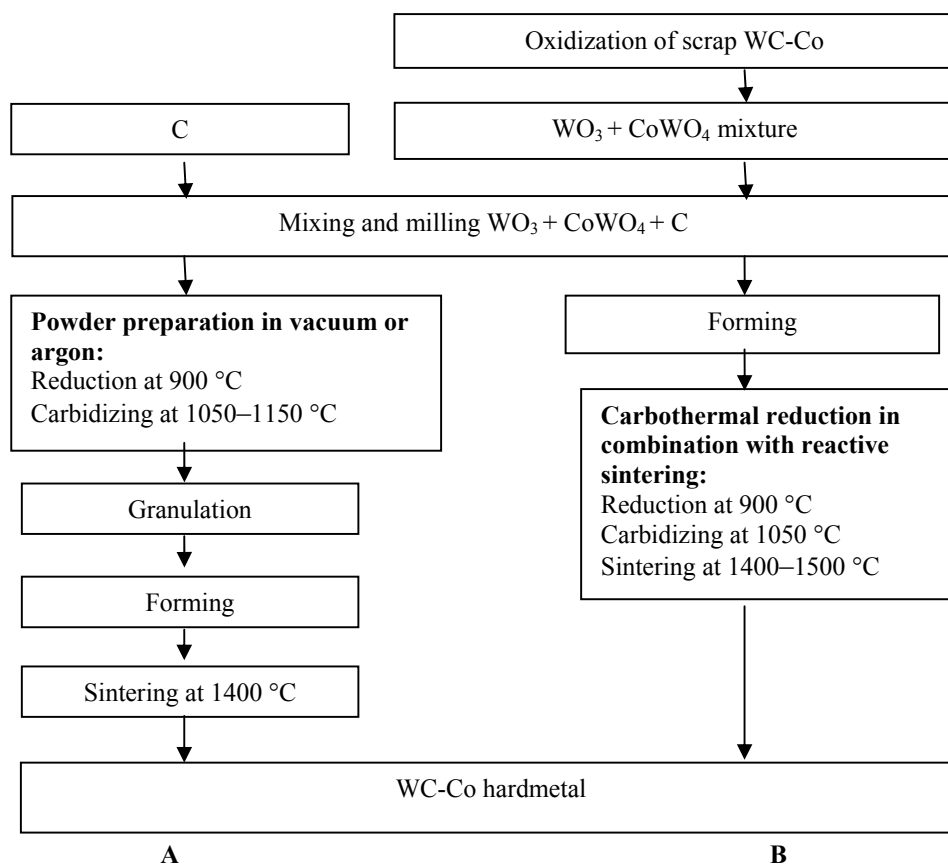


Figure 16. Producing routes of WC-Co by carbothermal reduction and sintering (A) conventional carbothermal reduction method, and (B) developed novel method

The WC-Co scrap was oxidized in a rotary kiln at 850 °C in a flowing stream of air. During oxidation the surfaces of the specimens developed a green-blue-yellow oxide coating, and many microcracks formed. As the tube inside the furnace rotated, the soft oxide layer was removed from the surfaces of the WC-Co specimens. Two oxide phases of  $\text{CoWO}_4$  and  $\text{WO}_3$  had formed during oxidation. The oxide of the WC-15 wt.% Co hardmetal had low strength due to its sponge-like microstructure and the presence of microcracks.

Fifteen types of hardmetals were investigated with the same chemical composition but different graphite content, milling procedures, plasticizer content and green density. Material notation and compositions are given in Tables 5. Milling and mixing were carried out in both an attritor (high energy milling) and ball mill (Fig. 15 A and B). The powders were mixed for 72 hours using a ball mill with WC-Co balls and pure ethanol as the liquid medium. The ball-to-powder weight ratio was 5:1, and the rotation rate of the mill was 60 1/min.

In the attritor the powders were mixed for 6 hours, using pure ethanol as the liquid medium. In order to minimize any possibility of contamination, the vial, impellers and milling balls were made from WC-Co hardmetals. The starting powder mixture was placed in the vial (1 l) with a ball-to-powder weight ratio of 5:1. The vial was cooled with water circulation throughout the process. The milling speed was set at 560 1/m. Paraffin wax solution in kerosene as a plasticizer was added into the some powder mixtures to improve the compacting properties.

#### **2.1.2.1 The preparation of powder and green parts from mixture of oxides and graphite**

The specific surface area (SSA) of oxide powder after milling in attritor and ball-mill were investigated. Results, compared those with the W-Co-C powders, are given in Table 2. As seen from the results, the oxide powder particle size decreased less during long time ball-milling then during high energy milling in attritor. It was seen that for the oxide mixtures nanoscale powder can be produced using high energy milling in attritor. Compared with W, Co and C elemental powders, the longer milling period is needed for the oxide mixtures. After mixing with additional carbon and milling, the powders were air-dried at 40 °C and palletized into small spheres about 200  $\mu\text{m}$  in diameter. The mechanically activated  $\text{WO}_3$ ,  $\text{CoWO}_4$  and C mixtures were compacted into 6×6×40 mm blocks and 12×12 cylinders by uniaxial pressing at 50, 80 and 100 MPa.

Table 2. Powder preparation and specific surface area

Powder type	Milling method	Milling time [hour]	Specific Surface Area [m <sup>2</sup> /g]	Particle size [nm]
WO <sub>3</sub> +CoWO <sub>4</sub> +C	Ball-Mill	72	7,58	149
WO <sub>3</sub> +CoWO <sub>4</sub> +C	Attritor	6	11,06	102
WO <sub>3</sub> +CoWO <sub>4</sub> +C	Attritor	12	12,66	89
W+Co+C	Attritor	0	1,02	370
W+Co+C	Attritor	2	5,06	75
W+Co+C	Attritor	4	5,72	66
W+Co+C	Attritor	8	6,58	57
W+Co+C	Attritor	12	7,02	54
W+Co+C	Attritor	16	8,36	45

In order to investigate the influence of plasticizer to the compatibility of the powders and to the properties of sintered material, mixtures with 0, 1, 2 and 3 wt.% of paraffin wax were produced, with the carbon addition 16,8 wt.%.

The green compacts were directly sintered at different temperatures for 0,5 hour in a graphite-heated furnace in a vacuum better than 10<sup>-4</sup> Bar. Interrupted sintering experiments were performed in the Sinter/HIP furnace.

### 2.1.2.2 Reduction and sintering process

Sinter/HIP sintering and vacuum sintering procedures were done in semi-industrial FPW-300/400-2-1600-100KS/SP Sinter/HIP furnace.

During the manufacturing of tested materials, no extra pre-sintering procedure was done. Pre-sintering and plasticizer out burn was done in same cycle with following sintering process at 450 °C, holding period 15 min. The vacuum level during the sintering was 10<sup>-4</sup> Bar. The parameters of finish-sintering varied in the range of temperatures 1390–1500 °C and in argon-gas compression 30 Bar.

An example schematic for sintering technology for conventional materials and carbothermal reduction is shown in Fig. 17. The first step (1 in Fig. 17) in sintering route is for the out burn of plasticizer (paraffin wax) at 450 °C for 15 min. The first step is the same for all three sintering technologies. Step 2 in carbothermal reduction route is needed for the reduction of oxides by carbon.

The reduction takes place at 900 °C and lasts 1-2 hours depending on the mass of oxide powder. Next step in (3 in Fig. 17) carbothermal reduction route is carburization which takes place at 1050 °C for 1–2 hours. The reduction and carburization thermodynamic, temperatures and results are analyzed in the first chapter of thesis.

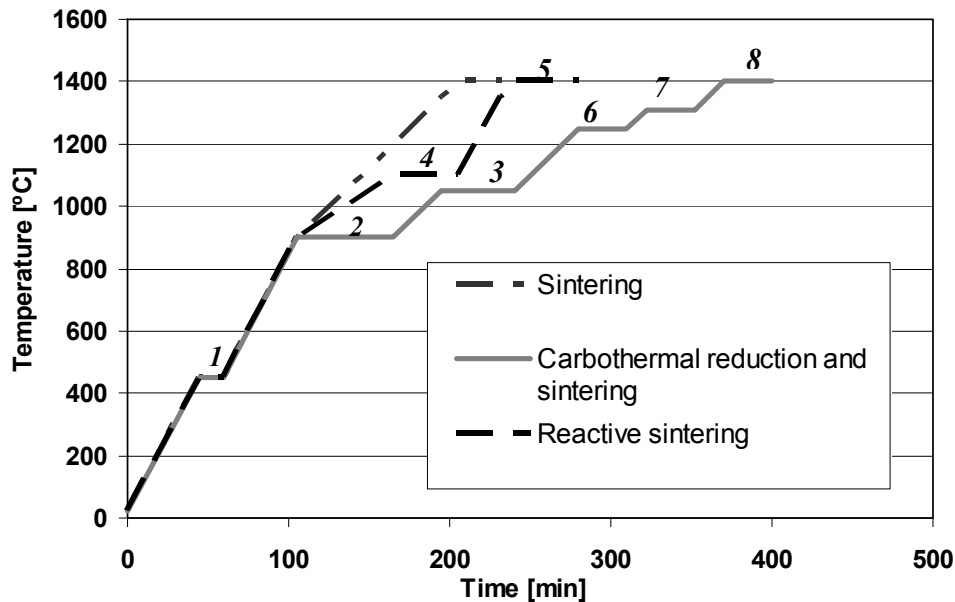


Figure 17. Schematic of Sinter/HIP sintering cycle for conventional route, reactive sintering and for materials produced via carbothermal reduction and reactive sintering

It was seen that 1050 °C is optimal temperature for the *in situ* carburization of tungsten. Step 4 is carburization in reactive sintering route, where the reaction between W and solid C takes place at ca 1100 °C. The presence of Co and previous mechanical activation during the milling play an important role in decreasing the carburization temperature. Several authors [42, 70, 71] have found that lower atmosphere pressure reduces the carburization temperature and is beneficial for full carburization during the shorter period of time. Steps 6 and 7 during the carbothermal reduction and reactive sintering process are shortstops before and after the liquid phase formation. The aim of those steps is to reduce the porosity which could appear if there is gas emission during the liquid phase sintering. Steps 5 and 8 are final sintering at 1400 °C for 30 min. The final sintering time was the same for conventional hardmetals and hardmetals produced by novel technology.

## 2.2 Materials tested

All materials described in this chapter were produced in the powder metallurgy laboratory of Tallinn University of Technology. The hardmetals were chosen for comparing the materials produced by conventional methods with materials produced by reactive sintering or carbothermal reduction method.

The composition and main production characteristics of investigated materials are provided in Tables 3–5. The microstructure evolution, grain size, mechanical properties and production parameters are given and were analyzed.

*Table 3. Tested conventional materials*

<b>Material notation</b>	<b>Binder content [wt.%]</b>	<b>Grain size [μm]</b>	<b>Density [g/cm<sup>3</sup>]</b>	<b>TRS [MPa]</b>	<b>Hardness HV10</b>
S13*	13	1-3	14,23	3250	1210
G30*	15	2,5	14,04	2400	1200
VK6	6	3-5	15,00	1370	1500
VK8	8	3-5	14,6	1700	1400
VK11	11	3-5	14,2	1900	1340
VK15	15	3-5	14,0	2100	1200
VK20	20	3-5	13,6	2500	920

\* data based on the Ref. [1]



Table 4 . Composition and mechanical properties of hardmetals produced by reactive sintering

Material notation	Binder content [wt. %]	Amount of graphite [wt. %]	Powder preparation method	Plasticizer [wt.%]	Additives [wt.%]
V1	15	6,12	Attritor	3 (Wax)	0
V16	15	6,65	Attritor	3 (Wax)	0
V24	15	7,12	Attritor	3 (Wax)	0
V17	15	7,70	Attritor	3 (Wax)	0
V5	15	9,10	Attritor	3 (Wax)	0
V6	6	7,12	Attritor	3 (Wax)	0
V8	8	7,12	Attritor	3 (Wax)	0
V11	11	7,12	Attritor	3 (Wax)	0
V24	15	7,12	Attritor	3 (Wax)	0
V20	20	7,12	Attritor	3 (Wax)	0
V41	15	7,12	Attritor	3 (Wax)	0,8 VC
V42	15	7,12	Attritor	3 (Wax)	0,8 Cr <sub>3</sub> C <sub>2</sub>
V43	15	7,12	Attritor	3 (Wax)	0,6 VC 0,2 Cr <sub>3</sub> C <sub>2</sub>
<b>Mechanical properties of hardmetals produced with 7,70 wt.% of graphite addition and 6–20 wt.% of Co</b>					
Material notation	Co [wt.%]	Density [g/cm <sup>3</sup> ]	Hardness HV10	TRS [MPa]	
V6	6	15	1740	1280	
V8	8	14,7	1700	1550	
V11	11	14,4	1520	1840	
V24	15	14,0	1380	2300	
V20	20	13,8	1145	2890	

*Table 5. Nominal composition and preparation method of WC-15 wt.% Co alloys produced by oxidation-reduction method.*

<b>Material notation</b>	<b>Amount of graphite [wt.%]</b>	<b>Powder milling method</b>	<b>Plasticizer [wt.%]</b>	<b>Pressure [MPa]</b>	<b>Green density [g/cm<sup>3</sup>]</b>
R16B	16,0 wt. % C	Ball mill	0	80	3,25
R16,5B	16,5 wt. % C	Ball mill	0	80	3,25
R16,8B	16,8 wt. % C	Ball mill	0	80	3,25
R17,0B	17,0 wt. % C	Ball mill	0	80	3,25
R16A	16,0 wt. % C	Attritor	0	80	3,25
R16,5A	16,5 wt. % C	Attritor	0	80	3,25
R17,0A	17,0 wt. % C	Attritor	0	80	3,25
R16,8A	16,8 wt. % C	Attritor	0	80	3,6
R16,8A-P	16,8 wt. % C	Attritor	0	50	3,1
R16,8A-T	16,8 wt. % C	Attritor	0	120	3,8
R16,8A-W1	16,8 wt. % C	Attritor	1	80	3,8
R16,8A-W1-P	16,8 wt. % C	Attritor	1	50	3,3
R16,8A-W1-T	16,8 wt. % C	Attritor	1	120	4,0
R16,8A-W2	16,8 wt. % C	Attritor	2	80	3,8
R16,8A-W3	16,8 wt. % C	Attritor	3	80	3,8

## **2.3 Property and wear testing methods**

### **2.3.1 Methods for microstructure and property testing**

The microstructure was investigated by SEM (JEOL JSM 840A) after various stages of sintering. Phase identification was carried out using X-ray diffraction (XRD) methods with CuK $\alpha$  radiation (Bruker AXS D5005). The size of the crystallites was determined by XRD peak broadening using Scherrer formula.

Sample length was measured with a precision of 0,01 mm before and after sintering. Relative density was calculated from green relative density and linear

shrinkage assuming isotropic densification. Shrinkage was determined from recorded changes in sample dimensions during heating at different temperatures. The hardness of the samples was measured using a Vickers pyramid indenter. Measurements were made under a load of 98 N using a load time of 30 s. An average hardness value was determined based on 5 indentations.

Transverse rupture strength was determined in accordance with the ASTM Standard B406-95 using device "Instron" (specimens grinded beforehand) [91]. Each test point indicates the average value of 5 measurement results.

The microstructure and mechanical properties of the recycled WC-Co materials were compared with those of the original conventional Boart Longyear G 30 and S13 hardmetal.

### 2.3.2 Erosive wear testing method

Erosion resistance of hardmetal was determined by centrifugal acceleration of abrasive particles with the help of CAK-3m, in accordance with standard methods [92]. The illustration of device operation scheme is provided on Fig. 18.

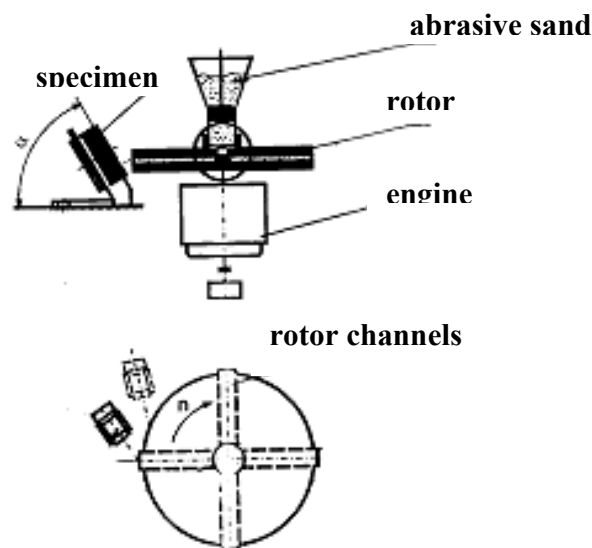


Figure 18. Principal scheme of abrasive-erosion tester

The test specimens with dimensions 23x14x5 mm were grinded, cleaned and weighed. Erosion rate was determined using 0,1 to 0,3 mm quartz sand stream. The specimen was weighed before and after testing, and the erosion rate was determined in volumetric loss per mass of used abrasive sand ( $\text{mm}^3/\text{kg}$ ) based on weighing results.

### 2.3.3 Abrasive wear test methods

Three-body abrasion tests were carried out using a block-on-ring tester (Fig. 19). Tests were performed in accordance with material testing standard ASTM B611-85. The mixture of 1500 g of abrasive particles ( $\text{SiO}_2$ , particle size 0,1 to 0,3 mm) and 0,94 l of distilled water was used as an abrasive medium. The blocks were pressed against steel disk ( $d=178$  mm) with normal load ( $F_n=40$  N) and constant sliding speed ( $2,2 \text{ m s}^{-1}$ ).

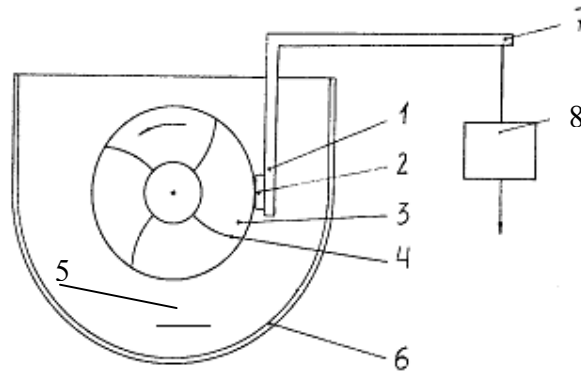


Figure 19. Block-on-ring tribometer. Sliding and abrasive wear testing scheme: 1-arm, 2-specimen, 3-rotating disk, 4-impeller, 5-slurry, 6-chamber, 7-arm, 8-weight

Carbon steel (0,45 wt.% C) with hardness 200 HB was chosen for counter body as a typical material for shafts and other machinery parts, working in sliding pairs with hardmetals. Specimen is pushed against carbon steel wheel rotating on a horizontal axis. Distilled water and abrasive particles ( $\text{SiO}_2$ ) are poured in chamber. Particles suspended in the liquid are drawn into gap between the specimen and the steel wheel. Sliding distance was set at 4 km run. The specimens were employed as the blocks with dimensions 22 mm x 12 mm x 5 mm. The surface roughness of both WC-Co specimens and steel ring were prepared under  $R_z \approx 1,0 \mu\text{m}$ .

Wear loss of the hardmetal blocks was obtained by weighting the block before and after the sliding using digital balance with a scale 0,1 mg. Since the wear of materials generally fluctuates, the sliding test was repeated at least four times under the same conditions.

### 3. Reactive sintering: development of method for hardmetal production from W, Co and C powders

#### 3.1 Changes in phase composition during reactive sintering process

Figure 20 shows the XRD patterns of W -15wt.% Co -9,1wt.% C powder mixture no milled, high energy ball milled for 8 hours, and heated at 800, 1000 and 1400 °C temperatures. W phase is only observed for high energy ball milling and the intensity of the W peak decreases with continued high energy ball milling due to W particle refining and accumulation of the strain energy by mechanical input energy. This explains the disappearance of the C and Co peaks, which is attributed to the mechanical input energy. Cobalt either distributes around the peripheral layer of W grains or dissolves into hard W phase. Therefore, the peak of Co is variable non-monotonically. Mi [93] have attributed the absence of the C Bragg peaks in their milled powders of W and C to the low scattering factor of C or to the amorphization.

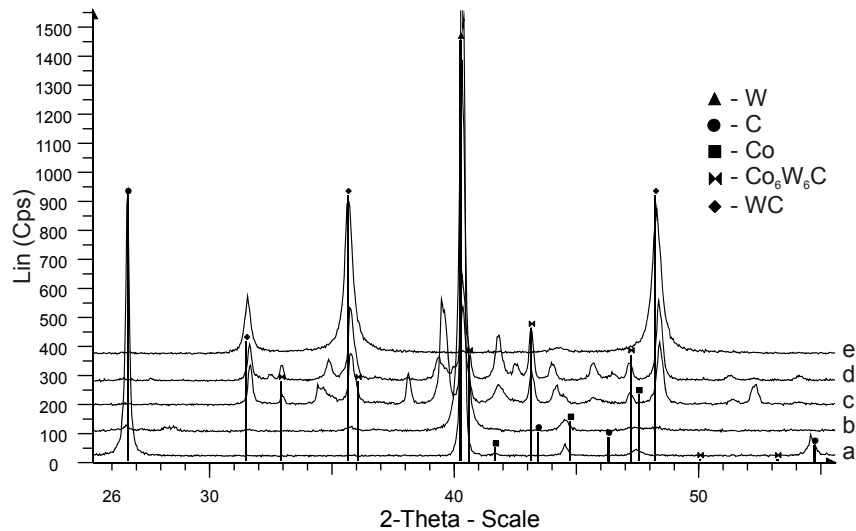


Figure 20. XRD patterns of W-C-Co no milled (a) and milled for 8 h (b) powder mixtures and the alloys sintered at 800 (c), 1000 (d) and 1400 °C (e)

W phase disappeared and W<sub>2</sub>C and Co<sub>6</sub>W<sub>6</sub>C intermediate carbides were formed at 800 °C, where Co<sub>6</sub>W<sub>6</sub>C carbide is dominating. WC is formed at 1000 °C. The tungsten phase disappeared gradually, the tungsten carbide was formed and its content increased

slowly. Small amount of ditungsten carbide ( $W_2C$ ) was formed at 1000 °C as indicated in the XRD pattern. Typically, direct carburization of W and C is carried out at higher temperature (~1400 °C), evidently the nanocrystalline W-Co-C is carburized at lower temperatures - about at 1000 °C. Cobalt acts also as a catalyst for the carburizing reaction. That is,  $Co_6W_6C$  forms at first in the carburizing initial step, later this  $Co_6W_6C$  combines with C and then decomposes to WC and Co. The decomposed Co then diffuses into  $W_2C$  and W again to form intermediate carbide ( $Co_6W_6C$ ). At 1400 °C, WC and Co are only observed without intermediate phase.

SEM micrographs of the samples sintered at different temperatures and time are presented in Fig. 21. The microstructure evolution of W-7,7C-15Co alloy sintered at different times in temperature range of 1250 °C to 1400 °C is observed. At the temperature of 1250 °C, the faceted WC grains were mixed, even no Co liquid phase was formed (Fig. 21 A). With the increase of the temperature, the average size of the aggregates grows. Up to 1250 °C, the aggregated particles develop a multi-faceted surface morphology that has the characteristics of layered structure of crystal platelets, suggesting a preferred orientation attachment of particles during aggregation. The results indicate that liquid phase sintering begins not below 1330 °C: some of the grains remain rounded, as in the starting powder (Fig. 21 B). The porosity of the sample is high. At 1330 °C, some WC grains have grown rapidly and transformed to triangular prism with truncated corners. These results confirm the results of [94], that the overall evolution of the original nanosized particles and the grain structure seems to occur via two processes: 1) the aggregation of the nanosized particles and 2) the transformation of aggregates to a single crystal.

The most active grain growth occurs at about 1380 °C: the micrograph in Fig. 21 C shows tungsten carbide grains, characteristic to the conventional WC-Co compositions. Similar, but less uniform microstructure was observed in samples sintered at 1400 °C during 30, 150 and 300 min (Fig. 21 D, E, F). As the sintering time was increased from 30 to 300 min the mean grain size increased from 0,69 to 1,44  $\mu m$ . As would be expected, the rate of grain growth increases rapidly with increasing sintering temperature. At a constant temperature the grain growth continues, but quite slowly. Grain growth during sintering is dependent upon relatively small changes in the graphite content, evidently because that factor can markedly alter the characteristics of the liquid phase. A high carbon content results in more rapid grain growth.

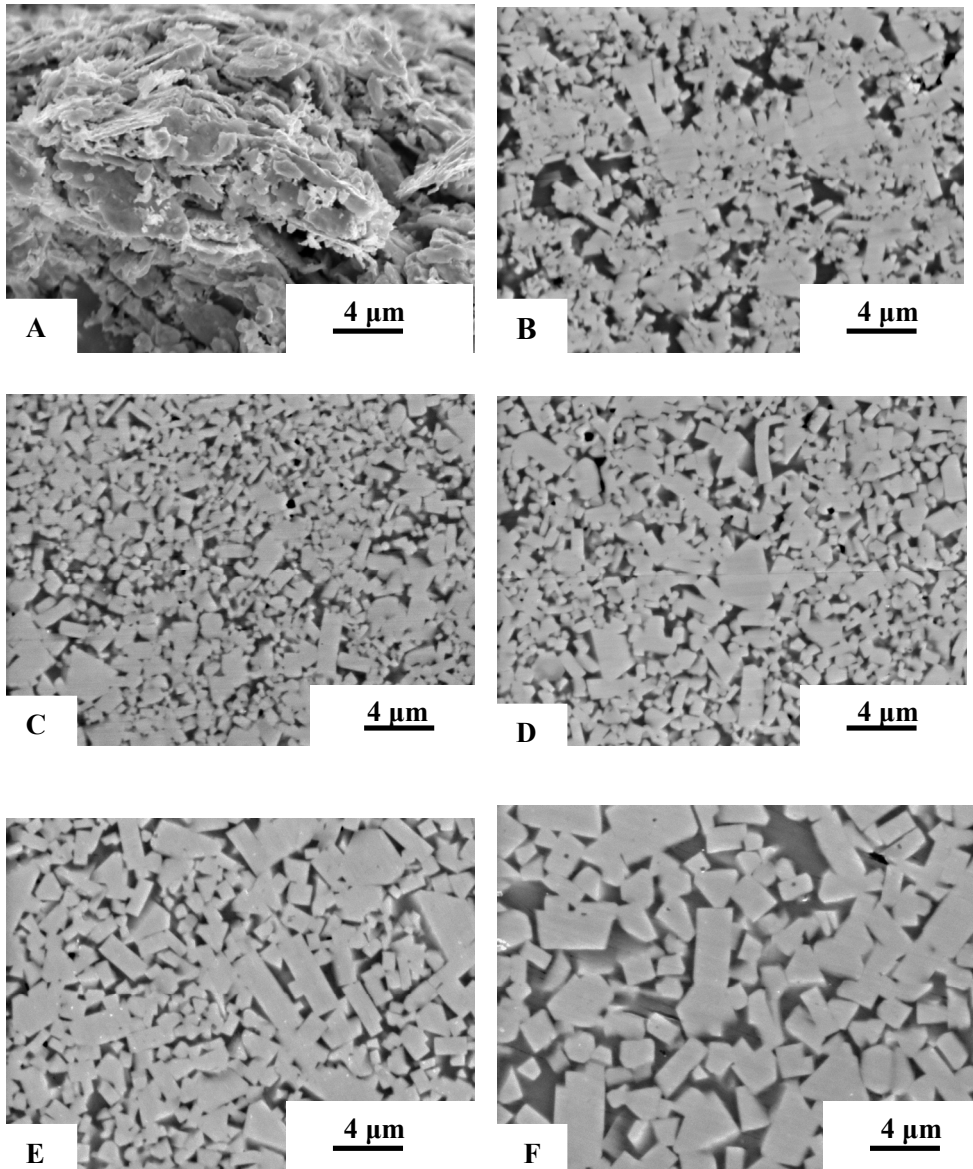


Figure 21. Microstructure of WC-15%Co composites with 7,12 wt.% of carbon addition sintered at various temperatures and time: (A) 1250 °C, 30 min, (B) 1330 °C, 30 min, (C) 1380 °C, 30 min, (D) 1400 °C, 30 min, (E) 1400 °C, 150 min, (F) 1400 °C, 300 min

The size of the W particles milled in attritor for 8 hours was 50–60 nm and the grain size of as formed WC in the sintered WC-Co composites was about 600 nm, meaning grain growth of the carbide of 10 times. The coarsening or growth of the carbide grains during liquid-phase sintering is usually explained in terms of Ostwald ripening (LSW) theory [50]. Grains below the average size are dissolved and larger ones grow. Such, the grain growth consists of two parts: the early stage grain growth that occurs during heat-up and the later stage during the isothermal hold. During the later stage the rate of grain growth is significantly slower than that during the early stage.

The microstructure of the WC-Co hardmetal consists of WC grains embedded in a cobalt-rich binder phase. Since WC is known to be accurately stoichiometric and does not dissolve any cobalt, the liquid cobalt phase ought to dissolve W and C in atomically equal proportions during liquid phase sintering. There is a very narrow range of  $6,13 \pm 0,1$  wt.% carbon where the WC-Co microstructure still remains in the two phase region. In practice the total amount of C in the material can be different from stoichiometric. It should be noted, that too much or too little of carbon results in the formation of graphite or  $\eta$ -phase ( $W_xCo_yC$ ) respectively. Figure 22 shows microstructure of W-xC-15Co composites sintered at 1400 °C during 30 min with different carbon content. The sintering process of the hardmetals also depends on the carbon content. The liquid phase appears at lower temperatures in C-rich mixtures (1290 °C) - not in the W-rich ones (1370 °C) - and the associated shrinkage is higher [95]. As seen in Fig. 22 A and B,  $\eta$ -phase was found in W-rich samples, but never in C-rich samples. Free carbon was found in C-rich samples (Fig. 22 E).

The properties of the WC-Co composites depend on the graphite content in the initial powder mixture. As it was difficult to predict how much carbon will burn out during sintering, graphite powder with 0–3 wt.% over stoichiometric content was added to initial W and Co powder mixture. The sintering process of the WC powder can be better understood if the results of the densification and shrinkage are linked to the microstructure and XRD characterization which are given in paragraphs 3.1 and 3.2.



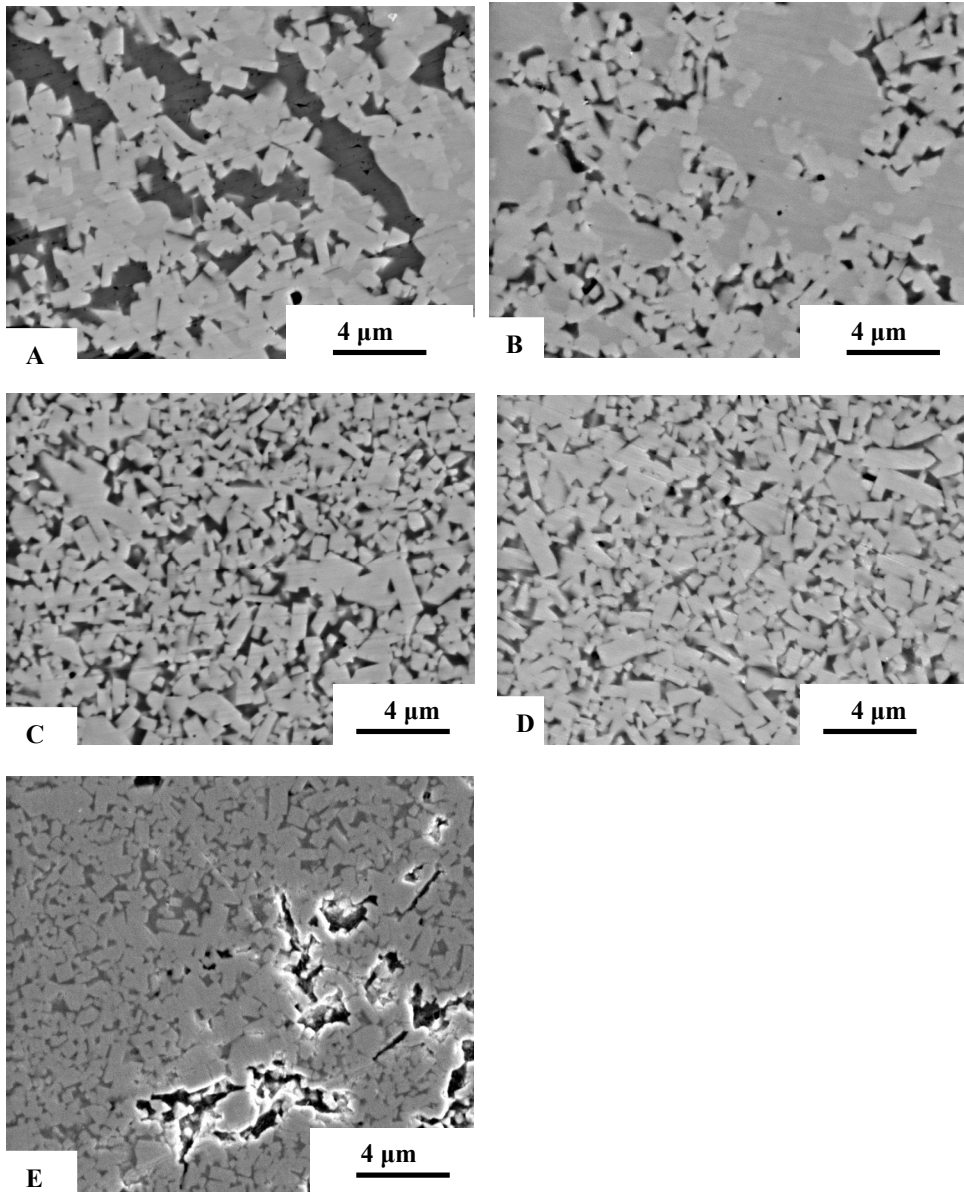


Figure 22. Microstructure of W-C-15wt%Co hardmetals sintered at 1400 °C during 30 min with different carbon content: (A) 6,13 wt.% C, (B) 6,67 wt.% C, (C) 7,13 wt.% C, (D) 7,7 wt.% C, (E) 9,1 wt.% C.

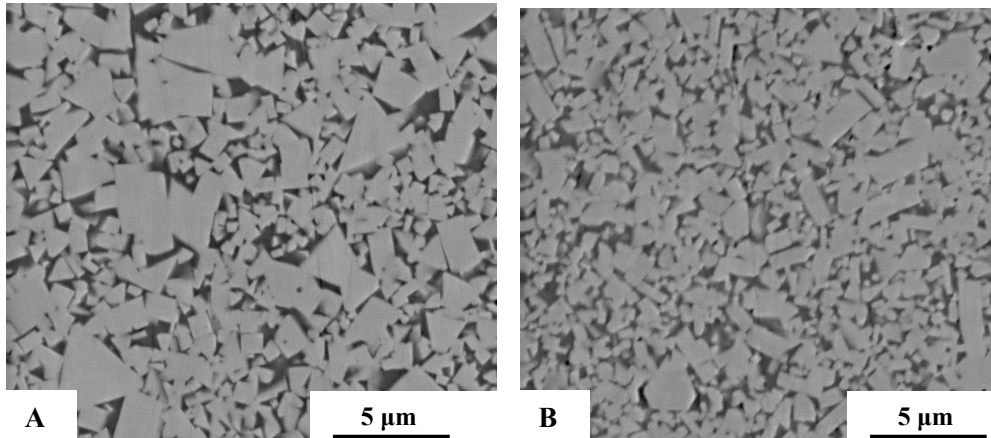


Figure 23. Microstructure of WC-15%Co hardmetal: (A) conventional and (B) produced by reactive sintering, with W:C 13:1

Figure 23 illustrates the difference between conventional hardmetal and material produced by reactive sintering method. It can be seen that reactive sintered hardmetall has fine grain and homogeneous microstructure.

### 3.2 Densification and shrinkage behavior

From the specific surface area (SSA) examinations we can conclude that the W-Co-C powder mixture, prepared by 8 hours of high energy milling has W particle size of 50–60 nm and the crystalline size by Warren-Averbach formula of 20–22 nm. The influence of milling parameters on the W-Co-C powder particles size described in details in [96]. For conventional WC-Co hardmetals, the densification phenomena are qualitatively understood [97].

The densification behavior of the W-xC-15 Co and WC-15Co powder compacts, sintered from 800 to 1400 °C is shown in Fig. 24. The shrinkage of the compacts increased with increasing of the sintering temperature. Sintering at the temperatures from 800 to 1000 °C has an insignificant effect on the sample dimensions, indicating that no densification occurs at these temperatures. As seen from Fig. 24 the shrinkage begins between 1100 and 1200 °C. This could be caused by reduction of the surface oxides and formation of the carbide. The intensive shrinkage by rearrangement of the particles can be explained by a low effective viscosity, generated by defects in the contact region between particles. The creep of the Co binder as the local process is producing solid state rearrangement.

The rapid densification occurred at 1200–1300 °C and after that the densification rate markedly decreased. In the most extreme case, 80% of the densification took place in solid phase sintering. The WC-15Co cemented carbide, sintered from nanocrystalline powders showed rapid shrinkage and full densification at lower temperature, compared to the conventional mixed powders. During heating the solubility of WC in the cobalt binder increases monotonously as the temperature increase. However, during isothermal holding the equilibrium solubility is quickly approached due to the very short diffusion distances in the binder phase and thereafter no further dissolution occurs. The linear shrinkage of the samples produced by reactive sintering was 20–25% higher than that of samples produced with conventional technology. However, the overall shrinkage at the end of the solid state sintering is also higher for C-rich alloys.

Archimedes' type density measurements show that the density of the samples depends on the graphite content in the initial W-C-Co powder mixtures (Fig. 25). The highest density is on the samples with 7,12 wt% graphite powder. It is 1% higher than in alloys with stoichiometric content (6,13 wt%). During sintering some carbon loss occurred. Samples with graphite content up to 6,67 %C have some  $\eta$ -phase in structure. On the other hand, samples with 7,7 and 9,1 %C in the powder mixture have free carbon in the structure. Thus, the optimal graphite amount in the initial powder mixtures is between 7,1 and 7,7 %. The structure of such alloys consists of WC grains and solid solution on the base of cobalt. No  $\eta$ -phase and free carbon was found.

During sintering the density increases to 55% at about 1100 °C when the first signs of the shrinkage are observed. At this temperature no grain or particle growth could be observed and therefore the shrinkage and the increase of the density can be attributed to rearrangement of the particles. Above 800 °C and up to 1100 °C negligible change in the linear dimensions is observed. By [98], the dissolution of the WC in solid Co begins at about 800 °C. It is noticed that the maximum in densification rate is reported at 1200–1280 °C. In the temperature range corresponding to the highest dissolution rate, significant dissolution of the WC in the Co binder takes place. The microstructural studies show neck formation between the particles and open porosity at the temperature of 1250 °C, which fits well in a conventional model of the first stage of sintering. The dominant physical process during heating is rearrangement of the individual carbide grains, causing small pores to disappear and larger ones to grow slightly.

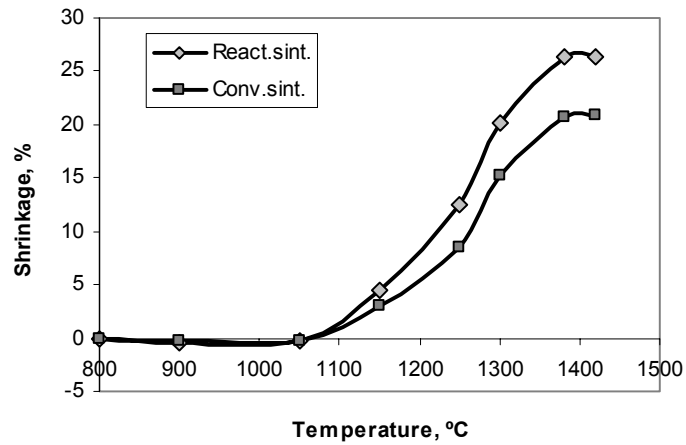


Figure 24. Linear shrinkage of reactive sintered  $W-7,12C-15Co$  and conventional  $WC-15Co$  samples

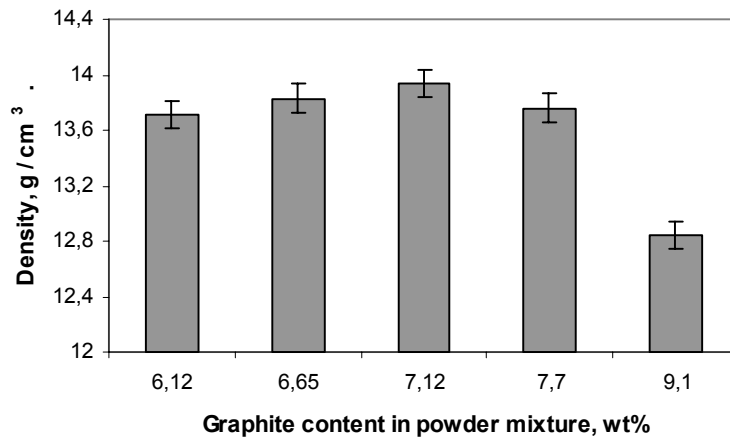


Figure 25. The influence of graphite content in initial powder mixture on the density of  $W-xC-15$  wt% Co samples

The solid-state shrinkage starts with the wetting of the WC grains by the Co binder, and is followed by the spreading of the binder into the porosity. This leads to the rearrangement of WC grains. The onset of shrinkage depends on the ability of the

binder to wet WC grains. At the temperature of 1275 °C an abrupt increase in the densification is observed that may indicate the formation of a liquid phase.

### 3.3 Effect of grain growth inhibitors

The SEM micrographs of nanocrystalline WC-15wt% Co are quite different from those of conventional WC-15 wt.% Co hardmetals as shown in Fig. 26. The carbide grains formed during reactive sintering have elongated form. The main problem is rapid carbide grain growth during solid state and liquid phase sintering in the nanocrystalline composites.

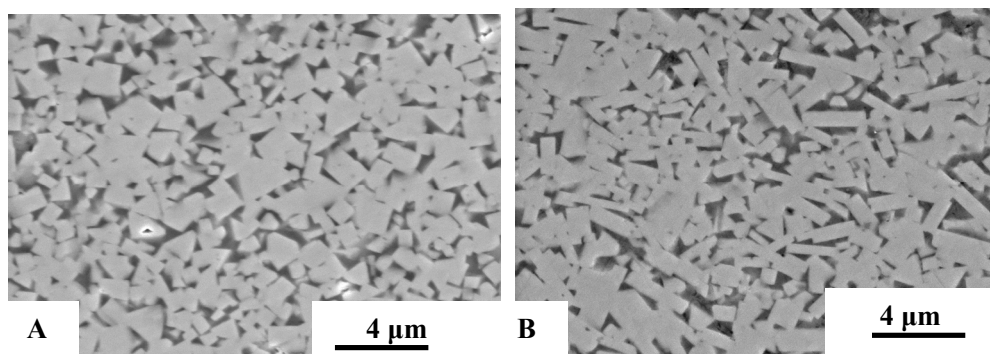


Figure 26. Microstructure of WC-15 wt% Co composites produced by different methods: (A) conventional technology, (B) reactive sintering

Studies of the grain growth behavior have found that the grains tend to grow extremely rapidly during the early stages of sintering. Fang and Eason [99] documented the densification and grain size versus the LPS (liquid phase sintering) time (5, 15, 30, 60, 90, 180, 360 min) and temperature (1630, 1670, 1710, 1750 K). It was found that the grain size of the samples was already dramatically increased from their initial nanometer sizes in the first 5 min. McCandlish [34] observed that the WC grain size in a WC-10 wt.%Co alloy, sintered from nanosized WC-Co powder (manufactured by Nanodyne, Inc.), after 30 s of sintering at 1400 °C was 200 nm, ending up to about 2 μm.

One way to decrease the grain coarsening is to use special alloying elements – so called grain growth inhibitors. Grain growth inhibitors have been used to mitigate grain growth during sintering. During the sintering process, small WC grains are dissolved into Co binder as W and C atoms and precipitated to large WC grains. The use of grain growth inhibitors is widely practiced in the industry for sintering ultrafine

WC-Co materials. Vanadium carbide (VC) and chromium carbide ( $\text{Cr}_3\text{C}_2$ ) are by far the most effective grain growth inhibitors due to their high solubility and mobility in cobalt phase at lower temperatures [100–103]. Additionally, the combinations of VC and  $\text{Cr}_3\text{C}_2$  have better inhibition effects than that doped alone [104]. Moreover, VC has been recognized as the most effective grain growth inhibitor to retard the WC grain growth [100].

To control the grain growth in nanostructured WC-Co composites, one of the keys is the proper selection of the second-phase additives as grain growth inhibitors.

When sintering of a 150 nm WC-Co powder grade without grain growth inhibitor it was observed that abnormally large WC grains form already during the heating-up period of the sintering cycle, well before the eutectic liquid is formed [105]. The normal and abnormal carbide grain growth during sintering is seen in Fig. 27.

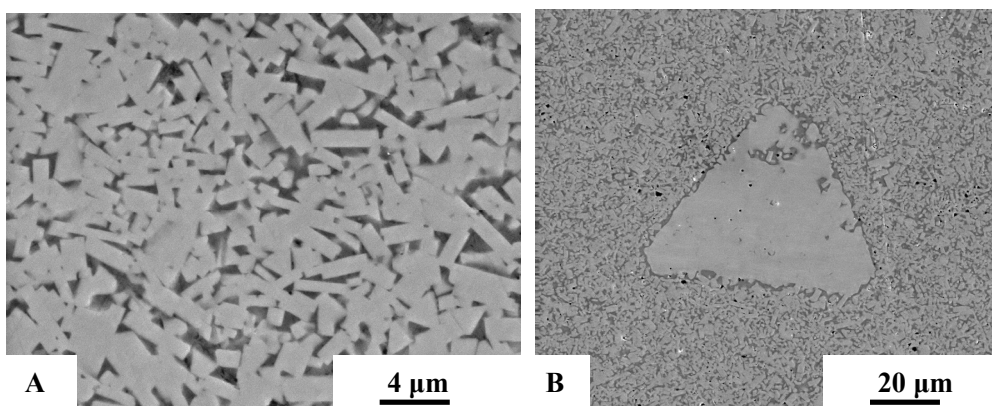


Figure 27. Grain growth in WC-15%Co hardmetals during reactive sintering at 1400 °C 60 min : A–normal, B– abnormal

The solubility of VC in the Co binder is 8,19 wt.% .The content of VC in WC-Co is usually kept at 0,7 wt.%, which is regarded as the practical upper limit, in order to avoid embrittlement due to (V,W)C precipitation at the interface of WC-Co [103]. Some investigations indicate that in order to achieve better overall properties, the weight ratio of VC/Co should be less than 5 wt.%.

Specifically, the grain growth of WC during sintering can be divided in two parts: during heat-up and during isothermal hold at liquid phase sintering temperatures. Until now, the most successful way of controlling WC grain growth during sintering is the addition of small amounts (about 1-2 wt.%) of several metallic carbides (as VC,  $\text{Cr}_3\text{C}_2$ ,

Mo<sub>2</sub>C, TaC etc) to the powder mixture. However, the physical mechanisms of the grain growth control are still unclear.

Figure 28 shows that alloyed WC-15wt% Co cermets have slightly higher hardness compared to the reactively sintered, non-alloyed cermets. It can be explained by somewhat finer structure of the alloyed cermets. Similar results are reported about alloyed WC-Co composites, prepared by different methods. M.A.Xueming et al had found, that VC-doped WC-Co alloys, directly synthesized from elemental powders, exhibit higher hardness than WC-Co alloys without doping with VC [106].

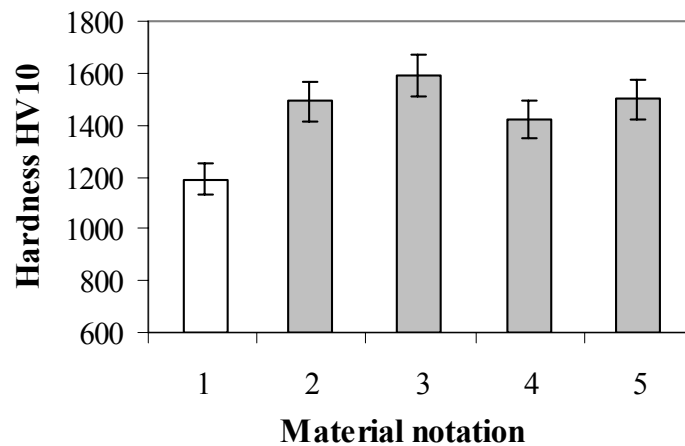


Figure 28. Hardness of WC-15wt.% Co hardmetals depending on alloying elements: 1 - WC-15Co (conv.), 2 - WC-15Co (react. sint. 7,12 wt.% C), 3 - WC-15Co-0.8VC, 4 - WC-15Co-0.8Cr<sub>3</sub>C<sub>2</sub>, 5 - WC-15Co-0.6VC-0.2Cr<sub>3</sub>C<sub>2</sub>

As seen in Fig. 29, reactively sintered WC-15wt%Co hardmetals, doped with grain growth inhibitors, exhibit lower TRS values, compared to the conventional WC-15%Co and non-alloyed hardmetals. Similar results have been reported in [102–104].

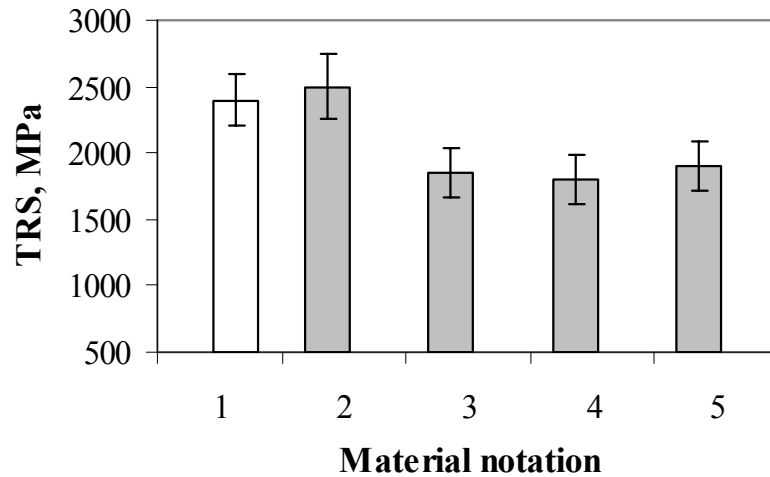


Figure 29. Transverse rupture strength of reactively sintered WC-15 wt% Co hardmetals with various grain growth inhibitors: 1 - WC-15Co (conv.), 2 - WC-15Co (react. sint. 7,12 wt.% C), 3 - WC-15Co-0.8VC, 4 - WC-15Co-0.8Cr<sub>3</sub>C<sub>2</sub>, 5 - WC-15Co-0.6VC-0.2Cr<sub>3</sub>C<sub>2</sub>

### 3.4 Mechanical properties

The Vickers hardness decreases with increasing the carbon content (Fig. 30). As was seen in Fig. 22 A and B the alloys consisting up to 7,12 wt.% C have hard and brittle  $\eta$ -phase in structure. The alloys with over 7,7% C have free carbon in the structure. The hardness decreases in this range with increasing of the cobalt content. The hardness of the reactive sintered hardmetals was higher than that of the conventional ones, which results not only from the submicron structure, but also from the alloy strengthening of the binder phase (Fig. 31).



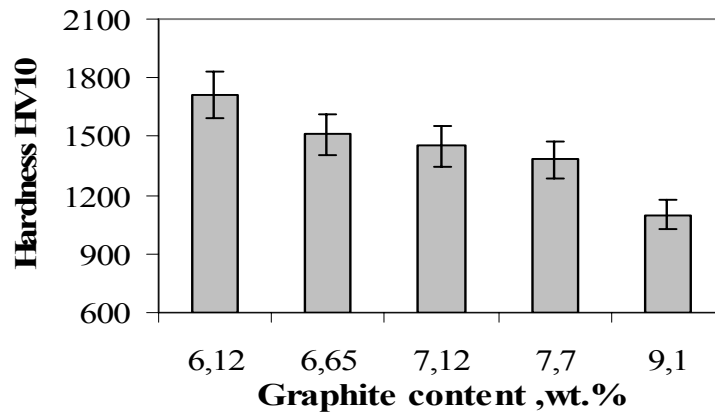


Figure 30. Hardness of WC-15wt % Co hardmetals depends on carbon content in the composites

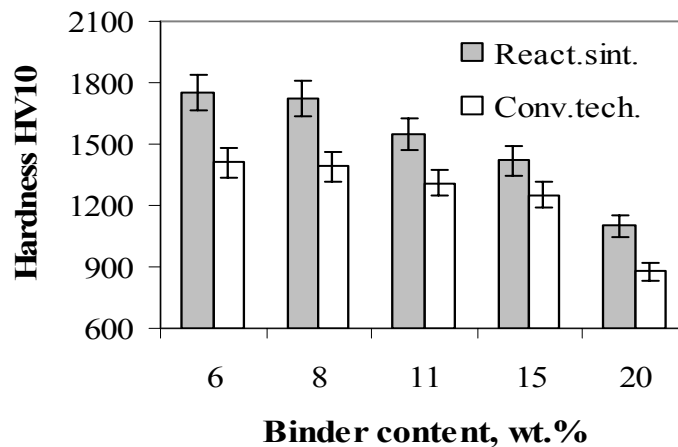


Figure 31. Hardness of hardmetals depending on binder content: conventional vs. reactive sintered with 7,7 wt.% of graphite

Transverse rupture strength (TRS) has historically being used as an indicator of the quality of materials [107]. As seen in Fig. 32 A, TRS of WC-Co composites, prepared by reactive sintering is nearly even than that of composites, prepared by conventional technology. The optimal graphite content with regard to tungsten in the initial powder mixture is 7,12–7,7 wt% (Fig. 32 B).

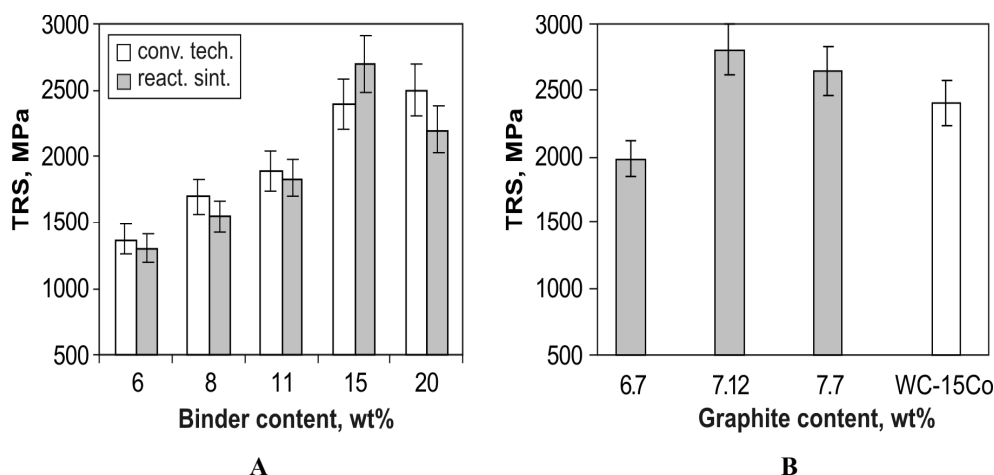


Figure 32. Transverse rupture strength of WC-Co hardmetals depending on binder content (A) and graphite content (in relation to W) in the initial mixture (B).

### 3.5 Conclusions to the chapter

1. A novel technology for production of submicron ( $d_c=0.6 \mu\text{m}$ ) WC-Co hardmetals from carbides acquired by way of reactive sintering was developed. The resulting alloys had higher hardness in comparison with the alloys produced with the conventional technologies.
2. Densification is achieved mainly by solid state shrinkage and completed by an LPS step at limited temperature. The linear shrinkage of samples produced by reactive sintering was 20–25% higher than that of samples produced by conventional technology.
3. During sintering some loss of carbon took place. The optimal graphite amount in the initial powder mixtures is between 7,1 and 7,7 wt.%. The structure of such alloys consists of the WC grains and solid solution on the base of cobalt, without  $\eta$ -phase and free carbon in structure.
4. Nanocrystalline W-Co-C powder after solid carburizing from 1000 to 1100 °C formed intermediate carbides ( $\text{W}_2\text{C}$ ,  $\text{Co}_3\text{W}_3\text{C}$ ). WC was formed at 1400 °C without intermediate carbide, because Co acts as a catalyst in the carburizing reaction. This lower carburizing temperature was found to minimize the WC grain growth.
5. The mechanical properties of the reactively sintered hardmetals depend on the carbide to binder ratio, graphite content in initial powder mixture and alloying additives.

## 4. Recycling by oxidation and carbothermal reduction

### 4.1 Oxidation process

Commercially available WC-Co hardmetal scrap was used as a raw material (Fig. 33). The particle size of WC in the hardmetal was 1–3  $\mu\text{m}$  and the content of Co binder phase was 6 and 15 wt.%. The specimens were washed with distilled water. After washing the specimen were oxidized at 850 °C in air in the rotary kiln (Fig. 34).

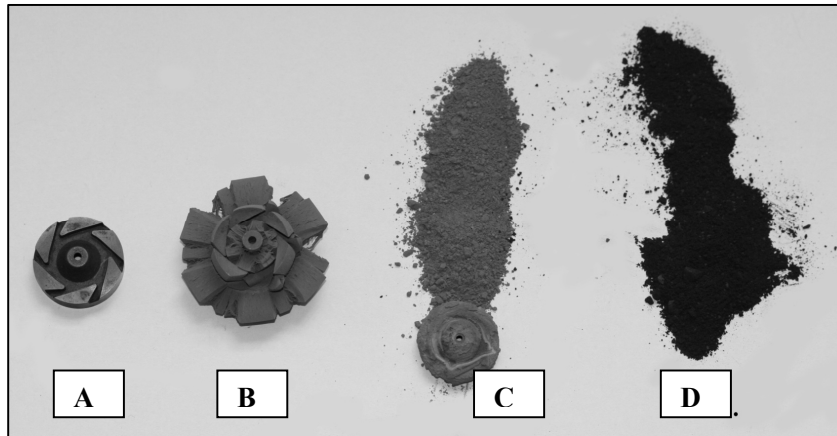


Figure 33.. Hardmetal scrap before oxidation process (A), during the oxidation (B and C) and after carburization (D)

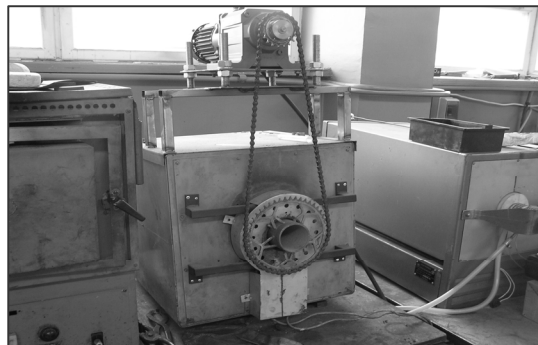


Figure 34. The furnace for oxidation process

In order to increase the speed of oxidation process the WC-Co was oxidized at 850 °C in a flowing stream of air. During the oxidation the surface of hardmetal specimens were covered with green-blue oxide and many microcracks formed. As the kiln rotated the soft oxide layer was removed from the surface of the WC-Co specimen. Two oxide phases of  $\text{CoWO}_4$  and  $\text{WO}_3$  formed during the oxidation (Fig. 35). The oxide mass of the WC-Co hardmetal has a low strength due to its sponge-like microstructure with microcracks.

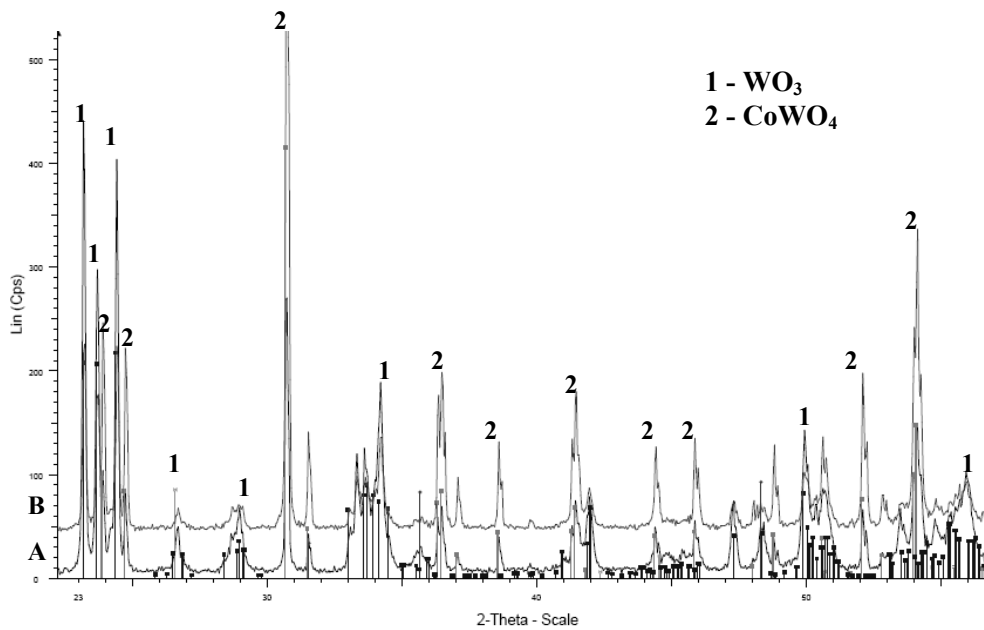


Figure 35. XRD patterns of oxidized (A) WC- 6 wt.% and (B) 15 wt.% of Co

The equations 24 and 25 below describe the oxidation reactions and reaction results of WC- 15 wt.% Co and WC- 6wt.% Co respectively:



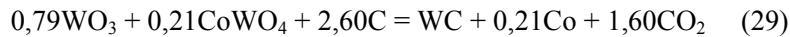
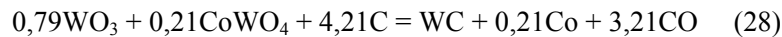
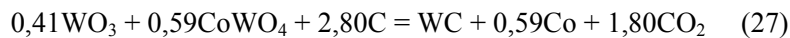
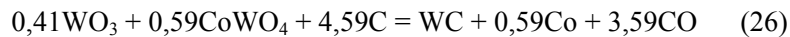
During the oxidation process not only volumetric but also mass increase occurs. The mass increase of solid material during the oxidation reactions (24) and (25) are 20,2% and 18,8% respectively.

After oxidization of hardmetals with different binder content, oxide mixtures with different  $WO_3/CoWO_4$  ratios formed. The  $CoWO_4$  content in oxidized WC-15 wt.% Co is 65% and in oxidized WC-6 wt.% Co is 26%. The mass percentage of different phases were calculated from the reaction equations 24 and 25, and proven by experimental way. From XRD analyses (Fig. 35) it was seen that cemented carbide with higher binder (Co) content has after oxidation higher  $CoWO_4$  content then cemented carbide with lower binder content, 63% and 25% respectively.

#### 4.2 The determination of content of additional carbon black

To achieve WC-Co hardmetals sintered material with high mechanical properties, it is important to obtain pure WC and  $\gamma$ -phases. For this purpose, the accurate content of carbon black addition in metal oxide powder mixture is one of the most important factors in the preparation procedures. Carbon in the form of graphite acts as the reduction reactant and the carburization medium in the *in situ* reaction.

There may be two kinds of gas products, i.e., CO and  $CO_2$ , when the oxides are reduced by the carbon according to the reaction equations as below:



For reaction equations (26) and (27) WC- 15 wt.% Co and for the equations (28) and (29) WC- 6 wt.% hardmetal bulk was regarded as the final target material. For Eqs. (26) and (27), the carbon addition 16,6 and 10,8 wt.% are needed and for Eqs. (28) and (29), the carbon addition 16,9 and 11,2 wt.% are needed, respectively. It is reasonable to predict that gas product from the reduction reactions is a mixture of CO and  $CO_2$ . The gas emission during the reactions (26) and (27) is 30,3 and 25,5 wt.% respectively. As described in the previous chapters there is higher thermodynamic probability to the formation of CO gas at higher temperature (above 900 °C) and therefore there is reasonable to predict that the carbon addition should be 16,6 wt.% . To determine precisely the content of carbon addition in the oxide powder mixture, a series of experimental investigations were carried out. Four kinds of raw powder mixtures containing different amounts of carbon (in the form of carbon black) additions, i.e., 15, 16, 17, and 18 wt.% respectively, were used to synthesize the WC-13 wt.% Co hardmetal powders by *in situ* reactions in vacuum furnace using the same

processing parameters for all mixtures. In order to investigate the carbothermal-reduction and reactive sintering process, powder mixtures with 16, 16,5, 16,8 and 17 wt.% of carbon addition were used to produce WC- 15 wt.% Co sintered parts. The composition of the alloys investigated, are given in Table 5. No grain growth inhibitors were added.

### **4.3 Carbothermal reduction of $WO_3$ , $CoWO_4$ and graphite mixture powders in vacuum**

The raw material for the tests were oxide powder obtained by the oxidation of WC-13 wt.% Co scrap, which was made from Boart Longyear TCD S13 hardmetal powder. Then the oxide mixture was crushed and mixed with graphite powder. Carbon black was added at 15, 16, 17 and 18 wt.%. The crushing and mixing were carried out for 72 hours using a ball mill with WC-Co balls and pure ethanol as the liquid medium. The ball-to-powder weight ratio was 5:1, and the rotation rate of the mill was 60 1/min.

The oxide and graphite mixtures were then heat treated (reduced) at 1080 °C and 1120 °C for 1 hour in a vacuum furnace. The mass of the reduced material was 200 g. After heat treatment the reduced powders were sieved and compacted to 18×28×5 mm test blocks by uniaxial pressing at 80 MPa. The pressed blocks were subsequently sintered at 1400 °C for 30 minutes in a vacuum furnace at  $10^{-4}$  Bar or in a Sinter/HIP furnace with pressure up to 50 Bar in an argon atmosphere. The mechanical properties of the produced materials were then determined.

The recycled WC-Co materials were compared with original Boart Longyear TCD S13 hardmetal in order to compare raw material and recycled material.

The phases produced from the reduction reactions at 1120 °C for 1 hour are shown in Fig. 36. It can be seen that for powder mixtures with a 17 and 18 wt.% carbon black addition, the majority of the phases are WC and Co in the products. The reaction product of the mixtures with lower carbon black addition content (15 and 16 wt%), consists of complex carbides, known as  $\eta$ -phases.

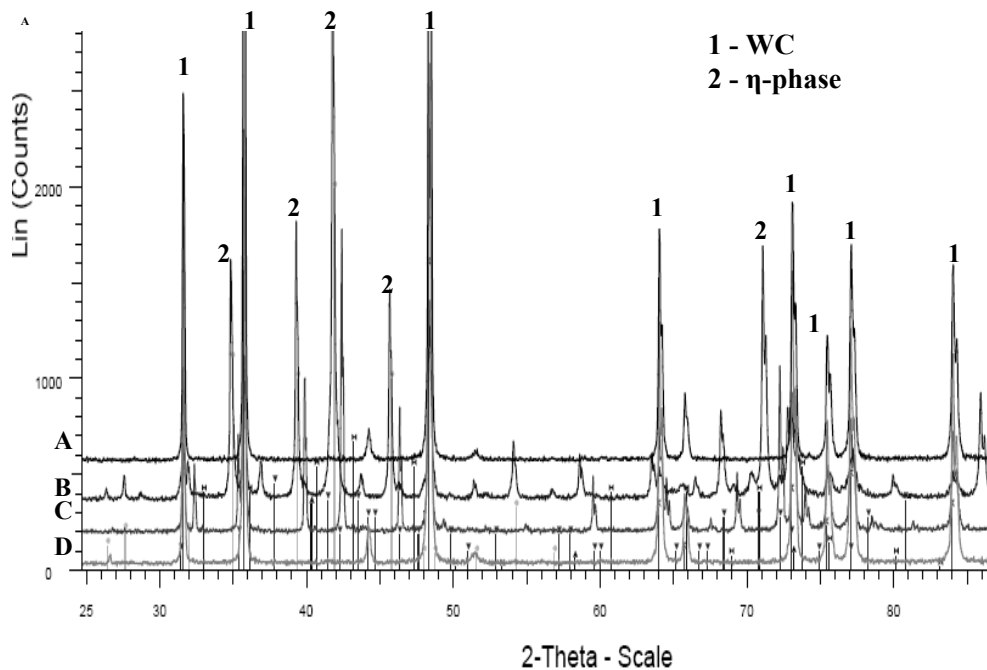


Figure 36. XRD patterns for powder mixes of  $WO_3$ ,  $CoWO_4$  and graphite after carbothermal reduction at  $1150\text{ }^\circ\text{C}$  for 1 hour: (A) with 17 wt.% graphite addition, (B) with 15 wt.% graphite addition, (C) with 16 wt.% graphite addition, (d) with 18 wt.% graphite addition

The microstructures for the reduced materials after sintering at  $1400\text{ }^\circ\text{C}$  for 30 min in vacuum and 20 min at 50 bars are shown in Fig. 37. It can be seen that the microstructure of the WC-Co composite with a graphite addition of 17 wt% (Fig. 37 B) is fine-grained, homogeneous, without porosity and free of complex carbides. Flakes of free graphite were not detected. The structure of material with a graphite addition of 16 wt.% is shown in Fig. 37 A. It can be seen that the majority of phases are complex carbides with a smaller amount of WC grains. It is also notable that due to the formation of complex carbides, there is a clear absence of Co binder in the structure of the material, resulting in a high rate of porosity. The SEM image (Fig. 37 A) shows that there is not enough binder between WC grains.

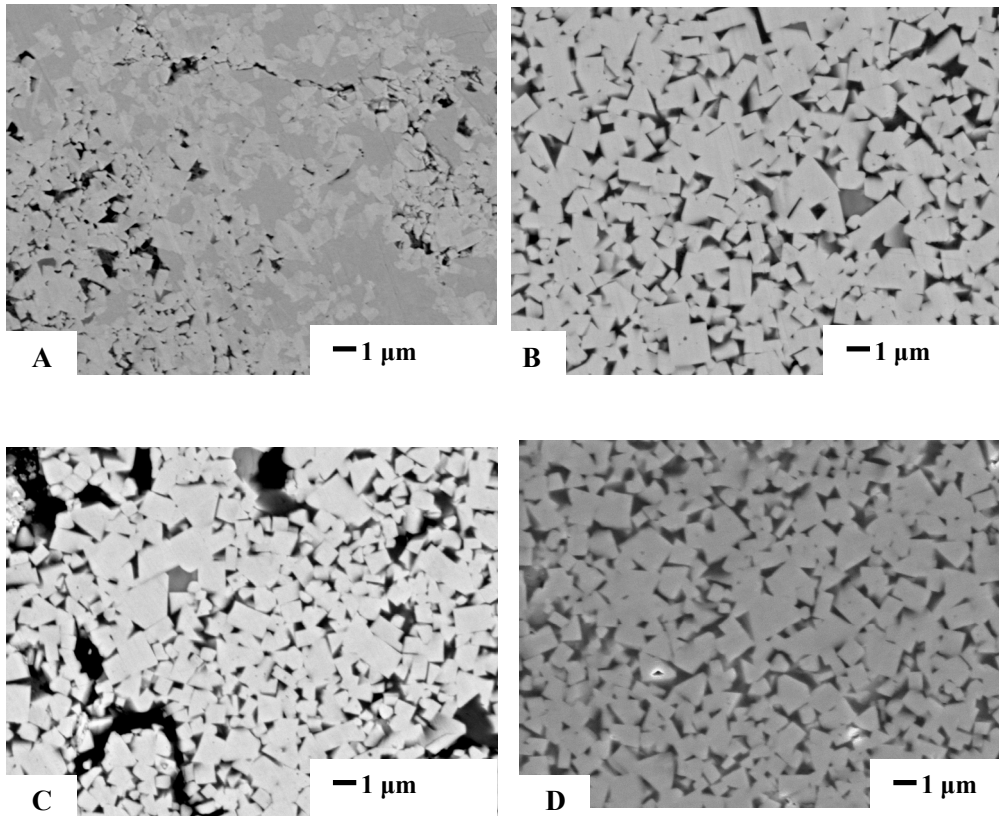


Figure 37. Structure of WC-13 wt% Co hardmetals: (A) 16 wt.% graphite, (B) 17 wt.% graphite, (C) 18 wt.% graphite, (D) conventional Boart Longyear TCD S13 hardmetal. All materials have been sintered in Sinter/HIP furnace.

A Sinter/HIP pressure of up to 50 Bars is for the conventional hardmetal clearly sufficient to produce material without porosity. Sintering of material with a graphite addition of 15 wt% was not possible, since the lack of graphite during the reduction reaction caused the formation of  $\eta$ -phases, which consists of W, Co and C, and there was not enough free Co binder in the structure of the sintered material.

In Figure 37 C, it can be seen that a graphite addition of 18 wt.% leads to the appearance of graphite flakes in the microstructure of the sintered materials. The WC structure is fine grained (1–3  $\mu\text{m}$ ), but there are graphite flakes between WC grains. As seen in Figure 37 B and D, the microstructures of conventional material and hardmetal produced from oxide powder show no significant differences. Analysis of



the experimental data makes it evident that a graphite addition of 17 wt% is suitable for the synthesis of pure WC - no free graphite flakes and  $\eta$ -phases.

A comparison of the data in Table 6 reveals that the amount of graphite addition has a remarkable influence on the mechanical properties of the hardmetal produced. Specimens with  $\eta$ -phase and graphite have lower hardness and transverse rupture strength values. The low density, TRS and hardness of material with a graphite addition of 16 wt.% can be explained with the absence of the Co binder phase.

Determined density values (Table 6) also clearly show that the use of Sinter/HIP is conducive to the production of materials with low porosity.

*Table 6. Composition and properties of the investigated WC-Co hardmetals*

<b>Powder preparation method</b>	<b>Graphite addition [wt.%]</b>	<b>Mode of sintering</b>	<b>Density [g/cm<sup>3</sup>]</b>	<b>HV10</b>	<b>TRS [MPa]</b>
Reduction reaction at 1120 °C, in vacuum for 1 hour	16	Sinter/HIP	13,55	1420	400
Reduction reaction at 1120 °C, in vacuum for 1 hour	17	Sinter/HIP	14,20	1580	1100
Reduction reaction at 1120 °C, in vacuum for 1 hour	18	Sinter/HIP	11,60	700	650
Reduction reaction at 1080 °C, in vacuum for 1 hour	17	vacuum	13,90	1500	1200
Conventional Boart Longyear TCD S13	0	vacuum	14,23	1500	2500

In this paragraph the technology for oxidation and reduction was presented. The WC-13 wt.% Co hardmetal alloy was fully transformed into an oxide mixture of CoWO<sub>4</sub> and WO<sub>3</sub> using oxidation and mechanical milling processes. The synthesized WC-Co composite material had an average particle size of 0,8  $\mu$ m.

The following conclusions can be drawn from this experimental study:

1. WC-Co hardmetal scrap can be recycled into a WC-Co composite material by a combination of oxidation, mechanical milling, carbothermal reduction in vacuum, compaction of green bodies and sintering in vacuum in combination with Sinter/HIP methods.

2. The graphite addition in the initial powder mixture had a significant influence on the phase configuration and mechanical properties of the WC-Co test blocks produced. The deficit of graphite leads to the formation of  $\eta$ -phase.
3. Sinter/HIP is conducive to the production of materials with low porosity.

#### **4.4 Carbothermal reduction of green parts in vacuum. The main parameters of process: carbon addition, temperature and time.**

A number of studies have shown that WC-Co composites can be synthesized from a mixture of metal oxides and graphite by carbothermal reaction at 950 °C to 1100 °C in a vacuum or in a flow of inert gas [42, 70, 72, 85, 108]. The synthesis of WC-Co powder from the oxide and graphite mixtures was described in previous paragraph. As it is economically advantageous to be able to combine the carbothermal reduction, carburization and reactive sintering processes, a series of tests were carried out.

##### **4.4.1 Phase formation in compacted green parts during carbothermal reduction and reactive sintering**

From the mixtures of the oxide powders and graphite addition green blocks were pressed. The green parts were reduced and sintered in a vacuum. The mechanical properties and wear resistance of materials produced were then determined. The chemical composition, manufacturing process and test methods were described in chapter 2. The material notation is given in Table 5.

Figure 38 shows the changes in chemical composition during carbothermal reduction at different temperatures in a vacuum. The oxide powder mixture consists of  $WO_3$  and  $CoWO_4$  (Fig. 38 line A). The dilatometer tests and TGA (Fig. 39) showed that the reduction process starts at 900° C, involving a mass loss of about 30%. After reduction for 1 hour at 900 °C, peaks of  $W_2C$  and WC appears, and the mixture also contains dual carbides and some remains of  $WO_3$  (Fig. 38 line B). It was found that 1 hour is not sufficient time for complete reduction of oxides in green parts with a weight of less than 10 g.

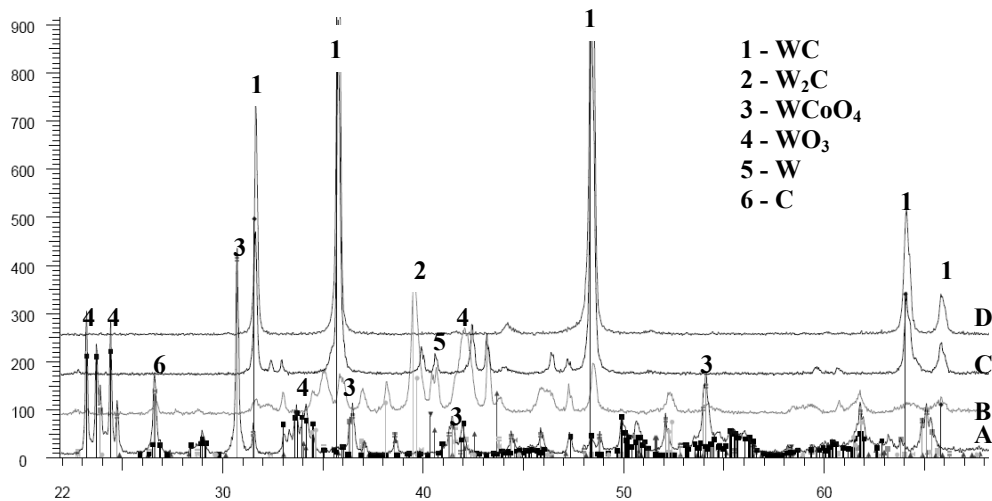


Figure 38. XRD patterns of green and sintered parts made from powder mixtures of  $WO_3$  and  $CoWO_4$  with a 16.8 wt% of additional graphite at different temperatures: (A) without carbothermal reduction, (B) reduction at 900 °C for 1 hour, (C) reduction at 1150 °C for 1 hour, (D) sintering at 1400 °C for 30 minutes

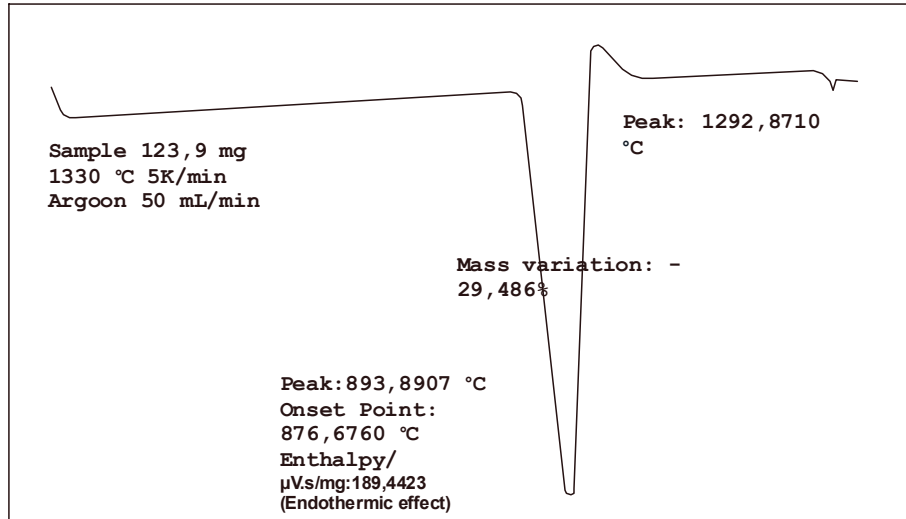


Figure 39. TGA curve

The phenomena can be explained by the different reduction conditions on the surface layer and at the core of the green parts. After reduction at 1150 °C, the material mainly consists of WC and Co (Fig. 38 line C). The appearance of W peaks show that the formation of WC continues at higher temperatures. After sintering at 1400 °C for 30 min., the recycled hardmetal consists of WC and Co.

Figure 40 illustrates microstructure evolution during sintering over a temperature range of 1250 °C to 1400 °C. During sintering a significant decrease of porosity was detected.

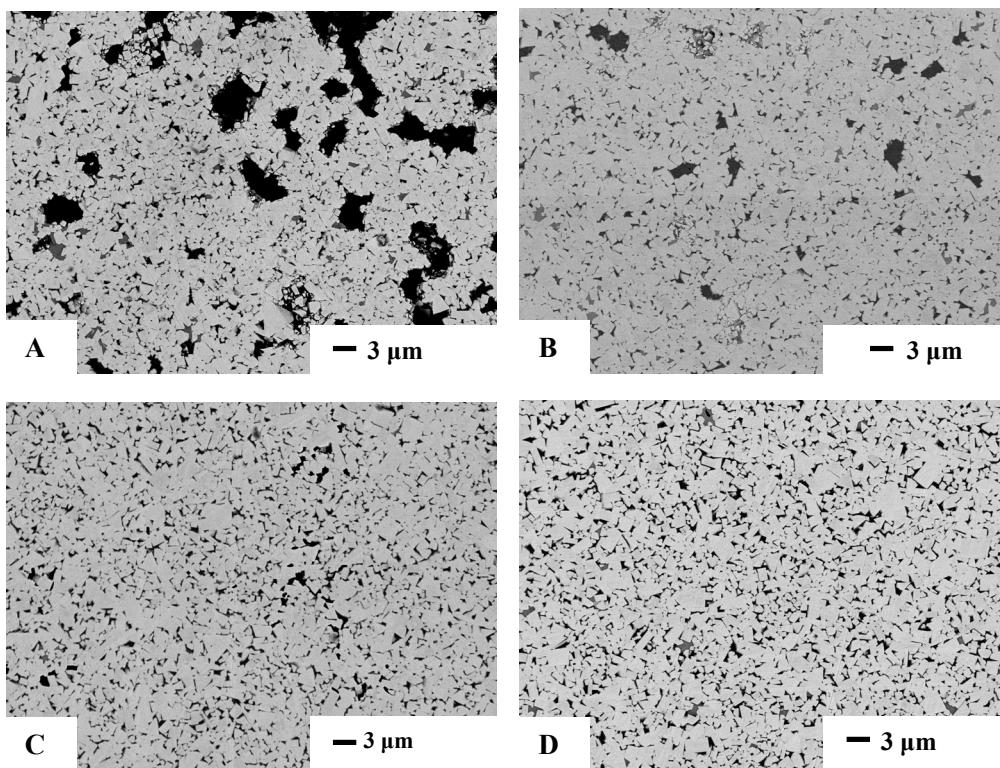


Figure 40. Structural evolution of WC-15 wt.% Co hardmetals at different temperatures during reactive sintering: (A) 1250 °C, (B) 1330 °C, (C) 1380 °C, (D) 1400 °C

As seen in Fig. 40 A, sintering at 1250 °C leads to a hardmetal microstructure with high porosity, which can be attributed to the lack of a liquid binder phase at lower temperatures. The liquid phase appears at about 1300 °C, but even after sintering at 1330 °C, the hardmetal still exhibits some porosity, due to the high viscosity of the

binder material (Fig. 40 B). A non-porous microstructure can be achieved by sintering at 1380 °C to 1400 °C (Fig. 40 C and D).

#### **4.4.2 Densification and shrinkage behavior during carbothermal reduction and following reactive sintering**

Densification behavior of the W-xC-15 Co powder compacts sintered between 900 °C and 1400 °C is shown in Fig. 41. The shrinkage of the compacts increased with an increase in sintering temperature. Sintering at temperatures between 900 °C and 1050 °C has a significant effect on the sample dimensions, indicating that remarkable densification occurs at these temperatures. As seen from Fig. 41, the linear shrinkage of sintered blocks at 900 °C is between 5 and 10%, depending on chemical composition and particle size distribution (attritor vs. ball mill). Shrinkage is caused by the reduction of oxides and the formation of carbides. Intensive shrinkage by the rearrangement of particles can be explained by a low effective viscosity generated by defects in the contact region between particles. The creep of the Co binder is assumed to be the local process producing solid state rearrangement.

It was found that the CO/CO<sub>2</sub> gas produced during the carbothermal reduction does not damage the green parts. This can be explained by the low green density and open porosity, which allow the gases to exit the compact without damaging the structure. The relatively high linear shrinkage rate at lower temperatures indicates that the sintering processes of mechanically activated materials starts at lower temperatures. As seen in Fig. 41, the mixtures prepared by high energy milling (R16,8A) have higher shrinkage rates at lower temperatures than the materials prepared by conventional ball milling (R16,8B).

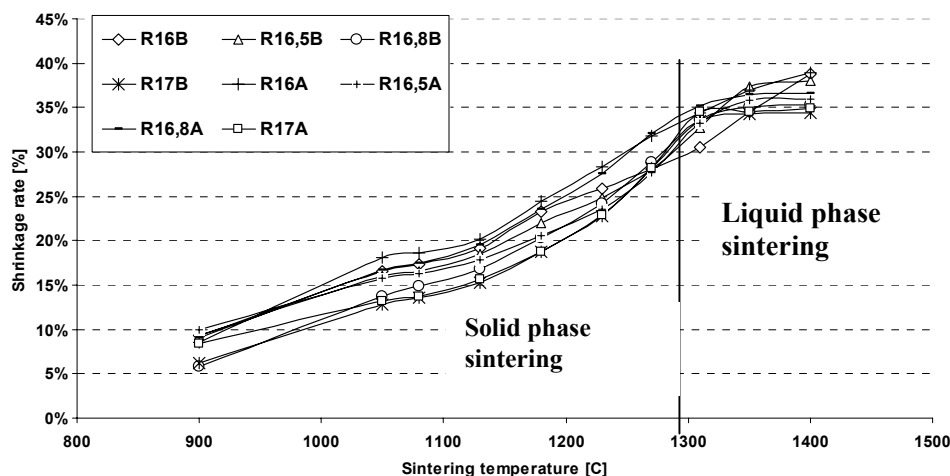


Figure 41. Linear shrinkage of  $W$ - $x$ C-15Co hardmetals with different amounts of graphite and different methods of powder preparation.

Rapid densification occurred at a temperature range of 900–1050 °C and 1130 °C to 1300 °C. Using TGA tests (Fig. 39), it was found that the liquid phase appears at 1295 °C. This shows that during carbothermal reduction and subsequent to reactive sintering more than 90% of the densification took place in solid phase sintering. The WC-15Co hardmetal sintered from oxide powders showed rapid shrinkage and full densification at a lower temperature than conventional W, Co and C powder mixtures which underwent reactive sintering [103]. During heating, the solubility of WC in the cobalt binder increases uniformly as the temperature increases. However, during isothermal holding, the equilibrium solubility is quickly reached due to very short diffusion distances in the binder phase, and thereafter, no further dissolution occurs. The linear shrinkage of the samples produced by carbothermal reduction in combination with reactive sintering was 40–45%, which is about 2 times more than that of samples produced with conventional technology.

The microstructure of the WC-Co hardmetals consists of WC grains embedded in a cobalt-rich binder phase. Since WC is known to be precisely composed stoichiometrically and does not dissolve any cobalt, the liquid cobalt phase ought to dissolve W and C in atomically equal proportions during liquid phase sintering. There is a very narrow range of  $6,13 \pm 0,1$  wt.% carbon where the WC-Co microstructure will remain in the two phase region. In practice, the total amount of C in the material may not agree with the stoichiometric ratio. It should be noted, that too much or too little carbon results in the formation of free graphite or  $\eta$ -phase ( $W_xCo_yC$ ) respectively.

Figure 42 shows the microstructure of the material produced by oxidation and carbothermal reduction with the optimal amount of graphite and the microstructure of the original hardmetal.

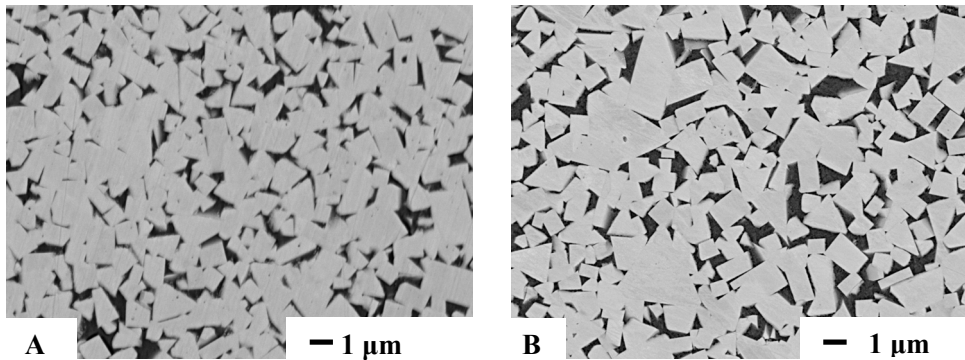


Figure 42. The microstructure of  $W-xC-15Co$  hardmetal: (A) 16,8 wt.% of graphite (B) original Boart Longyear hardmetal

The powder mixture of hardmetal in Fig. 42 A was prepared by ball milling and compacted by uniaxial pressing at 80 MPa and sintered at 1400 °C for 30 min. As seen in Fig. 42, the hardmetal produced by carbothermal reduction and reactive sintering have a fine-grained microstructure. However, an investigation of the cross-sections of the hardmetals produced revealed that depending on the content of additional carbon before carbothermal reduction and sintering, inner zones with abnormal phase compositions formed. Figure 43 illustrates the cross sections of sintered parts produced with the same production route, but different carbon addition. As seen in Fig. 43 A, the deficiency of graphite during WC phase formation leads to the formation of  $\eta$ -phase rich areas in the outer layer and to a lack of binder material at the core of the sintered specimen. This can be explained by the onset of WC formation and sintering on the surface layer of the blocks produced.

The lack of carbon black causes the formation of  $\eta$ -phase which results in the consumption of Co from the inner layers of the sintered part. Having too much additional carbon black in the mixture (Fig. 43 B) causes the formation of a graphite rich zone at the core of the sintered material.

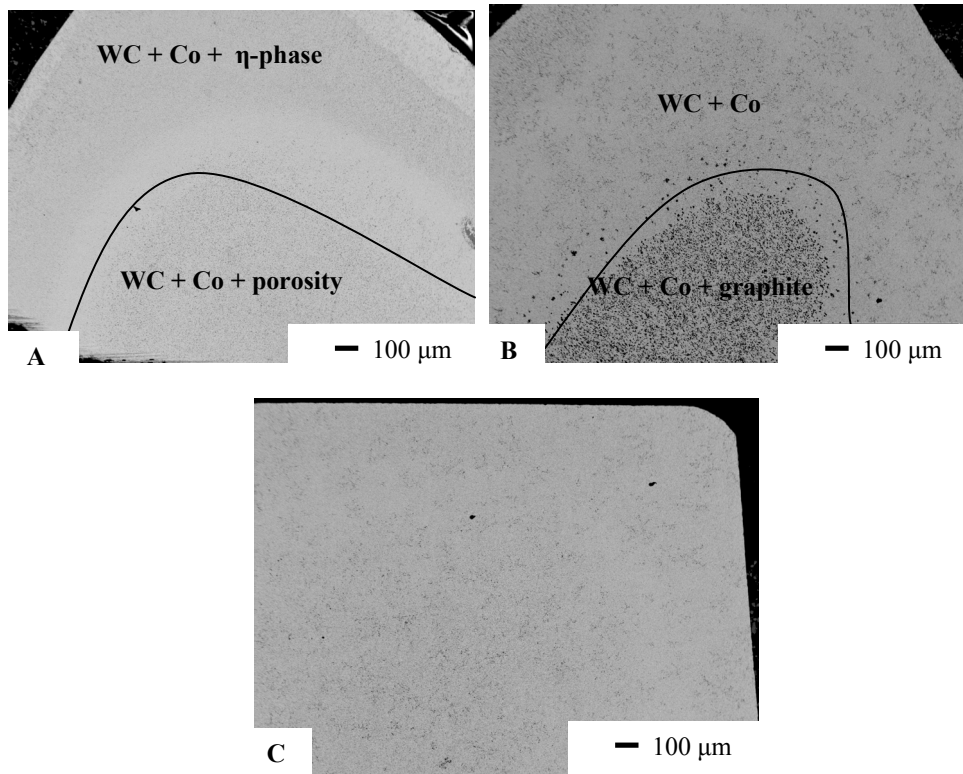


Figure 43. Phase formation after sintering: (A) 16.5 wt.% of graphite, (B) 17 wt.% of graphite, (C) 16.8 wt.% of graphite (all mixtures were milled in a ball mill)

It was noted that both porosity and graphite flakes arose only at the inner core of the sintered material. In both cases the microstructure of the outer layer of the sintered specimens consists of fine-grained WC and Co phases. In the case of compacts obtained from a mixture with 16,8 wt.% of graphite (Fig. 43 C), WC and Co phases filled the cross-sections of the specimens, and the formation of  $\eta$ -phase and free graphite was not detected.



### 4.4.3 The effect of milling technology

The influence of milling method was investigated. Figure 44 illustrates the microstructures of sintered hardmetals produced by ball milling and high energy milling in an attritor. It was found that the hardmetal prepared by high energy milling in an attritor has coarser WC grain than materials prepared by ball milling.

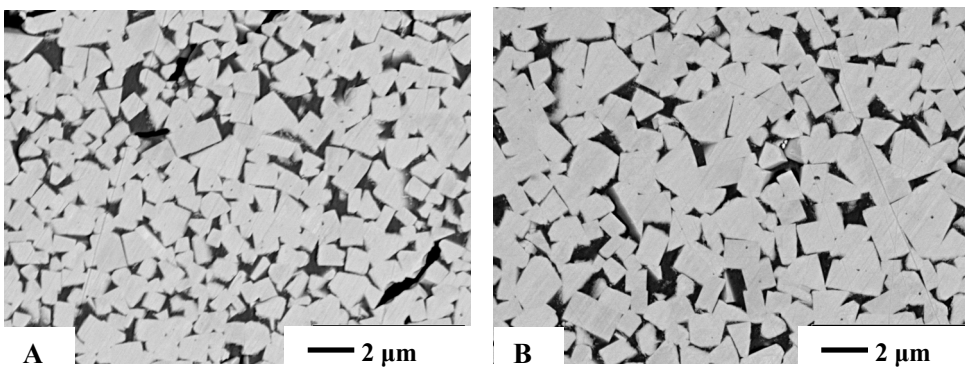


Figure 44. The microstructures of composites prepared by ball mill (A) and high energy milling in an attritor (B)

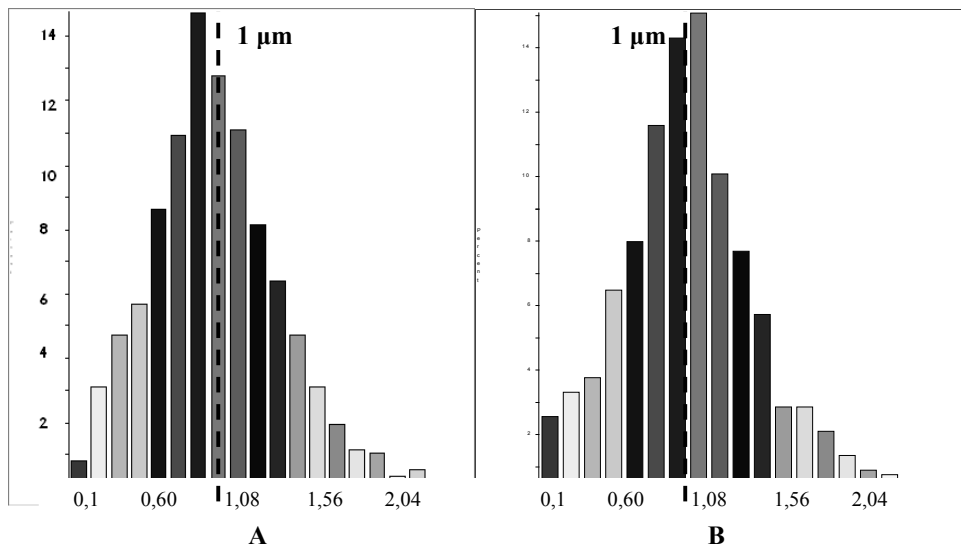


Figure 45. Grain size distribution of hardmetals prepared by ball mill (A) and high energy milling in an attritor (B)

Grain size analysis shows that the hardmetals prepared by attritor and ball mill have similar grain size distribution (Fig. 45 A and B), but the mean grain size of hardmetal prepared by ball milling is 0,88  $\mu\text{m}$  compared to 1,08  $\mu\text{m}$  for hardmetal prepared using an attritor. It can be explained by the faster grain growth of fine grain powders during the sintering process.

#### **4.4.4 The influence of plasticizer content and compaction pressure to the microstructure and mechanical properties**

Uniaxial powder pressing is the most common method used for high-volume production of cermets, hardmetal and ceramic components [109–110]. The object of a pressing process is to form a net-shaped, homogeneously dense powder compact that is nominally free of defects. A typical pressing operation has three basic steps: filling the mold or die with powder, compacting the powder to a specific size and shape, and ejecting the compact from die.

Pressing should be completed at a pressure high enough to achieve sufficient densification and strength for handling and green compact machining but low enough to avoid excessive wear on the press and tooling.

Dense packing increases particle coordination and green density, which increases the rate of densification during sintering while decreasing the concentration, size and size distribution of the porosity present. Generally, closely packed particles produce a finer and more uniform pore structure in a higher green-density compact that densifies more uniformly to a higher end-point density with less overall shrinkage on sintering [111, 112].

Producing sintered parts by carbothermal reduction and following sintering, the main problem arises as the warping process takes place (Fig. 46). Shape distortion or warping results from differential sintering shrinkage due to density gradients. During the interrupted sintering tests and determination of linear shrinkage at different temperatures, it was seen that the sintering process starts from the outer layer of compacted specimen. It can be explained by the density gradients in the green parts, where the surface layer of the material, which has direct contact with pressing tools, has significantly higher green density than that in the core of the green body.

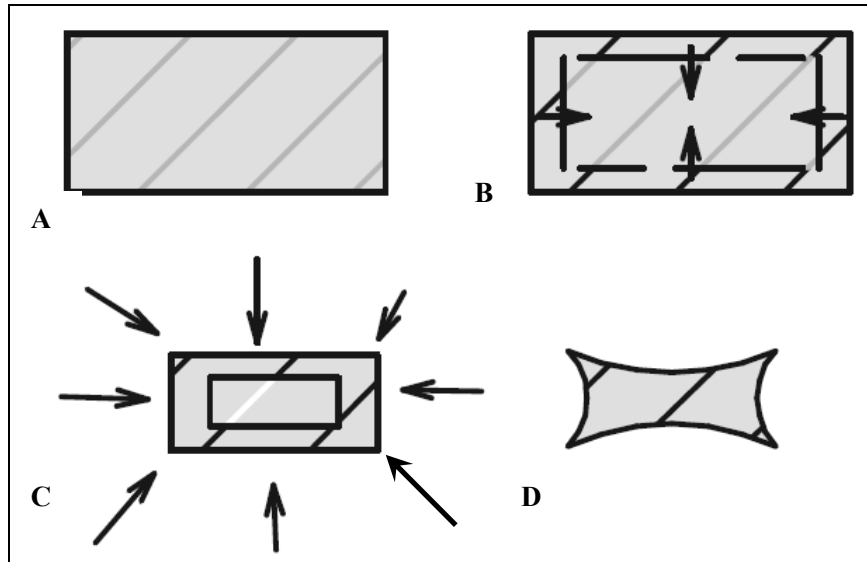


Figure 46. The sintering process: (A) the green body, (B) start of the sintering process on the outer layer of specimen, (C) formation of empty core of specimen, (D) end of the sintering process.

Therefore the sintering activity is higher in surface layer. In the early stage of the sintering (temperature range 1250–1350 °C), the formation of dense WC-Co structure in the surface layer of test specimen was detected (Fig. 46 B). The thickness of the sintered layer increases as the sintering temperature rises until the formation of dense WC-Co outer layer and porous core. At the end of the sintering the pores or channels were detected (Fig. 46 A and B). Using Sinter/HIP technology the bigger channels and pores in the microstructure can be avoided, but the changes of shape during the sintering still remains a problem (Fig. 46 C). Theoretically, the degree of warping depends on many factors, including the properties and characteristics of the powder and the granules, the die-fill density and uniformity, the die material and the size and shape of the die, the pressing pressure and rate, and the pressing conditions (uniaxial, isostatic, etc.) [113].

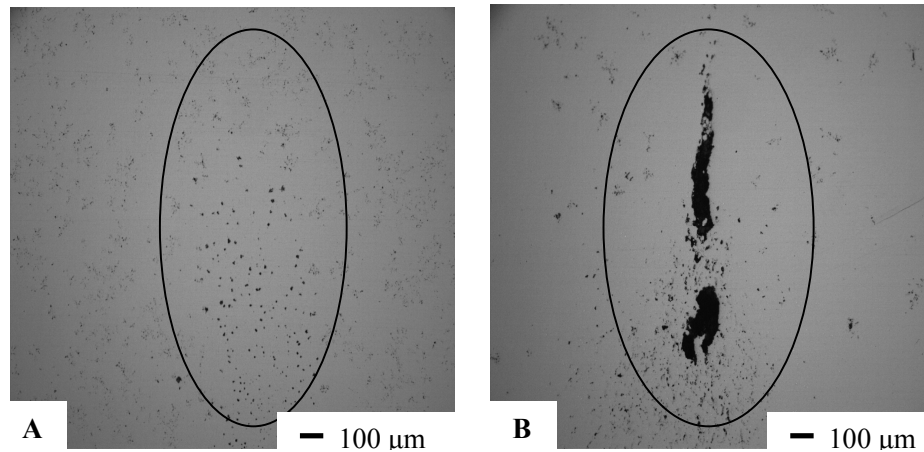


Figure 47. High porosity area (A) and shrinkage cavity (B) in the core of the sintered part

The pores in the WC-Co microstructure were investigated by optical microscope and the porous area was analyzed by program Omnimet. With the Omnimet software it was possible to separate black pore flakes from the hardmetal matrix and analyze the distribution of those flakes. The amount of pores was given in area percentage. It was seen that in the core zone of the sintered specimen the pores occupied ca 1% of the area (Fig. 47 A).

To produce process able powders, various organic additives are typically added to the slurry prior to spray drying. These include binders for strength, plasticizers that produce deformable granules and lubricants that mitigate frictional effects.

Managing friction is critical to successful pressing. Friction between the powder and die wall decreases the pressure available for compaction with increasing distance from the pressing punch. Because compact density is directly related to forming pressure, a forming pressure gradient becomes a density gradient in the compact [114]. Friction is influenced by the die material and its surface finish, as well as the powder and organic additives. Die-wall friction effects can be minimized with smooth surface dies. The effects are also minimized in simply shaped, low-aspect-ratio (height to diameter) parts. Internal and topical lubricants can aid processing .

Experiments revealed density gradients in isostatically pressed compacts where no die-wall frictional forces are present. This suggests that interparticle frictional forces also play an important role in compaction process and in determining the density gradients in a pressed compact [115]. Factors such as particle packing, pressing conditions, and discrete particle-particle and particle-die wall interactions all influence powder-compaction behavior. Compaction behavior is commonly assessed by monitoring how density changes as a function of the applied pressure

In order to investigate the influence of plasticizer to the compatibility of the powders and to the properties of sintered material, mixtures with 0, 1, 2 and, 3 wt.% of paraffin wax were produced, with the graphite addition 16,8 wt.% (Table 5). It was expected that paraffin wax addition reacts as a lubricant between oxide powder particles and therefore decreases the density gradient and changes of shape (warping) during sintering process. As the compaction pressure was expected to have significant influence to the green density gradient, the mixtures were pressed with 50, 80 and 120 MPa. The green parts were sintered according to the carbothermal reduction sintering route (Fig. 17).

The warping behavior and rate of sintered materials was investigated. Linear dimensions of sintered specimen cross sections were measured in different positions of specimen. The differences in the sintered part dimensions enables to estimate the warping rate after carburizing and sintering processes.

As seen in Figure 48 the specimen manufactured without additional plasticizer does not have pores neither in the core of the specimen nor in the outer layer. However, the specimen manufactured from the oxide mixture with 1 wt.% of additional plasticizer has significant porosity in the core zone of sintered body (Fig. 48 B).

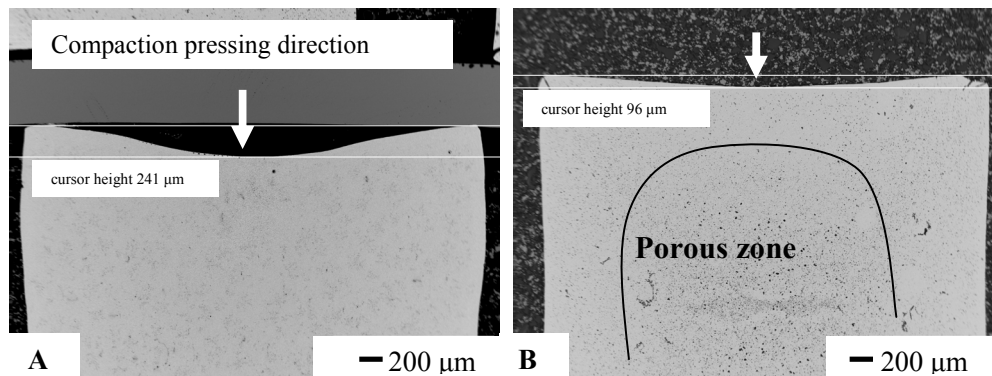


Figure 48. Cross sections of sintered parts: (A) without plasticizer and (B) with 1 wt.% plasticizer

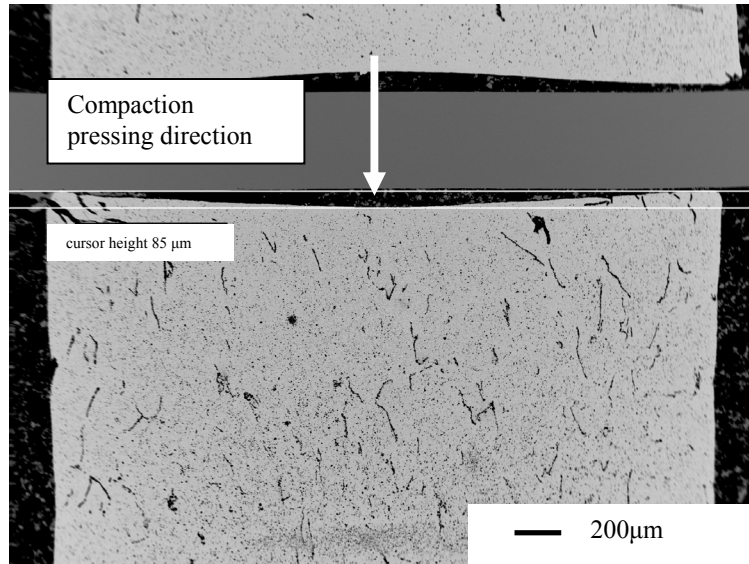


Figure 49. Cross sections of sintered part prepared with 3 wt.% of plasticizer addition

Figure 49 illustrates cross section structure of sintered material manufactured from the oxide powder with 3 wt.% of additional plasticizer. The high porosity and channels can be seen. The reason of highly porous microstructure can be the burnout of wax which causes the formation of long and broad channels through the WC-Co structure. However, as seen in Figs. 48 and 49 the warping rate of manufactured parts is different. The sintered body on Fig. 48 A has significantly bigger shape changes than parts in the Figs. 48 B and 49, which were manufactured using plasticizers. In conclusion, it was seen that utilization of plasticizers helps to reduce the shape changes caused by density gradients, but the burnout of plasticizers causes porosity which decrease mechanical properties of sintered hardmetal. The mechanical properties of hardmetals manufactured from mixtures with different plasticizer addition are presented in Table 8.

Pressing process must be designed and controlled to optimize green density and to minimize density gradients [114]. Density gradients, which are common in powder compacts, are undesirable because they promote differential densification that often results in warping and/or cracking during sintering. Uniform particle packing favors uniform compaction, and helps to ensure homogeneous densification and shrinkage during sintering [113, 116].

During powder pressing, the compaction pressure promotes consolidation by granule rearrangement and granule deformation. Particle-coordination number (the

number of nearest neighbors), green density, and compact strength all increases with increasing pressure, while the volume and size of the porosity in the compact decreases [117, 118].

Pressure of 80–200 MPa is common in hardmetal forming [2]. Though, the oxide powder mixture can't be used as conventional WC-Co because of the specific characteristics of oxides. So the optimum compaction pressure has to be determined by experimental way.

As the compaction pressure influences consolidation of powder particles and higher green density is achievable using higher pressure, the series of tests were made with compaction pressure 50, 80 and 120 MPa. The achieved green densities are given in Table 5.

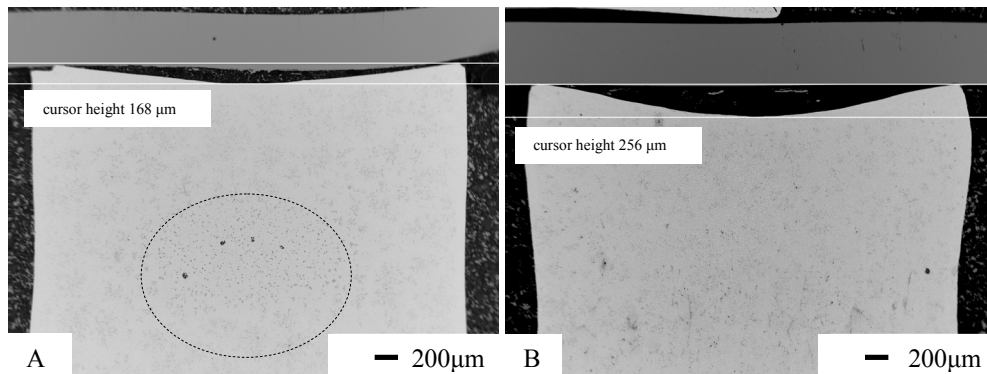


Figure 50. Cross sections of sintered parts produced with different compaction pressure: (A) 50 MPa and (B) 120 MPa. Both parts are manufactured without plasticizer

Figure 50 illustrates cross sections of sintered hardmetal manufactured by using different compaction pressures, 50 and 120 MPa, Fig. 50 A and B respectively. It can be seen that the specimen produced with lower compaction pressure (Fig. 50 A) has smaller shape changes as the specimen produced with higher pressure. Though, the core of the specimen in Fig. 50 A has porous microstructure. Specimen in Fig. 50 B has no porosity, but the shape of specimen has significantly changed during the sintering.

It was seen that the amount of plasticizer and compaction pressure influences the porosity and shape changes (see cursor height in Fig. 48, 49 and 50) of sintered specimens. Influence of green density of and density gradients in green parts needs further investigation.

#### 4.4.5 Mechanical properties of hardmetal produced by carbothermal reduction in combination with reactive sintering

The mechanical properties of tested materials are presented in Table 7. It was found that materials with a sufficient amount of additional graphite have the same mechanical properties as the hardmetal before recycling. The density of hardmetal produced using 16,8 wt% of graphite was  $14,0 \text{ g/cm}^3$ , which is the same as that of the hardmetal produced using conventional WC-Co powder and the conventional production method. The relatively high hardness and very low strength of hardmetals produced using a smaller amount of additional carbon can be explained by the formation of hard but brittle  $\eta$ -phase in the sintered specimen, as seen in Fig 37 A and Fig. 43. Due to the formation of  $\eta$ -phase the microstructure of hardmetal has some porosity which is caused by the lack of binder phase (Co).

Table 7 Mechanical properties of W-xC-15Co hardmetals with different levels of graphite, and methods of powder preparation

Material notation	Amount of additional carbon black [wt.%]	Hardness HV10	TRS [MPa]
R16B	16,0 wt. % C	1350	-
R16,5B	16,5 wt. % C	1200	1500
R16,8B	16,8 wt. % C	1350	2500
R17,0B	17,0 wt. % C	1100	2100
R16A	16,0 wt. % C	1300	-
R16,5A	16,5 wt. % C	1250	1300
R16,8A	16,8 wt. % C	1300	2500
R17,0A	17,0 wt. % C	1200	2100
Original Boart Longyear G30		1300	3000

Table 8 Mechanical properties of tested materials

Material notation	Density [ $\text{g/cm}^3$ ]	Hardness HRA (core)	Hardness HRA (surface)	TRS [MPa]
R16,8A	14,0	88	88	2500
R16,8A-P	13,5	85	88	2500
R16,8A-W1	13,4	83	89	1300
R16,8A-W2	13,1	78	89	1000
R16,8A-W3	12,9	77	88	600



The mechanical properties of recycled hardmetal with plasticizers addition in the manufacturing process are given in Table 8. As analyzed in previous chapter the plasticizer addition causes porosity, which reduces also mechanical properties of hardmetal. Data in Table 8 shows that compositions where wax was used, have on the surface same hardness values as original hardmetal, but the hardness in the core zone is much lower. It is in the correlation with microstructure analysis, which showed porosity specially, in the core of sintered specimens.

#### **4.5 Conclusions to the chapter**

A novel technology for production of hardmetal, from the mixture of  $WO_3$  and  $CoWO_4$  powders, was proposed using a combination of carborthermal reduction, carburizing and reactive sintering. The method has advantages of high productivity, since many production steps involved in the recycling of hardmetals can be eliminated. The preliminary calculations of energy consumption by recycling from oxidation to the sintered hardmetal was 4,5 kWh/kg. In Zinc process is it ca 5,5 kWh/kg. Though there are many aspects which have to be investigated further, the following conclusions can be drawn from the present data:

1. It is technically possible to combine reduction, carburization and reactive sintering. The gas emission during the sintering does not damage the green part and the sintering process can continue with carburization and liquid state sintering.
2. A pure phased, fine-grained WC-15 wt.% Co with excellent mechanical properties was obtained.
3. Densification is achieved mainly by shrinkage during solid state sintering. The linear shrinkage of samples was up to 40%.
4. The recycled hardmetal has the same chemical composition as the original material, as well as similar grain size and mechanical properties.

## 5. Wear resistance of hardmetals produced by reactive sintering method

Mechanical and tribological properties of cermets depend on the carbide/binder ratio, alloying compounds, and structure, but also on the technology used for manufacture of the carbide and the alloy. The size of carbide grains exerts significant influence on mechanical and tribological properties of hardmetals. It has been discovered that fine grained cermets are usually more erosion and wear resistant than middle-sized and coarse-grain cermets of the same chemical composition [119–121].

Abrasive wear is a detachment of the material from the surfaces in relative motion, caused by the sliding and rotating hard particles between the opposing surfaces; it is the most important one due to its destructive character [122]. The situation where an abrasive particle can freely slide and rotate between the two surfaces is known as a three-body abrasion [123]. In case of three-body abrasive wear the WC-Co hardmetals wear occurs through several processes, such as plastic deformation and extrusion of the binder phase [124–125], fragmentation [125–127] and separation of the carbide grains [128–130]. According to the literature [131] abrasive wear mechanism depends on the hardness ratio between the abrasive ( $H_a$ ) and material ( $H_m$ ). In case of WC-Co cermets with  $H_a/H_m$  ratio below 1.2 wear occurs through the preferential removal of the binder phase in conjunction with the fracture and detachment of the carbide grains. In case of hardness ratio above 1.2 the wear mechanism leads to fracture of WC grains and plastic deformation of WC and binder phase, due to the fact that the indentation of the abrasive grits into the materials surface is possible [131].

### 5.1 Abrasion

Abrasive wear coefficient of WC-Co cermets is predicted using Lancaster model [132]. In Figure 51 is exhibited the effect of the binder content on the wear coefficient on the WC-Co compositions. The wear coefficient increases in increase of Co volume fraction in compositions. The wear coefficient increases approximately linearly in increase of the binder content from 6 to 15 wt.% Co. The wear coefficient of materials with 20 wt.% Co is somewhat higher. This could be explained by decreasing hardness in increase of binder content. According to [132] the low or high level of abrasive wear occurs through hardness ratio between the abrasive ( $H_a$ ) and the worn material ( $H_m$ ). The hardness of hardmetals with 6–15 wt% Co (Table 4) is higher than for quartz sand (1100 HV) and therefore the abrasive grits are incapable of direct plastic deformation of material. Consequently the abrasive wear is low and does not depend on binder phase. The hardness of materials with binder content 20 wt.% is lower or close to the

hardness of quartz sand, consequently the abrasive particles have capability to penetrate into the material, plastically deform the material and consequently the volume wear of these composites is at high level. The wear coefficient however in case of all investigated binder contents is lower for reactive sintered hardmetals due to their more fined grained and homogeneous microstructure resulting in higher hardness.

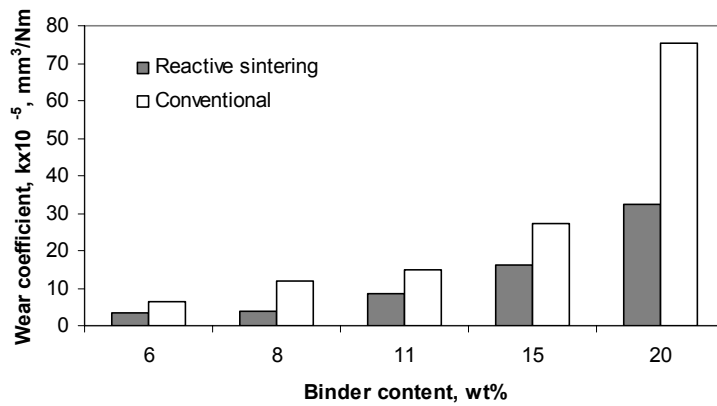


Figure 51. Wear coefficient of WC-Co hardmetals vs. binder content  $P=222\text{ N}$ ,  $s=263\text{ m}$

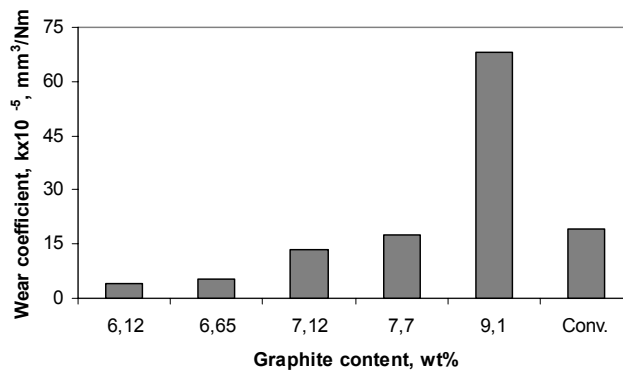


Figure 52. Wear coefficient of  $W-C_x-15\text{wt}\%Co$  hardmetals depending on graphite content in initial powder mixture

Wear resistance of reactive sintered WC-Co hardmetals also depends on the graphite content in initial powder mixture (Fig. 52). The three body abrasive wear resistance of W-C<sub>x</sub>-15wt.% Co hard metals decreases with increase of the graphite content in the initial powder mixture. As seen in Fig. 22, the alloys with graphite content below 7,12 wt.% contain hard and brittle η-phase in the structure, which results in increasing hardness and higher wear resistance. The alloys with graphite content over 7,7 wt.% have free graphite in the structure and as a result the wear resistance of those materials is low. Figure 53 shows that the volume loss of WC-Co hardmetals increases with the increase of the sliding distance as predicted by the Lancaster equation.

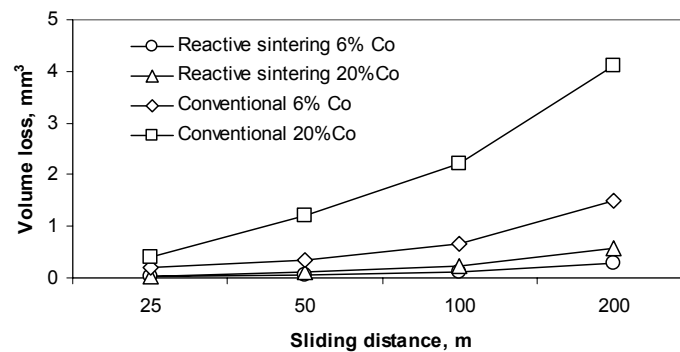


Figure 53. Volumetric wear of differently produced WC-Co hardmetals, depending on binder content and sliding distance,  $P=222\text{ N}$

Figure 54 indicates how the volume loss depends on bulk hardness of investigated composites. The volume loss decreases in increase of the bulk hardness of WC-Co alloys. The indentation depth of the abrasive particles into the surface increases as the hardness decreases. Increase in the binder content results in the decrease of the bulk hardness and following increase in the wear coefficient.

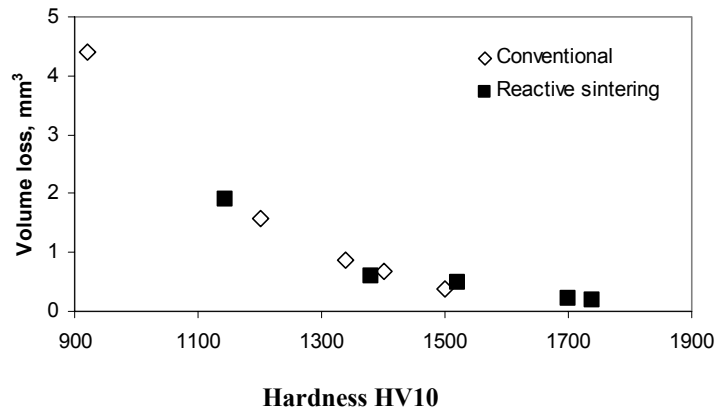


Figure 54. Volume loss vs. bulk hardness of WC-Co hardmetals produced by different technologies

Figures 55 and 56 illustrate the wear resistance of recycled hardmetals versus conventional hardmetals. It was seen that the volume loss of recycled hardmetal is on the same level with conventional materials or even better in the case of lower binder content (Fig. 56).

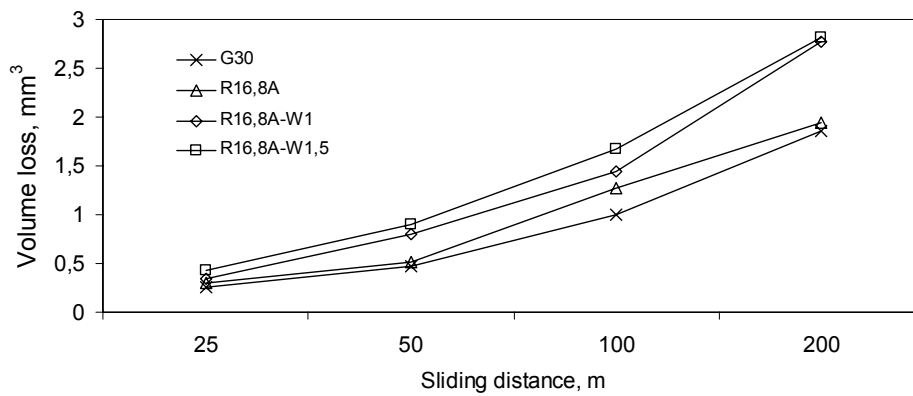


Figure 55. Volume wear of original vs. recycled WC-15 wt.% Co hardmetals, depending on content and sliding distance,  $P=40\text{ N}$

As it was shown in the previous chapter, the use of plasticizers in the recycling process affects the density of sintered materials. It was seen that the porosity is located

in the core of the sintered body, since the surface layer is mostly free of pores. Taking that fact into account, the density of all tested WC- 15 wt.% Co materials was taken 14,04 according to the density of conventional G30 hardmetal. The porosity in the core of sintered materials were not attended to the calculations of volumetric loss, because only the surface layer of the tested materials was worn. Figure 55 shows that the recycled materials with plasticizer addition have lower wear resistance then the conventional material. It can be explained by several bigger pores or channels which were detected in the surface layer of sintered hardmetal. The channels can be generated by the burnout of plasticizer during the sintering process.

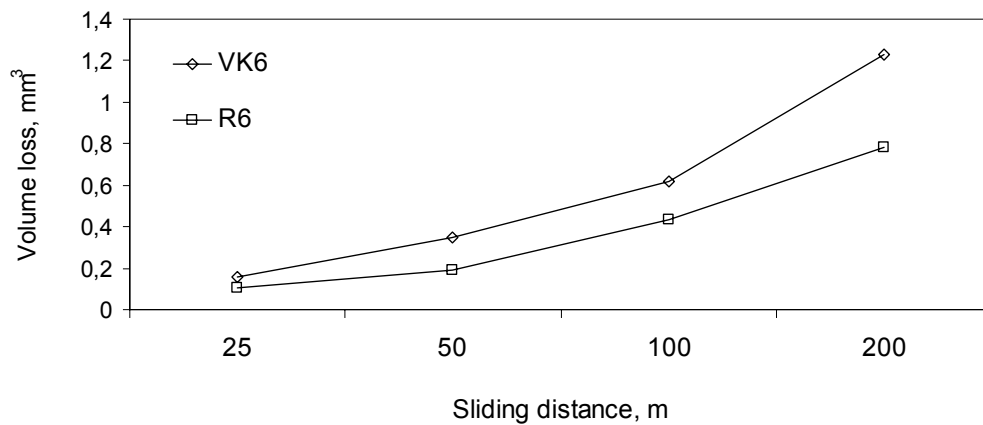


Figure 56. Volumetric wear of original(VK6) vs. recycled WC- 6 wt.% Co hardmetal (R6), depending on sliding distance,  $P=40\text{ N}$

## 5.2 Wear mechanism in abrasion

The mechanism of material removal in case of three - body abrasive wear of the hardmetal by  $\text{SiO}_2$  grits has not been studied in details. In Figure 57 is exhibited a wear track in the surface of WC-6wt.% Co grade cermets.

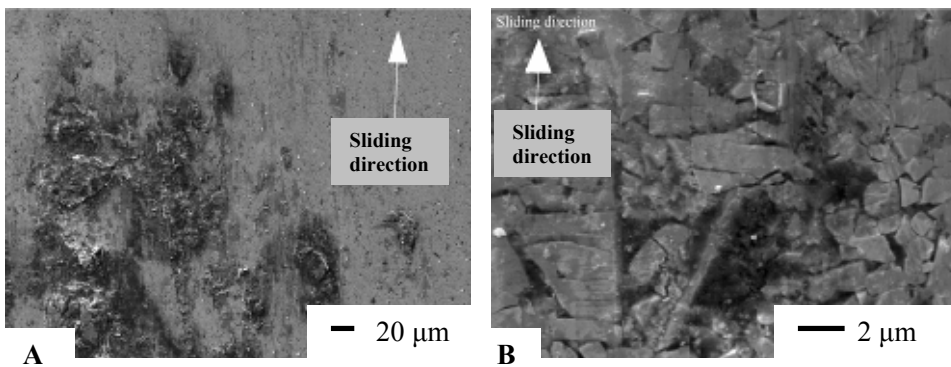


Figure 57. Worn surface of WC-6wt.% Co hardmetal

Since the tungsten carbide grains are harder (WC-HV2240), than the abrasive  $\text{SiO}_2$  grits (HV1100), the latter cannot penetrate into the carbide phase. At a ratio of about 1,2  $H_a/H_m$  there is a change in wear mechanism, because above of this ratio the indentation of the abrasive particle into the material surface is possible. First marks of damage in the surface of WC-Co hardmetals are visible after a couple of meters. Rolling silica sand particles are not able to damage the carbide grains, but they deform plastically the softer binder phase below and between carbide grains.

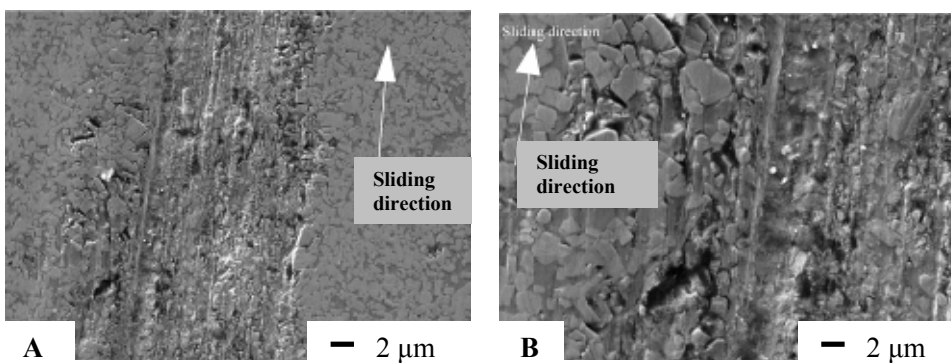


Figure 58. Worn surface of WC-20wt.%Co hardmetal

In case of low binder content material i.e. the materials which are harder than the abrasive a plastic deformation of the carbide framework takes place, leaving behind shallow grooves or craters (Fig. 57 A); it is followed by the fragmentation of the carbide phase with removal of those fragments until all grain is removed (Fig. 57 B). In Figure 57 B is visible the grain debonding and pullout and fracturing of carbide grains.

In case of WC-Co hardmetals with high binder content (Fig. 58), when the material is softer than the abrasive the crushing of carbide framework takes place at the beginning of wear process. In Figure 58 is exhibited the worn surface of WC-20wt.% Co material, which is filled with deep grooves and craters. After crushing the carbide framework, its fragments are pressed into materials surface; some of the binder is squeezed out onto the surface and then wiped off. Material loss from the surface leaves behind various shape and size wear scars and holes (Fig. 58 B). It is evident that the binder extrusion is rate controlling factor and the wear rate depends on the binder content. Fatigue of surface layers of the material occurs through the mechanical deformation of the surface, which results in spalling type of failure; subsurface fatigue leads to cracks formation (Fig. 59 B), which penetrates deeper into the material.

As seen in cross section view (Fig. 59), then in case of high binder content materials (Fig. 59 B) the formation of sub surface cracks of carbide grains and extrusion of binder phase is visible. In case of low binder content material the extrusion of binder phase and although some cracks crosswise to the material surface is visible, due to the brittleness of the material (Fig. 59 A).

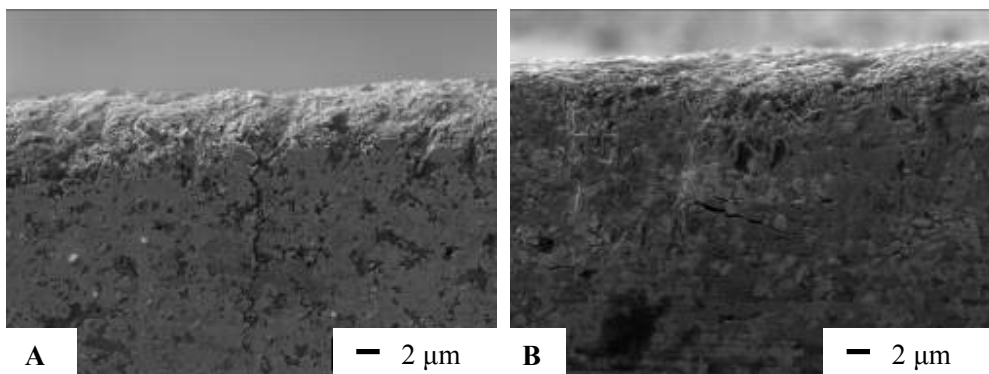


Figure 59. Cross section of the wear spot of WC-Co hardmetals: (A) 6wt.% Co, (B) 20wt.% Co



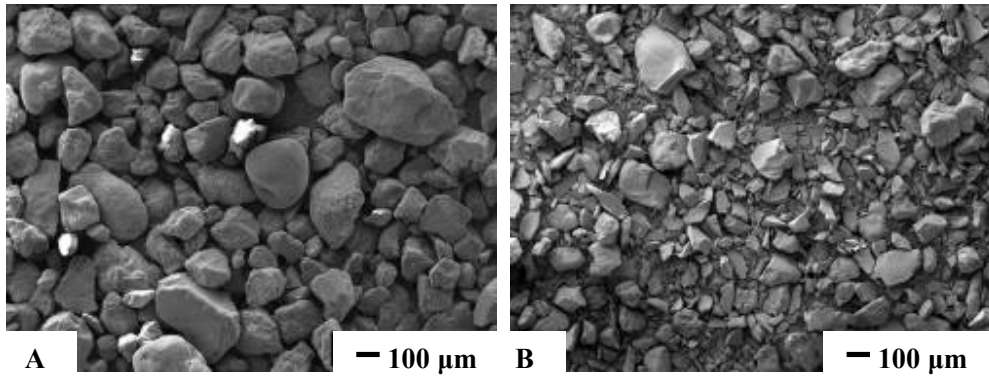


Figure 60. Abrasive used in tests: (A) before test and (B) after test

In Figure 60 is exhibited the abrasive used in tests before and after the test. Because the high pressure is applied during the tests most of the abrasive is crushed into smaller particles.

#### 5.4 Erosion

The abrasive erosion rate of the WC-Co composites depends on the graphite content in the initial powder mixture (Fig. 61 A). If the graphite content in the initial powder exceeds 7,7% the erosion resistant fall abruptly. The erosion rate of the WC-Co hardmetals depends also on the carbide/binder ratio (Fig. 61 B). If the amount of the binder increases, the erosion rate increases in the cases of both conventional and reactive sintered alloys. This is associated with the decrease in the hardness of the composites with higher binder content. The reactive sintered composites are somewhat harder than conventional composites of the same chemical composition and as a result more wear resistant.

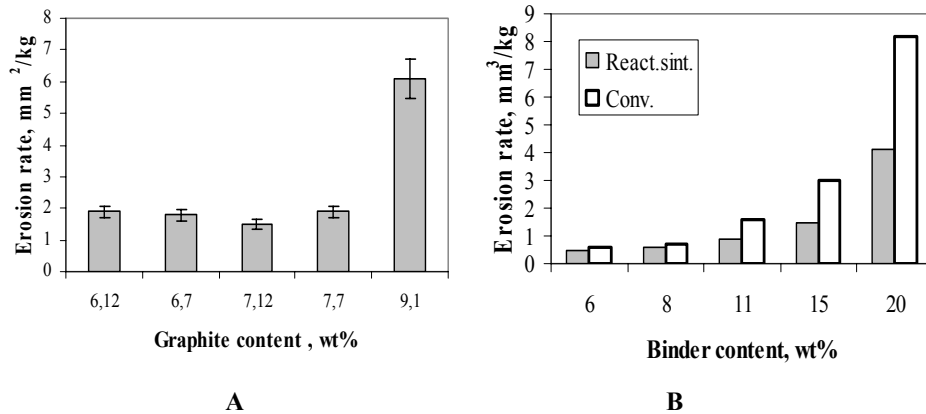


Figure 61. Erosion rate of the WC-Co composites vs. graphite content in the initial powder mixture (A) and binder content (B)

Figure 62 shows the erosion wear rates of conventional and recycled hardmetals. It was seen that the recycled hardmetal has the same wear resistance as the conventional material. It can be explained with the similar mechanical properties. Also it was seen that close correlation exists between abrasive wear and abrasive-erosion.

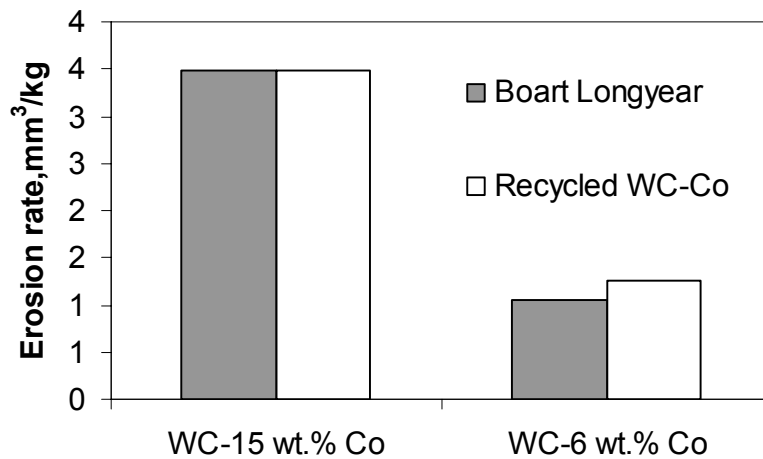


Figure 62. Erosion rates of the conventional Boart Longyear and recycled hardmetals

## 5.4 Conclusions to the chapter

The following conclusions can be drawn from the experimental study:

1. Investigated materials were produced via reactive sintering. Reactive sintering method enables to produce fine grained hardmetals with superior properties with lower costs compared to materials produced via conventional technology;
2. Wear performance of WC-Co hardmetals depends on the carbide to binder ratio and on the materials producing method. Reactive sintered hardmetals exhibited 10 – 40 % higher wear resistance compared to hardmetals produced by conventional technology. Wear rate increases with an increase in binder content, which corresponds to a decrease in the bulk hardness.
3. The optimal amount of carbon content in initial powder mixture on the abrasive wear resistance of those materials were investigated, higher wear resistance exhibited hardmetals with lower carbon content due to the higher hardness of those compositions. According to the experiments, maximum hardness and wear resistance can be achieved by reactive sintering using less than 7,12 wt.% of graphite.
4. Three-body abrasive wear mechanism of the WC-Co hardmetals depends on the hardness  $H_a/H_m$  ratio. When hardness of the abrasive particles is higher compared to materials hardness, plastic deformation of surface takes place. The materials loss during abrasive wear is a result of the extrusion of the binder phase, fracturing of the carbide grains and carbide network and moving carbide grains. If hardness of the abrasive particles is lower than materials hardness, deformation the carbide framework takes place, followed by the fragmentation and removal of the carbide phase by low-cycle fatigue mechanism.

## Conclusions

Technology for the production of bulk WC-Co hardmetal from a mixture of  $\text{WO}_3$ ,  $\text{CoWO}_4$  and graphite by way of carbothermal reduction and reactive sintering was investigated. The main conclusions of the present thesis are as follows:

1. A novel cost-effective (low investments costs, low energy consumption) technology for hardmetals recycling was proposed. It was proven, that the hardmetals can be synthesized directly from the mixture of  $\text{WO}_3$ ,  $\text{CoWO}_4$  and graphite powders, using a combination of carbothermal reduction, carburizing and reactive sintering. The method has advantages of high productivity, since many production steps involved in the conventional recycling routes can be eliminated.
2. Studied method for recycling lies in the carbothermal reduction of compacted  $\text{WO}_3+\text{CoWO}_4+\text{C}$  green parts in combination with subsequent reactive sintering in a vacuum furnace. The test showed that despite the gas emission during the reduction, it is possible to combine reduction with reactive sintering. It was seen that the mechanical properties of achieved hardmetals are on the same level with the conventional ones.
3. A technology for production of submicron ( $d < 1 \mu\text{m}$ ) hardmetal from elemental powders of W, Co and C (in the form of graphite) by way of reactive sintering was developed. The resulting alloys had higher hardness, erosion and wear resistance in comparison with the alloys produced with the conventional technologies. Grain growth inhibitors (VC,  $\text{Cr}_3\text{C}_2$ ) addition before reactive sintering reduced carbide grain size and rise hardness remarkably.
4. Dense WC-Co formed during liquid phase sintering. Carburization takes place in temperature range 1050–1200 °C because Co acts as a catalyst in the carburizing reaction and preferably milled powder mixtures. This low carburizing temperature was found to minimize the WC grain growth.
5. The mechanical properties of the reactively sintered hardmetals depend on the carbide to binder ratio, graphite content in initial powder mixture and alloying additives. During sintering some loss of carbon took place. This drawback can be avoided, adding some “extra” carbon black to the W and Co powder mixture in order to compensate the decarburization in the furnace during sintering.

## References

- [1] K.J.A. Brookes, World Directory and Handbook of Hardmetals and Hard Materials 6th ed., International Carbide Data, Hertfordshire (1996) 9.
- [2] B. Aronsson, H. Pastor, Cemented Carbide Powders and Processing, Powder Metallurgy: An Overview, The Institute of Metals, London GB, (1991).
- [3] B. Aronsson, Influence of processing on properties of cemented carbide, Powder Met., 30 3 (1987) 175-181.
- [4] A.N. Zelikman and L.S. Nikitina, Wolfram, (Tungsten), Izdat. Metallurgiya, Moskva, (1978) 272.
- [5] F. Bensovsky, K. Swars, Wolfram, Ergänzungsband Al Metall, Technologie, Gmelin Handbuch der Anorganischen Chemie, System Nr.54 Springer Verlag, Berlin, (1979) 241.
- [6] B.D. Kieffer, Recycling systems with particular reference to the zinc process, Proceedings of the second International Tungsten Symposium, San Francisco, (1982) 103-114.
- [7] K. Vadasdi, R. Olah, I. Szylassy and A. Jeszensky, Preparation of APT, by means of electrodialysis and solvent extraction, Proceedings of the 11th International Plansee-seminar'85: New applications, recycling and technology of refractory metals and hard materials, 1 (1985) 77-89.
- [8] G. S. Upadhyaya, Cemented tungsten carbides: production, properties, and testing, Noyes Publications, Westwood, New Jersey, 1998.
- [9] A.I. Vasil'eva, Ya. I. Gerasimov and Ya. P. Simanov, Equilibrium constant for the reaction of reduction of tungsten oxides by hydrogen, (in Russian) Zhur. Fiz. Khim., 31 3 (1957) 682-691.
- [10] R. Haubner, W.D. Schubert, E. Lassner and B. Lux, Über den Einfluss von P und Si auf die Reduktion von  $WO_3$  zu W mit Wasserstoff, Intern. J. Refract. & Hard Metals, 6 2 (1987) 111-116.
- [11] R. Haubner, W.D. Schubert, E. Lassner and B. Lux, Einfluss von Eisen und Nickel auf die Reduktion von Wolframoxid zu Wolfram, Intern. J. Refract. & Hard Metals, 7 1 (1988) 47-54.
- [12] D.S. Parsons, The reduction of tungsten oxides by hydrogen, Electrochem. Technol., 3, 9/10 (1965) 280-283.
- [13] J. Qvick, Use of oxygen probes to study and control the atmosphere during reducing of tungsten oxide, Intern. J. Refract. & Hard Metals, 7 4 (1988) 201-205.
- [14] T.Z. Ji, W.Y. Fang and L.J. Bo, Multidimensional regression equations for forecasting particle size of tungsten powder, Intern. J. Refractory & Hard Metals, 4 4 (1985) 166-171.

- [15] Z. Tao, Production of submicron tungsten powder by hydrogen reduction of  $WO_3$ , Intern. J. Refract. & Hard Metals, 5 2 (1986) 108-112.
- [16] P. Borchers, Processing of tungsten, Proceedings of the First International Tungsten Symposium. Stocholm, (1979) 64-77.
- [17] E. Rudy, St. Windisch and J.R. Hoffman, Ternary phase equilibria in transition metal-boron-carbon-silicon systems. Part I. Related binary systems. Volume VI: W-C system: supplemental information on the Mo-C system, Technical Report no. AFML-TR-65-2, I VI (1966) 79.
- [18] B. Uhrenius, Calculation of the Ti-C, W-C and Ti-W-C phase diagrams, Calphad, 8 2 (1984) 101-119.
- [19] A. Hara and M. Miyake, Studies on the formation process of tungsten carbide powder from tungsten powder, Planseeber. Pulvermetall., 18 (1970) 90-110.
- [20] L.V. McCarty, R. Donelson and R.F. Hehemann, A diffusion model for tungsten powder carburization, Metall. Trans., 18A (1987) 969-974.
- [21] T. Zhengji, Production of fine quality tungsten carbide, Intern. J. Refract. & Hard Metals, 7 4 (1988) 215-218.
- [22] U. Seeker and H.E. Exner, Eigenschaften unterschiedlich hergestellter wolframkarbidpulver und ihr Verhalten bei der Hartmetallherstellung, Metall, 40 12 (1986) 1238-1247.
- [23] F.C. Nava Alonso, M.L. Zambrano Morales, A. Uribe Salas and J.E. Bedolla Becerril, Tungsten trioxide reduction carburization with CO-CO<sub>2</sub> mixtures: kinetics and thermodynamics, Intern. J. Mineral Processing, 20 (1987) 137-151.
- [24] J. M. Gomes, A. E. Raddatz and T.G. Carnahan, Preparation of tungsten carbide by gas sparging tungstate melts, Proceedings of the third International Tungsten Symposium. Madrid, (1985) 96-112.
- [25] T.D. Halliday, F.H. Hayes and F.R. Sale, Thermodynamic considerations of the production of Co/WC mixture by direct gas phase reduction/carburization reactions, in Industrial Use of Thermochemical data, Proc. Conf. Chem. Soc. 1979; Spec. Publ. Chem. Soc. 34 (1980) 291-300.
- [26] Ushijima K. Production of WC Powder from  $WO_3$  with Added  $Co_3 O_4$ . Japan Metal Society Journal, 42 (1978) 871-875.
- [27] S. Takatsu, A new continuous process for production of WC-Co mixed powder by rotary kilns, Powder Metal International, 10 (1978) 13-15.
- [28] W.D.Schubert, A.Bock, B.Lux, General Aspects and Limits of Conventional Ultrafine WC Powder Manufacture and Hard Metal Production, Int. J. Refr.Metals & Hard Mater. 13 (1995) 281-296.
- [29] L.J.Prakash, Application of Fine Grained Tungsten Carbide Based Cemented Carbides, Int. J. of Refr. Metals & Hard Materials, 13 (1995) 257 - 264.

- [30] G.Gille, B.Szesny, K.Dreyer, H.van.den Berg, J.Schmidt, T.Gestrich, G.Leitner, Submicron and Ultrafine Grained Hardmetals for Microdrills and Metal Cutting Inserts, *Int. J. of Refr. Metals & Hard Materials*, 20 (2002)3-22.
- [31] Ban ZG, Shaw LL. Synthesis and processing of nanostructured WC-Co materials. *J Mater Sci*, 37 (2002) 3397-403
- [32] Berger S, Porat R, Rosen R. Nanocrystalline materials: a study of WC-based hard metals, *Prog. Mater. Sci.*, 42 1-4 (1997) 311-20.
- [33] L.Gao,B.H.Kear, Synthesis of nanophase WC powder by a displacement reaction process, *Nanostructured Materials*, 9 (1997) 205-208.
- [34] L.E.McCandlish, B.H. Kear, Processing and properties of nanostructured WC-Co, *Nanostructured Materials*, 1 (1992) 119-124.
- [35] Z.Fang, J.W.Eason, Study of nanostructured WC-Co composites, *Int. J. of Refr. Metals & Hard Materials*, 13 (1995) 297-303.
- [36] M-H. Lin, Synthesis of nanophase tungsten carbide by electrical discharge machining, *Ceramic International*, 31 (2005)1109-1115.
- [37] J.C.Kim, B.K.Kim, Synthesis of nanosized tungsten carbide powder by the chemical vapor condensation process, *Scripta Materials*, 50 (2004) 969-972.
- [38] W.Chang, G.Skandan, S.C. Danforth, B.H.Kear and H.Hahn, Chemical apor processing and applications for nanostructured ceramic powders and whiskers, *Nanostructured Materials*, 4 (1994) 507- 520.
- [39] J.Grabis, I.Zalite, D.Jankovica, D.Rasmane, Preparation of nanosized W and WC based powders and their processing, *Proc. of Estonian Academy of Science, Engineering*, 4 (2006) 349-357.
- [40] C.Koch, Synthesis of nanostructured materials by mechanical milling: problems and opportunities, *Nanostructured Materials*, 9 (1997) 13-22.
- [41] L.L.Shaw, Synthesis and processing of nanostructured WC-Co materials, *J.of Materials Science*, 37 (2002) 3397-3403.
- [42] W.Liu,X. Song, J. Zhang, Guozhen Zhang, X. Liu, Thermodynamic analysis for in situ synthesis of WC-Co composite powder from metal oxides, *Materials Chemistry and Physics*, 109 2-3 (2008) 235-240.
- [43] M. Sherif El-Eskandarany, Amir A.Mahday, H.A.Ahmed, A.H.Amer, Synthesis and Characterizations of Ball-Milled Nanocrystalline WC and Nanocomposite WC-Co Powders and Subsequent Consolidations, *J. of Alloys and Compounds*,312 (2000) 315-325.
- [44] M. Sherif El-Eskandarany, Fabrication of nanocrystalline WC and nanocomposite WC-MgO refractory materials at room temperature, *J.of Alloys and Compounds*, 296 (2000) 175-182.
- [45] J.Gurland, A study of the effect of carbon content on the structure and properties of sintered WC-Co alloys”, *Trans.AIME*, 200 (1954) 285-290.

- [46] A.Petersson. Sintering shrinkage of WC-Co and WC-(Ti,W)C-Co materials with different carbon contents, *Int. J.of Refr. Metals & Hard Materials*, 22 (2004) 211-217.
- [47] M.Sommer, W-D Shubert, E.Zobetz, P.Warbachler, On the Formation of Very Large WC Crystals During Sintering of Ultrafine WC-Co Alloys, *Int.J. of Refract. Metals & Hard Materials*, 20 (2002) 41-50.
- [48] P.Arato, L.Bartha, R.Porat, S.Berger, A.Rosen, Solid or liquid phase sintering of nanocrystalline WC-Co hardmetals, *Nanostructured Materials*, 10 (1998) 245-255.
- [49] J.-H. Ahn, Y.Kim, Activated and/or liquid phase sintering of mechanically milled nanocrystalline powders, *J. of Metastable and Nanocrystalline Materials*, 2-6 (1999) 147-152.
- [50] B. Meredith, D.R.Milner, Densification mechanisms in the tungsten carbide-cobalt system, *Powder Metallurgy*, 19 (1976) 38-45.
- [51] D.F. Carroll, Sintering and microstructural development in WC-Co-based alloys made with superfine WC powder, *Int. J. of Refr. Metals & Hard Materials*, 17 (1999) 123-132.
- [52] A. Lackner, M. Rieder, Recycling of cemented carbides, EURO-PM 2008, EPMA European Hard Materials Group, (2008).
- [53] K.Stjernberg, J.Jr. Johnson, Proc. International Conference on Powder Metallurgy and Particulate Materials, (1998) 173.
- [54] Reporte of the Rare Metal Brach, Mining Council in Ministry of Economy, Trade and Industry of Japan, Going Steady Supply of Rear Metals Supporting Frontier, 2000 21.
- [55] K. Vadasdi, Effluent-free manufacture of ammonium paratungstate (APT) by recycling the byproducts, *Int. J. of Refractory Metals and Hard Materials*, 13 (1995) 45-59.
- [56] G.Lee, G.H. Ha, Synthesis of WC/Co composite powder from waste WC/Co hard metal alloy, *Proceedings of Euro PM2004, PM Tool Materials* (2004).
- [57] S. Venkateswaran, W.D. Schubert, B. Lux, *Int. J. of Refractory Metals and Hard Materials*, 14 (1996) 263.
- [58] ASTM International Handbook Committee: *ASTM Handbook Vol.7 Powder Metal Technologies and Applications*, ASM International, New York, 1998 194.
- [59] F. Clin and H. Pastor, Sur une technique de tri par densité de déchets de carbures cimentés en vue de leur valorisation et recyclage, *Industrie Minérale, Mines et Carrières, Les Tehniques*, 1987.
- [60] B.F. Kieffer and E. Lassner, Reclamation of tungsten containing scrap material: economic and technical aspects, *Proceedings of the fourth International Tungsten Symposium. Vancouver*, (1987) 59-67.



- [61] T.Kojima, T. Shimizu, R. Sasai, H. Itoh, *Journal of Material Science*, 40 (2005) 5167-5172.
- [62] R. Sasai, A. Santo, T. Shimizu, T. Kojima, H. Itoh, Development of new recycling system of WC-Co cermet scraps, *Proc. 1st International Conference on Waste Management and the Environment*, (2002) 13.
- [63] N.F. Gao, R. Sasai, H. Itoh, Y. Suzumura, Recycling process for yttria-stabilized tetragonal zirconia ceramics using a hydrothermal treatment, *Journal of Material Cycles and Waste Management*. Jpn 9 1 (2007).
- [64] N.Gao, F.Inagaki, R.Sasi, H.Itoh, K.Watari, *Key Engineering Materials*, 280-283 (2001) 1480
- [65] Y. Fujiwara, *Metall Powder Report*, 42 (1987) 871.
- [66] J.L. Dassel and D.R. de Halas, Applications for zinc-reclaimed powders in the cemented carbide industry, *Proceedings of a M.P.R. Conference held in London, UK, Paper no.7* (1988) 15.
- [67] Pat. 3595484 USA, Reclamation of refractory carbides from carbide materials, 27.07.1971
- [68] B.F. Kieffer and E. Lassner, *Tungsten Recycling in Today's Environment*, BHM 139 (1994) 340.
- [69] Pat. 3953194 USA, Method for regenerating cemented carbides, 06.02.75.
- [70] Liu W, Song X, Zhang J, Zhang G, Liu X. Preparation of ultrafine WC-Co composite powder by in situ reduction and carbonization reactions, *International J. of Refractory Metals & Hard Materials*, 27 (2009) 115-121
- [71] Liu W, Song X, Wang K, Zhang J, Zhang G, Liu X. A novel rapid route for synthesizing WC-Co bulk by in situ reactions in spark plasma sintering. *Materials Science and Engineering*, A499 (2009) 476-481.
- [72] C. Meissl, Edtmaier C, Schubert WD, Schön A, Bock A, Zeiler B. Sintering of Tungsten Carbide - Cobalt Composite Powders, *Proc. 16th Plansee Seminar*, 2 (2005) 631-640.
- [73] T.E.Babutina, I.V.Uvarova, L. D.Konchakovskaya and L.N. Kuzmenko, *Powder Metallurgy and Metal Ceramics*, 43 (2004) 3-4.
- [74] Z.G. Ban and L.L. Shaw, On the reaction sequence of WC-Co formation using an integrated mechanical and thermal activation process, *Acta Mater.*, 49 (2001) 2933-2939.
- [75] B.K. Kim, G.H. Ha, G.G. Lee, D.W. Lee, Structure and properties of nanophase WC/Co/VC/TaC hardmetal, *Nanostructured materials*, 9 (1997) 233-236.
- [76] P. Arato, L. Martha, R. Porat, S. Berper, A. Rosen, Solid or liquid phase sintering of nanocrystalline WC/Co hardmetals, *Nanostructured Materials* 10 (1998) 245-255.

- [77] S. Decker, A. Lofberg, J.M. Bastin, A. Frennet, *Catalysts Lett*, 44 (1997) 229-239
- [78] H.Yuehui, Chen Libao, Huang Baiyun, P. K. Liaw, Recycling of heavy metal alloy turnings to powder by oxidation–reduction process, *International J. of Refractory Metals&Hard Materials*, 21 (2003) 227-231.
- [79] L. Erik,S. Wolf-Dieter, *Tungsten:Properties, Chemistry, Technology of the Element Alloys, and Chemical Compounds*, NY, Kluwer Academic /Plenum Publishers, 1999.
- [80] G. Kris Schwenke, Thermodynamic of the hydrogen-carbon-oxygen-tungsten system as applied to the manufacture of tungsten and tungsten carbide,15th Int. Plansee Seminar, 2 (2001) 647-661.
- [81] Vanables DS, Brown ME. Reduction of tungsten oxides with hydrogen and with hydrogen and carbon. *Thermochimica Acta*, 285 (1996) 361-382.
- [82] V. I. Tret'yakov, V. K. Senchikhin, N. K. Vaskevich, et al., Effect of cobalt on carbidizing treatment of tungsten with methane, *Poroshk. Metall.*,11 (1990) 32–36.
- [83] V.P. Bondarenko, E.G. Pavlotskaya, L.M. Martynova, Thermochemical method for regeneration of hard alloys waste in methane-hydrogen gas ambient of precision composition, *Methods and Means of Providing high Quality Preparation of Machine Components*, Nizhnii Novgorod, 2001.
- [84] M.Miyake,A.Hare,T.Sho,Y.Kawabata, *P/M'78 SEMP*, 2 (1978) 94
- [85] H.S. Im,J.M. Hur, W.J. Lee, A Study of reduced and carburized reactions in dry-milled  $WO_3+Co_3O_4+C$  mixed powders with different carbon content,*Materials Science Forum*, (2001) 534-536
- [86] Vanables DS, Brown ME. Reduction of tungsten oxides with carbon.Part1- Thermal analyses, *Thermochimica Acta* , 282/283 (1996) 251-264.
- [87] Jing-Chie Lin JC, Jain-Yuan Lin JY, Shie-Peir Jou SP. Selective dissolution of the cobalt binder from scraps of cemented tungsten carbide in acids containing additives.*Hydrometallurgy*, 43 1-3 (1996) 47-61.
- [88] K. Ushijima, K. Fuqii, Mechanism of WC formation from  $WO_3$  and added  $Co_3O_4$  and Co, *J. Jap. Int. Met.*, 9 (1978) 876-881.
- [89] K. Ushijima, *Powder Metallurgy International*, (1979) 158.
- [90] W.R. Blumenthal, H. Sheinberg, S.A. Bingert, Compaction issues in powder metallurgy, *MRS Bulletin*, 22 (1997) 12.
- [91] ASTM Standard B406-95 ,Standard Test Method for Transverse Rupture Strength of Cemented Carbide. published in *Annual Book of ASTM Standards*, 1995.
- [92] *Wear Resistance Assurance: gas-abrasive wear testing of materials and coatings with centrifugal accelerator*, GOST23.201-78, Publishing House of Standards, Moscow, 1978.

- [93] S. Mi, T. H. Courtney, Synthesis of WC and WC-Co Cermets by Mechanical Alloying and Subsequent Hot Isostatic Pressing, *Scripta Materialia*, 38 (1998) 171-176.
- [94] X. Wang, Z. Z. Fang, H. Y. Sohn, Grain growth during the early stage of sintering of nanosized WC-Co powder, *Proc. of European Conference of Hard Materials*, 1 (2006) 83-88.
- [95] V. Bounhoure, Influence of the C-potential and of Cr<sub>3</sub>C<sub>2</sub> Addition on the Solid-State Sintering Mechanisms of the WC-Co Alloys, *Proc. Of European Powder Metallurgy Congress*, 3 (2007) 343-348.
- [96] M. Viljus, J. Pirso, S. Letunoviš, Low temperature synthesized of WC and its usability for fine-grained hardmetal, *Proc. of European Powder Metallurgy Conference PM2006 – Hard Materials Powders*, (2006) 281-285.
- [97] C. H. Allibert, Sintering features of cemented carbides WC-Co processed from fine powders, *Int. J. Refr. Metals and Hard Mater.*, 19 (2001) 53-61.
- [98] A. Upadhyaya, D. Arathy, G. Wagner, *Advances in Sintering of Hard Metals, Materials and Design*, 22 (2001) 499-506.
- [99] T. Ya. Kosolapova, *Carbides: Properties, Production, and Applications*, New York, Plenum, 1971.
- [100] F. Arenas, I. B. de Arenas, J. Ochoa, S.-A. Cho, Influence of VC on the microstructure and mechanical properties of WC-Co sintered cemented carbides, *Int. J. Refract. Met. Hard Mater.* 17 (1999) 91-97.
- [101] S.-A. Cho, A. Hernandez, J. Ochoa, J. Lira-Olivares. Phase relations, microstructure and mechanical properties of VC substituted WC-10Co cemented carbide alloys. *Int. J. of Refractory Metals & Hard Materials*, 15 (1997) 205-214.
- [102] L. H. Zhu, Q. W. Huang, H. F. Zhao, Preparation of nanocrystalline WC-10Co-0.8VC by spark plasma sintering, *Journal Mater Science Letter*, 22 (2003) 1631-1633.
- [103] C. Lin, E. Kny, G. Yuan, B. Gjuricic, Microstructure and properties of ultrafine WC-0,6VC-10Co hardmetals densified by pressure-assisted critical liquid phase sintering. *J. of Alloys and Compounds*, 383 (2004) 98-102.
- [104] S. Luyckx, M. Z. Alli, Comparison between V<sub>8</sub>C<sub>7</sub> and Cr<sub>3</sub>C<sub>2</sub> as grain refiners for WC-Co Mater. *Design*, 22 (2001) 507-510.
- [105] M. Sommer, W.-D. Schubert, E. Zobetz, P. Warbichler. On the formation of very large WC crystals during sintering of ultrafine WC-Co alloys. *Int. J. of Ref. Metals & Hard Materials*, 20 (2000) 41-50.
- [106] M. A. Xueming, J. I. Gang, Z. Ling, D. Yuanda, Structure and properties of bulk nano-structured WC-Co alloy by mechanical alloying, *J. of Alloys and Compounds*, 264 (1998) 267 – 270.

- [107] Z.Z. Fang, Correlation of transverse rupture strength of WC-Co with hardness, *Int. J. of Refractory Metals & Hard Materials*, 23 (2005) 119 – 127.
- [108] Lee DR, Lee WJ. Fabrication of Nano-sized WC/Co Composite Powder by Direct Reduction and Carburization with Carbon. *Materials Science Forum*, 534-536 (2007) 1185-1188.
- [109] B.J. McEntire, in *Ceramic and Glasses, Engineered Materials Handbook vol. 4*, ASM International, 1991, 141
- [110] J.S. Reed, *Introduction to the Principles of Ceramic Processing*, John Wiley & Sons, New York, 1988, 329.
- [111] M.A. Occhionero, J.W. Halloran, *Sintering and Heterogeneous Catalysis, Materials Science Research*, vol. 16, Plenum Press, New York, 1984, p.89
- [112] M.D. Sacks, T.S. Yeh, S.D. Vora, *Ceramic Powder Processing Science*, Deutsche Keramische Gesellschaft, Köln, 1989, 693
- [113] J.S. Reed, *Introduction to the Principles of Ceramic Processing*, 2<sup>nd</sup> ed., John Wiley & Sons, New York, 1995, 397.
- [114] T. Garino, M.J. Readey, F.M. Mahoney, K.G. Ewsuk, J. Gieske, G. Stoker, S. Min, *Diversity into the next century*, SAMPE International, 1995, 610.
- [115] F.M. Mahoney, M.J. Readey, *Ceramic Compaction Models: Useful Design Tools or Simple Trend Indicators*, 1996.
- [116] K.G. Ewsuk, *Characterization of Ceramics*, Greenwich, (1993) 77
- [117] R.M. German, *Particle Packing Characteristics*, Metal Powder Industries Federation, New York, 1989.
- [118] E. Artz, *Acta Metall*, 30 (1982) 1883.
- [119] H.O. Pierson, *Handbook of Refractory Carbides and Nitrides*, 1996, 101-110.
- [120] E.T. Jeon, J. Joardar, S. Kang. Microstructure and tribo-mechanical properties of ultrafine Ti(CN) cermets. *Int. J. of Refractory Metals & Hard Materials*, 20 (2002) 207-211.
- [121] R. Chattopadhyay. *Surface wear: analysis, treatment and prevention*. ASM international. Materials Park. Ohio, 2001.
- [122] S. Letunovits, *Tribology of Fine Grained Cermets*, PhD Thesis of TUT, TTU Press, Tallinn, 2003.
- [123] J.A. Hawk, R.D. Wilson, *Tribology of Earthmoving Mining and Minerals Processing*, *Modern Tribology Handbook*, Vol.1-2., CRC Press, USA, 2001.
- [124] J. Larsen-Basse, C.M. Perrott, P.M. Robinson, *Abrasive wear of tungsten carbide/ cobalt composites*, *Mater Sci Eng*, 13 (1974) 83–91.
- [125] J. Larsen-Basse, *Friction in two-body abrasive wear of a WC-Co composite by SiC*, *Wear*, 205 (1997) 231–235.
- [126] A.J. Gant, M.G. Gee, *Abrasion of tungsten carbide hardmetals using hard counterfaces*, *Int. J. Refr. Metals & Hard Materials*, 24 (2006) 189–198.

- [127] B. Roebuck, M.G. Gee, Abrasion resistance of wide grained WC/Co hardmetals, In Proc of European powder metallurgy congress. PM 2002, 129–135.
- [128] K. Jia, T.E. Fischer, Abrasive wear of nanostructured and conventional cemented carbides, *Wear*, 200 (1996) 206–214.
- [129] C. Allen, M. Sheen, J. Williams, V.A. Pugsley, The wear of ultrafine WC–Co hard metals, *Wear* 250 (2001) 604–610.
- [130] P.H. Shipway, J.J. Hogg, Dependence of microscale abrasion mechanisms of WC–Co hardmetals on abrasive type, *Wear*, 259 (2005) 44–51.
- [131] I.M. Hutchings, *Tribology-friction and wear of engineering materials*, Edward Arnold, London, 1992.
- [132] J.K. Lancaster. The influence of substrate hardness on the formation and endurance of molybdenum disulphide films, *Wear*, 10 (1967) 103-107.

## List of publications

The majority of the contents of dissertation have been published in following authors original papers:

1. R. Joost, J. Pirso, T.Tenno, M. Viljus, Effect of Free Carbon on the Mechanical and Tribological Properties of Cemented Carbides. In: Proceedings of 7th International Conference of DAAAM Baltic Industrial Engineering, April 22–24 (2010) 450–455.
2. R. Joost, J. Pirso, M. Viljus, The Structure and Properties of Recycled Hardmetals. In: Proceedings Vol. 2 P/M Hard Materials: 17th Plansee Seminar 2009 International Conference on High Performance P/M Materials, Reutte, Austria, May 25–29 (2009) HM25/1–HM25/7.
3. J. Pirso, M. Viljus, R. Joost, K. Juhani, S. Letunoviš, Microstructure evolution in WC-Co composites during reactive sintering from nanocrystalline powders, In: Proceedings of the PM08 World Congress on Powder Metallurgy and Particulate Materials, Metal Powder Industry Publications Washington, NY, USA, June 12–16 (2008) CD-ROM.
4. R. Joost, J. Pirso, M. Viljus, The effect of carbon content on the mechanical and tribological properties of WC-Co cemented carbides, In: Proceedings of the 13th Nordic Symposium in Tribology, Nordtrib 2008, Tampere, Finland: June 10–13 (2008).
5. R. Joost, J. Pirso, M. Viljus, Recycling of hardmetal scrap to WC-Co powder by oxidation-reduction process, Proceedings of the 6th international conference of DAAAM Baltic industrial engineering, April 24–26 (2008) 449–454.

## **Abstract**

### **"Novel methods for hardmetal production and recycling"**

A new cost-effective technology for the production of bulk WC-Co composites from a mixture of  $WO_3$ ,  $CoWO_4$  and graphite by way of carbothermal reduction in combination with reactive sintering was developed. Waste hardmetals parts were fully oxidized into a mixture of  $WO_3$  and  $CoWO_4$ . Dense fine-grained compositions were produced from the oxide powder mixtures of  $WO_3$ ,  $CoWO_4$  and graphite by high energy milling in an attritor and a ball mill. The oxide powder mixtures containing carbon in the form of nanocrystalline graphite were pressed into compacts. The green parts were carbothermally reduced into WC and Co in a vacuum furnace. During carbothermal reduction tungsten monocarbide and cobalt were formed, and during liquid phase sintering the WC-Co alloy was formed in one cycle.

In order to investigate phase formation, microstructure evolution and mechanical properties, dense fine-grained WC-Co compositions were fabricated from the elemental powders of W, Co and C by high energy milling and following reactive sintering. The powders with nanocrystalline size were pressed to compacts and sintered. During solid state sintering the tungsten carbide was formed and during liquid phase sintering the WC-Co alloy was formed in one cycle.

The influence of different carbon content on phase composition, mechanical properties and linear shrinkage during solid and liquid state sintering is discussed. The microstructure of reactive sintered WC-Co hardmetal is fine-grained and identical to that of the original WC-Co microstructure. The reactive sintered WC-Co compositions are fine-grained, resulting with higher hardness, erosion and wear resistance, compared with conventional WC-Co hardmetals. The amount of additional carbon has a significant influence on the phase composition and mechanical properties of recycled hardmetals.

**Keywords:** Hardmetal, Recycling, Reactive Sintering, Microstructure Evolution, Carbothermal Reduction

## Kokkuvõte

### "Uudsed meetodi WC-Co kõvasulamite valmistamiseks ja taaskasutamiseks"

Doktoritöö käigus töötati välja ökonoomne ja uudne meetod WC-Co kõvasulamite valmistamiseks WO<sub>3</sub>, CoWO<sub>4</sub> ja grafiidi segust. Meetod põhineb karbotermilisel taandamisel ja sellele järgneval reaktsioonpaagutamisel. Väljatöötatud tehnoloogia aluseks on kõvasulamjäätmete oksideerimine WO<sub>3</sub> ja CoWO<sub>4</sub> seguks. Tekkinud segule lisatakse grafiit ning seejärel teostatakse kõrgenergeetiline jahvatus atriitoris või tavajahvatus kuulveskis. Peale jahvatamist pressitakse grafiidi ja oksiidide segust sobiva kujuga detailid. Detailide paagutamise käigus vaakumahjus taandab süsinik oksiidi ja reageerides wolframiga moodustuvad WC ning Co. Paagutamise vedelas faasis paakub WC-Co.

Faaside moodustumise, mikrostruktuuri arengu ja mehaaniliste omaduste uurimiseks viidi läbi katsed ka W, Co ja C pulbritega, mis jahvatati ja pressiti detailid. Järgneva reaktsioonpaagutuse käigus moodustus WC ning toimus detaili paakumine. Uuriti karbidiseerumise ja reaktsioonpaagutuse temperatuure ning paagutusaja mõju mikrostruktuurile. Katsed näitasid, et karbidiseerimise ja paagutamise saab läbi viia ühe tsüklina.

Töös uuriti lisatud grafiidi koguse mõju faaside moodustamisele, mehaanilistele omadustele ja paakumisel tekkivale joonkahanemisele. Reaktsioonpaagutamisega ümbertöödeldud materjali iseloomustab peeneteralne mikrostruktuur, mis on sarnane ümbertöödeldud materjali algse struktuuriga. Reaktsioonpaagutatud kõvasulami peeneteraline mikrostruktuur annab tavameetodidega võrreldes valmistatud kõvasulamitega suurema kõvaduse ning seepärast on uudsel meetodil valmistatud kõvasulamid ka suurema kulumiskindlusega. Töös on näidatud, et põhiline parameeter reaktsioonpaagutatud kõvasulamite omaduste mõjutamiseks on lisatud süsiniku hulk, mis määrab valmistatud materjali faasilise koostise.

**Märksõnad:** kõvasulam, taaskasutamine, reaktsioonpaagutus, mikrostruktuuri areng, karbotermiline taandamine.



## ELULOOKIRJELDUS

### 1. Isikuandmed

Ees- ja perekonnanimi Renee Joost  
Sünniaeg ja -koht 09.11.1978, Pärnu  
Kodakondsus Eesti

### 2. Kontaktandmed

Aadress Allika 1-36, Keila, 76610  
Telefon +372 5043239  
E-posti aadress renee.joost@ttu.ee

### 3. Hariduskäik

Õppeasutus (nimetus lõpetamise ajal)	Lõpetamise aeg	Haridus (eriala/kraad)
Nõo Realgümnaasium	1997	keskharidus
Tallinna Tehnikaülikool	2001	tootmistehnika, B Sc.

### 4. Keelteoskus (alg-, kesk- või kõrgtase)

Keel	Tase
eesti keel	emakeel
inglise keel	kõrgtase
saksa keel	kõrgtase
vene keel	kesktase

### 5. Teenistuskäik

Töötamise aeg	Tööandja nimetus	Ametikoht
2001 - 2003	AMI Doduco GmbH	insener
2003 - 2006	Lidl Eesti UÜ	projektijuht
2006 - 2007	Alka WMT OÜ	arendusjuht
2007 - ...	Tallinna Tehnikaülikool	teadur

6. Teadustegevus  
Kõvasulamite ümbertöötlemise ja reaktsioonpaagutuse tehnoloogia arendamine.
7. Kaitstud lõputööd  
T. Tenno, M Sc.
8. Teadustöö põhisuunad  
Loodusteadused ja tehnika. Protsessitehnoloogia ja materjaliteadus.
9. Teised uurimisprojektid  
TiC-NiMo reaktsioonpaagutus. Hõõrdelaagri materjalide uurimine.

## CURRICULUM VITAE

### 1. Personal data

Name Renee Joost  
Date and place of birth 09.11.1978, Pärnu

### 2. Contact information

Address Allika 1-36, Keila, 76610  
Phone +372 5043239  
E-mail renee.joost@ttu.ee

### 3. Education

Educational institution	Graduation year	Education (field of study/degree)
Nõo Realgümnaasium	1997	High school
Tallinna University of Technology	2001	Bachelor of Science

### 4. Language competence/skills (fluent; average, basic skills)

Language	Level
Estonian	mother tongue
English	fluent
German	fluent
Russian	average

## 5. Professional Employment

Period	Organisation	Position
2001 - 2003	AMI Doduco GmbH	engineer
2003 - 2006	Lidl Eesti UÜ	project manager
2006 - 2007	Alka WMT OÜ	development manager
2007 - ...	Tallinna Tehnikaülikool	researcher

## 6. Scientific work

Development of hardmetal recycling technology

## 7. Defended theses

T. Tenno, M Sc.

## 8. Main areas of scientific work/Current research topics

Natural Science and Engineering. Process Technology and Materials Science.

## 9. Other research projects

Reactive sintering of TiC-NiMo alloys. Investigation of sliding wear.

**DISSERTATIONS DEFENDED AT  
TALLINN UNIVERSITY OF TECHNOLOGY ON  
*MECHANICAL AND INSTRUMENTAL ENGINEERING***

1. **Jakob Kübarsepp**. Steel-bonded hardmetals. 1992.
2. **Jakub Kõo**. Determination of residual stresses in coatings & coated parts. 1994.
3. **Mart Tamre**. Tribocharacteristics of journal bearings unlocated axis. 1995.
4. **Paul Kallas**. Abrasive erosion of powder materials. 1996.
5. **Jüri Pirso**. Titanium and chromium carbide based cermets. 1996.
6. **Heinrich Reshetnyak**. Hard metals serviceability in sheet metal forming operations. 1996.
7. **Arvi Kruusing**. Magnetic microdevices and their fabrication methods. 1997.
8. **Roberto Carmona Davila**. Some contributions to the quality control in motor car industry. 1999.
9. **Harri Annuka**. Characterization and application of TiC-based iron alloys bonded cermets. 1999.
10. **Irina Hussainova**. Investigation of particle-wall collision and erosion prediction. 1999.
11. **Edi Kulderknup**. Reliability and uncertainty of quality measurement. 2000.
12. **Vitali Podgurski**. Laser ablation and thermal evaporation of thin films and structures. 2001.
13. **Igor Penkov**. Strength investigation of threaded joints under static and dynamic loading. 2001.
14. **Martin Eerme**. Structural modelling of engineering products and realisation of computer-based environment for product development. 2001.
15. **Toivo Tähemaa**. Assurance of synergy and competitive dependability at non-safety-critical mechatronics systems design. 2002.
16. **Jüri Resev**. Virtual differential as torque distribution control unit in automotive propulsion systems. 2002.
17. **Toomas Pihl**. Powder coatings for abrasive wear. 2002.
18. **Sergei Letunovitš**. Tribology of fine-grained cermets. 2003.
19. **Tatyana Karaulova**. Development of the modelling tool for the analysis of the production process and its entities for the SME. 2004.
20. **Grigori Nekrassov**. Development of an intelligent integrated environment for computer. 2004.
21. **Sergei Zimakov**. Novel wear resistant WC-based thermal sprayed coatings. 2004.
22. **Irina Preis**. Fatigue performance and mechanical reliability of cemented carbides. 2004.
23. **Medhat Hussainov**. Effect of solid particles on turbulence of gas in two-phase flows. 2005.

24. **Frid Kaljas**. Synergy-based approach to design of the interdisciplinary systems. 2005.
25. **Dmitri Neshumayev**. Experimental and numerical investigation of combined heat transfer enhancement technique in gas-heated channels. 2005.
26. **Renno Veinthal**. Characterization and modelling of erosion wear of powder composite materials and coatings. 2005.
27. **Sergei Tisler**. Deposition of solid particles from aerosol flow in laminar flat-plate boundary layer. 2006.
28. **Tauno Otto**. Models for monitoring of technological processes and production systems. 2006.
29. **Maksim Antonov**. Assessment of cermets performance in aggressive media. 2006.
30. **Tatjana Barashkova**. Research of the effect of correlation at the measurement of alternating voltage. 2006.
31. **Jaan Kers**. Recycling of composite plastics. 2006.
32. **Raivo Sell**. Model based mechatronic systems modeling methodology in conceptual design stage. 2007.
33. **Hans Rämmal**. Experimental methods for sound propagation studies in automotive duct systems. 2007.
34. **Meelis Pohlak**. Rapid prototyping of sheet metal components with incremental sheet forming technology. 2007.
35. **Priidu Peetsalu**. Microstructural aspects of thermal sprayed WC-Co coatings and Ni-Cr coated steels. 2007.
36. **Lauri Kollo**. Sinter/HIP technology of TiC-based cermets. 2007.
37. **Andrei Dedov**. Assessment of metal condition and remaining life of in-service power plant components operating at high temperature. 2007.
38. **Fjodor Sergejev**. Investigation of the fatigue mechanics aspects of PM hardmetals and cermets. 2007.
39. **Eduard Ševtšenko**. Intelligent decision support system for the network of collaborative SME-s. 2007.
40. **Rünno Lumiste**. Networks and innovation in machinery and electronics industry and enterprises (Estonian case studies). 2008.
41. **Kristo Karjust**. Integrated product development and production technology of large composite plastic products. 2008.
42. **Mart Saarna**. Fatigue characteristics of PM steels. 2008.
43. **Eduard Kimmari**. Exothermically synthesized B<sub>4</sub>C-Al composites for dry sliding. 2008.
44. **Indrek Abiline**. Calibration methods of coating thickness gauges. 2008.
45. **Tiit Hindreus**. Synergy-based approach to quality assurance. 2009.
46. **Karl Raba**. Uncertainty focused product improvement models. 2009.

47. **Riho Tarbe**. Abrasive impact wear: tester, wear and grindability studies. 2009.
48. **Kristjan Juhani**. Reactive sintered chromium and titanium carbide- based cermets. 2009.
49. **Nadežda Dementjeva**. Energy planning model analysis and their adaptability for Estonian energy sector. 2009.
50. **Igor Krupenski**. Numerical simulation of two-phase turbulent flows in ash circulating fluidized bed. 2010.
51. **Aleksandr Hlebnikov**. The analysis of efficiency and optimization of district heating networks in Estonia. 2010.